A novel liquid nitrogen fill level meter for the AGATA triple cluster detector

Diplomarbeit von: Daniel Lersch
Unter der Leitung von: Prof. Dr. Peter Reiter

Institut für Kernphysik der Universität zu Köln

Dezember 2009

Contents

Chapter 1

Introduction

High resolution γ-spectroscopy is the underlying method to investigate excited stats in nuclei and to understand nuclear structure physics. Since the complexity of nuclear structure experiments is still increasing, the requirements on an efficiently and accurately working γ-spectrometer are considerably high.
AGATA (Advanced GAmma Tracking Array) is an European project to establish a new γ-spectrometer which is based on modern electronics with the encapsulated, highly segmented germanium-crystal-technology. A characteristic of these complex detector-systems is the continuous operation at liquid nitrogen temperature. A lack of cooling would cause a severe damage of these delicate detectors and major losses in operation time and financial losses would be related to such a warmup event. Therefore the determination of the liquid nitrogen consumption and the direct monitoring of the liquid nitrogen level inside the detector are of great importance.
The subject of this thesis is a novel liquid nitrogen fill level meter for the AGATA-triple-cluster detectors. The consumption of liquid nitrogen depending on different setups of the AGATA-detector is investigated with the newly developed device.
Due to various AGATA detector positions the affect of the consumption of liquid nitrogen and the influence on the liquid-nitrogen-level-read-out itself was subject of this thesis.

Chapter 2

The AGATA-spectrometer

The AGATA-spectrometer is designed as a 4π γ-spectrometer and will consist of 60 antisymmetric triple cluster (ATC) detectors (see fig. 2.1) in its final configuration. Each cluster contains three 36-fold-segmented, encapsulated high purity n-type Germanium (HPGe) crystals [DB01]. The geometry of the

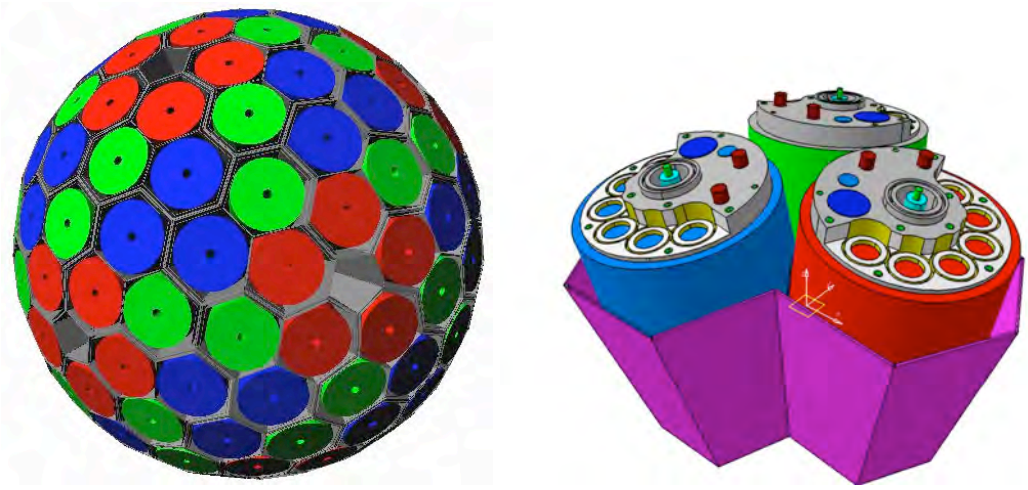

Figure 2.1: **Left:** *Drawing of the AGATA-array consisting of* 180 *hexagonal shaped crystals. The inner radius of the shell is* 23.5 cm *[JE08], as* 82 % *of the solid angle are covered by the Ge-crystals. The total amount of germanium needed for this configuration is* 362 kg *[JE08].* **Right:** *The Ge-crystals inside one triple cluster are not shaped symmetrically, three different asymmetric types are used instead: A-type (red), B-type (green) and C-type (blue).*

AGATA-array is determined by the following requirements [DB01]:

- Full energy efficiency and spectral response for γ-rays in the energy range from 10 keV to 10 MeV
- Symmetry of the configuration
- Modularity
- Available inner space (inner radius of shell)
- Amount of germanium used (cost)

The final design of the array is shown in fig. 2.1. The AGATA-spectrometer will be used for several types of experiments which are characterised by a

γ-radiation after a reaction zone. Thus a spherical configuration of the Ge-crystals around a target provides the highest detection efficiency [DB01]. Many methods of γ-spectroscopy (e.g angular distribution, correlation measurements etc.) take advantages of a symmetric arrangement of the detectors which is given by the configuration shown in fig. 2.1 [DB01]. In order to realise a full solid angle coverage in a spherical arrangement, the detectors are shaped asymmetrically.
Figure 2.1 displays the predicted performance for the future AGATA-spectrometer at energies of 1 MeV. The efficiency for a single γ-particle is determined by the amount of detection material which surrounds the radiation source [DB01]. γ-rays with energy $E_\gamma = 1\,\text{MeV}$ for example are detected with an efficiency of 43.3 %. According to the attenuation law $I = I_0 \cdot e^{-\mu\Delta x}$ for gamma rays, the thickness of the surrounding Ge-material becomes more important for higher γ-energies [DB01]. If the γ-multiplicity M_γ increases then the number of detecting elements has to increase too, in order to distinguish between different γ-rays. Considering this, simulations have shown that $6000 - 8000$ detection elements are required which is realised by 6660 channels for the AGATA-spectrometer. The peak-to-total ratio P/T describes the spherical response of

Multiplicity	1	10	20	30
Efficiency [%]	43.3	33.9	30.5	28.1
Peak to total ratio [%]	58.2	52.9	50.9	49.1

Table 2.1: *Predicted performance of* 180 *triple cluster detectors in the AGATA for* γ*-energies of* 1 MeV *[JE08].*

the detector. A high position resolution is assured by the segmentation of the Ge-crystals, as the segments are sufficiently small [DB01].

2.1 The AGATA-triple-cluster

Each AGATA-triple cluster (see fig. 2.4) consists of two main parts: on the one hand the Ge-crystals which are detecting the γ-rays and the cryostat on the other hand. The cryostat connects the crystals with the high front end read-out-electronics and keeps the crystals at an temperature near $-196\,^\circ\text{C}$ since they are cooled with liquid nitrogen.

2.1.1 The AGATA-capsule

The high angular resolution and position sensitivity of the AGATA-spectrometer is related to the fact that all Ge-crystals in the array are segmented. Each Ge-crystal comprises 36 segment-electrodes and one core-electrode. In order to separate the delicate Ge-crystals from the cryostat and to protect them during repairs of the electronics, all crystals are encapsulated. Figure 2.2 shows an

Figure 2.2: **Left:** *CAD-drawing of an encapsulated, segmented hexagonal Ge-crystal [DB01].* **Middle:** *Labeling of the segmented detector: The rows are labelled from 1 to 6, as no. 6 is the upper segment. The rings are labelled from A to F.* **Right:** *Photograph of an AGATA-detector. In order to read out the signals of the segments a board is mounted on top of the crystal which connects the first preamplifier stage with the segments.*

encapsulated AGATA-detector with a board mounted on top. The capsules are made of aluminium with a 8 mm wall thickness. The space between the detector and the Al-caspule is about 0.5 mm. The whole detector has a weight of 2 kg.
The AGATA-capsules are manufactured by the company Canberra, Lingolsheim (Strasbourg), France. Before these crystals are mounted in the AGATA triple cryostat, they have to pass a customer acceptance test (CAT) which is done at IKP (Institut für Kernphysik) Cologne. The results of such a test are displayed in fig. 2.3. All segments and the core of this detector are performing well. The FWHM of segment B3 for example is 1 keV for a γ-energy $E_\gamma = 59.6\,\mathrm{keV}$.

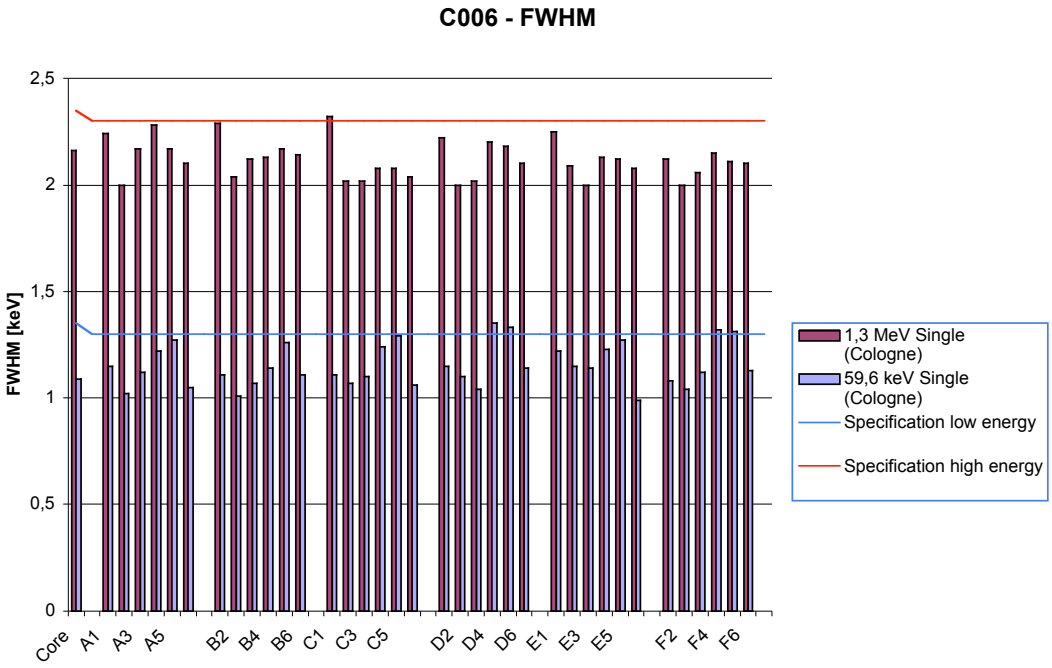

Figure 2.3: *Results of a customer acceptance test done at IKP Cologne for an asymmetric C-type AGATA-detector. The full width at half maximum (FWHM) of a measured energy peak is specified for the segments and the core. The specifications for the segments are:* 1.3 keV *for an energy of* 59.6 keV, 2.3 keV *for* 1.3 MeV *and for the core:* 1.35 keV *at* 122 keV, 2.35 keV *at* 1.3 MeV. *The measured FWHM of the segments and core of this detector are performing well within the specifications.*

2.1.2 The cryostat

Each AGATA-cryostat (see fig. 2.4) may in principle be divided in three main sections:

1. The cold part: Three asymmetric, hexagonal, encapsulated Ge-crystals and the first amplifying stage are operated under a high vacuum of $p < 10^{-7}$ mbar and a temperature near $-196\,^{\circ}\mathrm{C}$. The cold part is covered by an aluminium endcap with a length of 27.5 cm and a weight of 420 g.

2. The warm part: The warm preamplifiers are connected by feedthroughs with the amplifying stage in the cold part. The amplifiers in the cold and warm part are operated with a low-voltage of ± 6 V and ± 12 V.

3. The liquid nitrogen is hosted inside a dewar.

Since all AGATA-detectors are cooled with LN_2, the dewar is linked by a cooling finger with the cold part (see chapter 3) where the crystals are attached. The whole cryostat has a total length of 92 cm, as the dewar has a length of 38 cm. The total weight of the cryostat without liquid nitrogen inside is 38 kg. Figure 2.4 shows a symmetric triple cluster where symmetric detectors are mounted inside. But the working principle is identical to that of an asymmetric triple cluster.

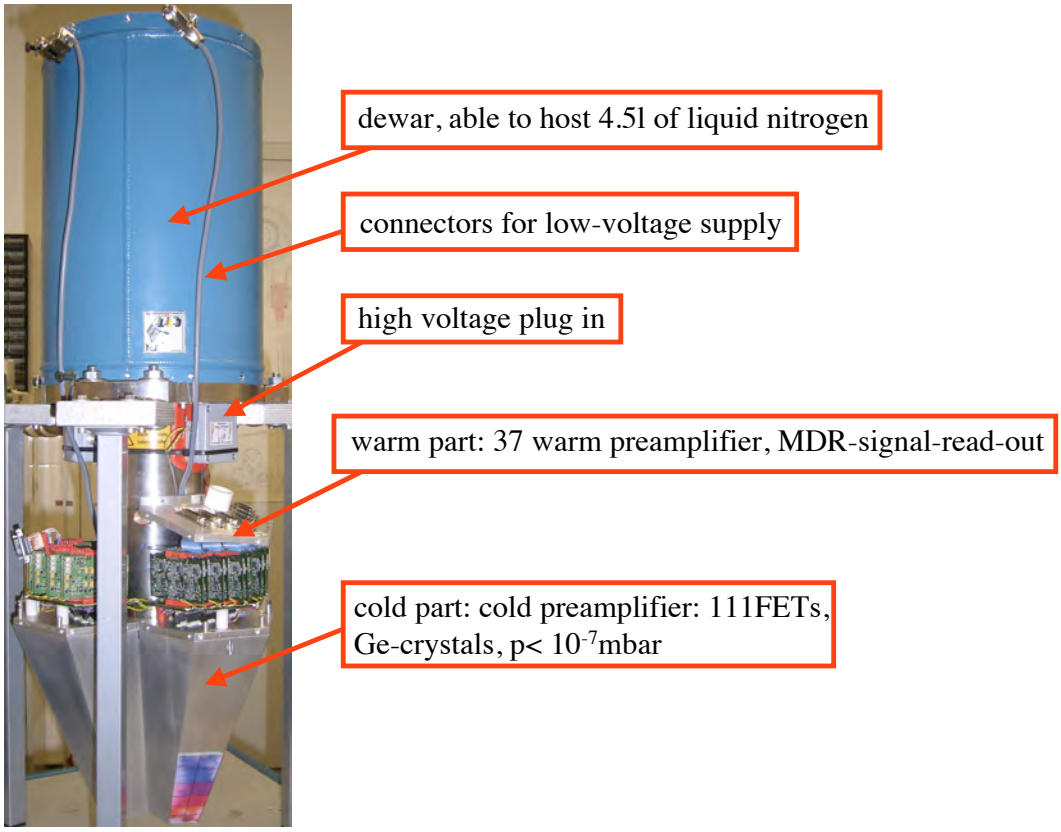

Figure 2.4: *Symmetric AGATA-triple-cluster (STC) at IKP Cologne. The only difference between a symmetric and an asymmetric triple cluster is given by the shape of the detectors and the endcap. The amplifying stage in the cold part comprises* 111 *(*3×36 *segments* $+$ 3 *cores) feld-effect-transistors (FETs). The signals coming from the cold part pass the warm preamplifiers (*2 *warm preamplifier provide six segments, whereas each core-signal is read out by one warm preamplifier* $\rightarrow$ 37 *warm preamplifiers in total) and are read out by a MDR-cable afterwards.*

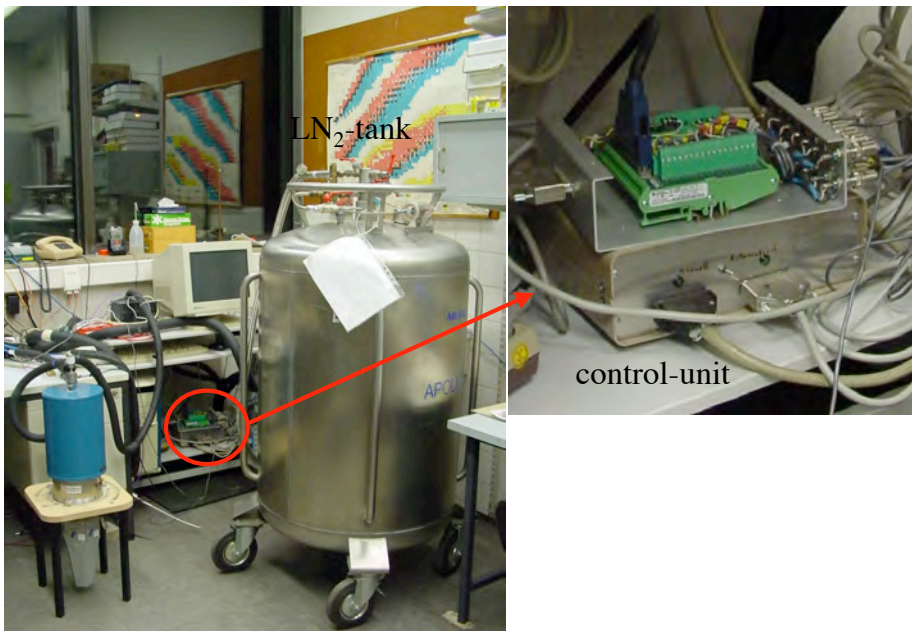

Figure 2.5: *Automatic cryogenic filling system at IKP Cologne. The* LN_2*-tank is able to host* 45 l *of liquid nitrogen and linked by a valve with the control unit. The control unit itself is linked to a PC where the start of a filling and the filling period are adjusted. The control unit drives several valves which are connected by filling-nozzles with the detectors. Each filling-nozzle is equipped with an overflow, as the overflow itself is controlled by a PT100-sensor. If this sensor detects a temperature of* $-196\,°C$ *the control unit shuts the valve and the filling is terminated. The adjusted filling period of the Cologne-filling-system is* 8 h*. The liquid nitrogen is filled with a pressure of* $1.5-2$ bar *into the dewar. The duration of the filling for an AGATA-triple dewar varies between* $5-12$ min *depending on the pressure inside the tank.*

2.2 The cryogenic filling system

All detectors in the AGATA-array are linked to an automatic cryogenic filling system which provides every cluster with liquid nitrogen. The requirements to such an automatic filling system are:

- Reliability
- The filling should start automatically at a given point in time and end automatically when a certain liquid nitrogen level inside the dewar is reached.
- A warning signal has to be sent out by the system if the filling is somehow interrupted or impeded.
- A force filling has to be done in the case the regular filling is interrupted or the detectors is warming up above a temperature treshold.

Figure 2.5 shows the automatic cryogenic filling system which is used in Cologne. The control unit is driven by a Linux-PC which is connected to the Internet. If a filling process was successful (or not) an email is sent out. The reliability of this system depends strongly on the pressure inside the LN_2-tank. Thus it is of great importance that the tank is equipped with a self-adjusting pressure unit which keeps the pressure always at a constant level. The Cologne-filling-system

is able to provide two AGATA-trilpe-clusters and one AGATA-single-detector at once with liquid nitrogen.
The filling-system for the AGATA-array is more complex but mainly working in the same way. Figure 2.6 displays the general layout of a cryogenic system at the LNL (Laboratori Nazionali di Legnaro) in Legnaro. The liquid nitrogen is hosted in the outer tank which is connected by a pipeline with the detectors. Each detector is equipped with a gas-exhaust. The nitrogen gas is collected in a vessel (lime-green coloured box) which is equipped with a PT100-sensor and connected to the outflow watchdog. If the gas becomes liquid the PT100 sensor at the vessel gives a signal to the watchdog which stops the filling automatically [Koj07]. Each detector has an extra PT100-sensor (DPT) which

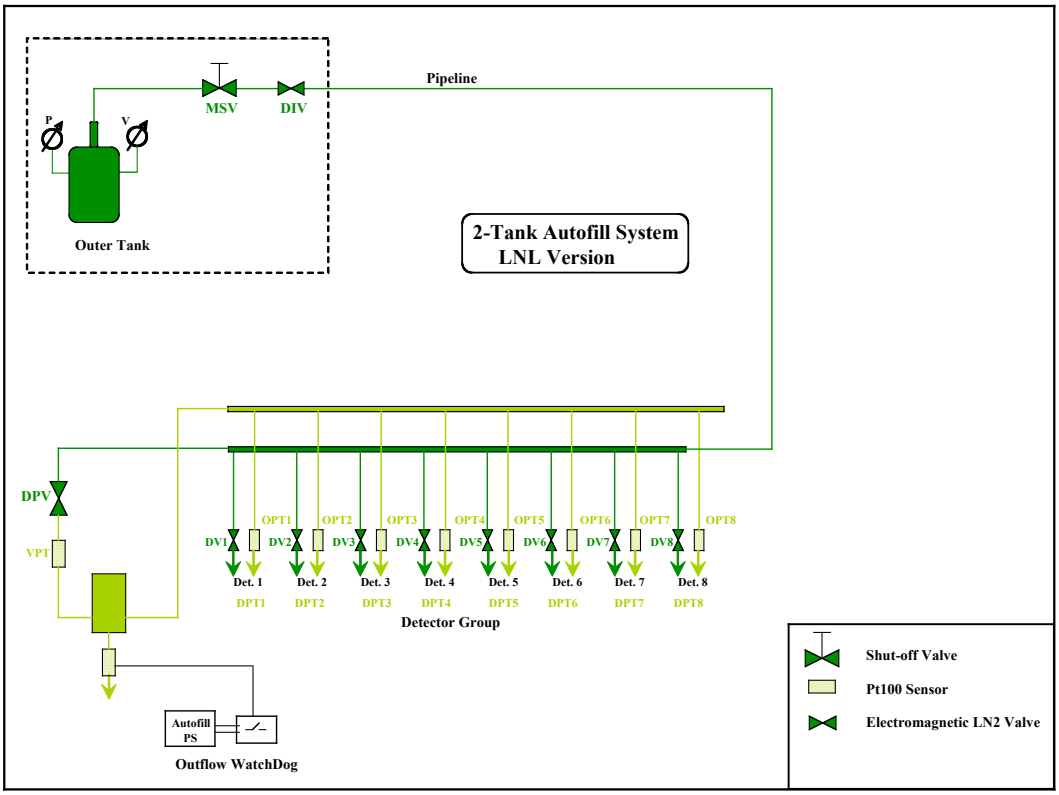

Figure 2.6: *General structure of the cryogenic system at Legnaro [Koj07]*

monitors its temperature. In the case that the temperature exceeds a certain value the detector valve (DV) opens and the DPT gives a signal to the watchdog and a force-fill is done. Due to the complexity of such a system it is not unlikely that a failure may occur and prevent the automatic filling which would be crucial for any detector in the array. A missing liquid nitrogen fill causes an uncontrolled warming up of the detector. This leads to an overheating of the crystals while they are operated under high voltage. Moreover the electronics inside the cold part might be damaged by high voltage sparks.
Thus an independent liquid nitrogen monitor is a necessary extension of the control system. The new monitor is directly linked to the liquid nitrogen level inside the dewar. In case the LN_2-level falls below a certain value, the monitor will cause a force-fill. The working principle of such a LN_2-monitor and the difference with respect to a PT100-sensor inside the detector is discussed in the following section.

Chapter 3

The LN_2-monitor

The AGATA-detectors have to be kept at a low temperature $\sim -190\,°C$ and monitoring of the LN_2-level is of great importance. In this chapter the basic concepts and prerequisites of the new LN_2 monitor are introduced.

3.1 Cooling with liquid nitrogen

The detectors used for the AGATA-triple-clusters are 36-fold segmented high purity germanium detectors. Germanium is a chemical element of the fourth main group and thus is a semiconductor which has a temperature dependent conductivity. The electrical conductivity σ_{el} inside a semiconductor depends on the **intrinsic carrier concentration** $n_i(T)$ [EH05]:

$$\sigma_{el} \sim n_i(T) \tag{3.1}$$

The temperature dependency of n_i determines the conductivity and is discussed in the following section.

3.1.1 Characteristics of a semiconductor

A solid is characterised as conductor, semiconductor or isolator by the bandgap $E_g = E_c - E_v$ between the valence band and conduction band (see fig. 3.1 left). Considering a semiconductor the bandgap is in a region of: $E_g \cong 0.5 - 1\,\text{eV}$ [Dem05]. The probability that an electron inside a solid occupies a state with energy E at a given temperature T is described by the **Fermi-Dirac-distribution** [Dem05]:

$$f(E) = \left[\exp\left[\frac{(E - E_F)}{k_B T}\right] + 1\right]^{-1} \tag{3.2}$$

As E_F is the Fermi-energy. A plot of equation 3.2 is shown on the right hand side of fig. 3.1. If the temperature T of the system is 0, no state with energy $E > E_F$ can be occupied by electrons. When temperature is finite, states with energies $E > E_F$ may be occupied. Therefore for a certain temperature T the probability exists that an electron inside a semiconductor may transcendent through E_g into the conduction band. The electrical conductivity of a solid is determined by the concentration n of electrons in the conduction band which is given by: [Kit06]

$$n = \int_{E_c}^{\infty} \rho_e(E) \cdot f(E) dE \tag{3.3}$$

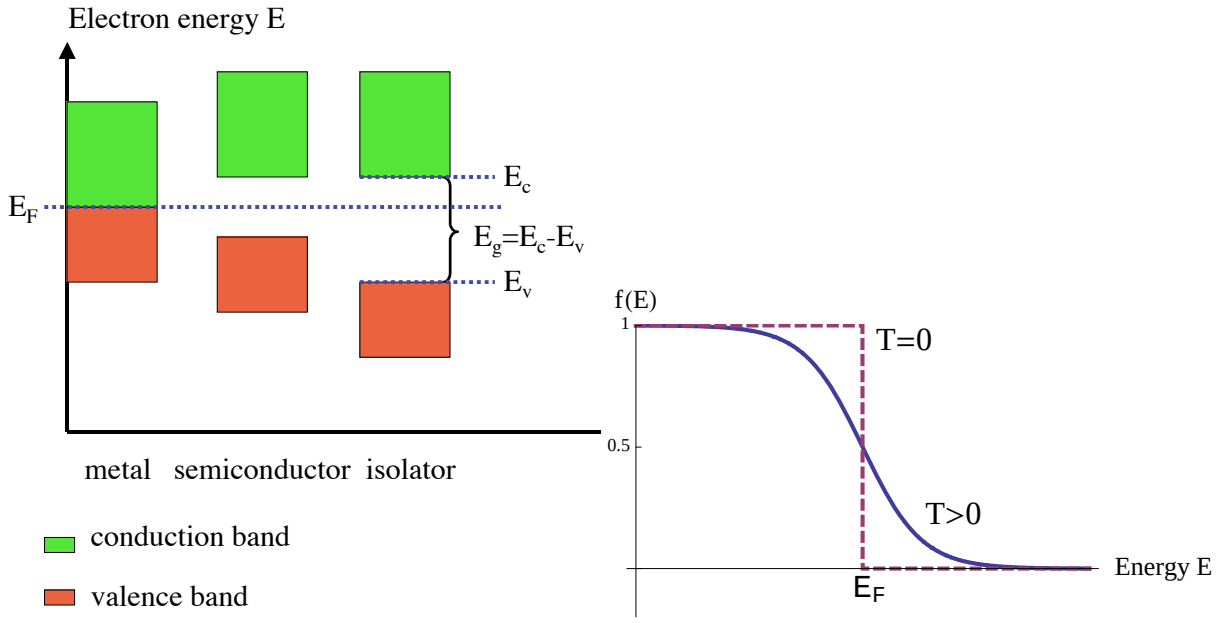

Figure 3.1: **Left:** *Schematic drawing of the band model for solids. The conduction band has a minimum energy E_c whereas the valence band has a maximum energy E_v [Dem05]. The energy E_F is the* **Fermi-energy** *and denotes the highest energy state at $T = 0$ which is still occupied with electrons [Dem05].* **Right:** *Plot of the Fermi-Dirac-distribution $f(E)$ as a function of the energy E. If the energy is $E = E_F$, the distribution takes the value $f(E_F) = 0.5$. For the temperature $T = 0$ the distribution is equal to the Θ-function.*

As ρ_e is the density of states for electrons and $f(E)$ the Fermi-Dirac-distribution [Kit06]. Each electron in the conduction band causes a positive charge called **hole** in the valence band. Referring to equation 3.3 the concentration of holes in the valence band is given by [Kit06]:

$$p = \int_{-\infty}^{E_v} \rho_h(E) \cdot f_h(E) dE \tag{3.4}$$

ρ_h describes the density of states for holes and $f_h(E) = 1 - f(E)$ [Kit06] the corresponding distribution. The temperature dependent intrinsic carrier concentration is then given by [EH05]:

$$n_i(T) = \sqrt{n \cdot p} = n_{i0} \cdot T^{3/2} \cdot \exp\left[\frac{-E_g}{2k_B T}\right] \tag{3.5}$$

Considering germanium for example, the bandgap is $E_g = 0.66\,\text{eV}$ and $n_{i0} = 1.57 \cdot 10^{15}\,\text{cm}^{-3}\text{K}^{-3/2}$ [EH05]. Equation 3.4 is shown in figure 3.2, where $\log[n_i]$ is plottetd with respect to the inverse temperature $1/T$. For high temperatures the charge carrier concentration is considerably high. In order to measure only electron-hole-pairs created by radiation, the semiconductor has to be kept at low temperature: $T \sim 98\text{K}$. The most common cooling techniques applicable are:

1. Cooling with liquid nitrogen LN_2
2. Cooling with liquid helium

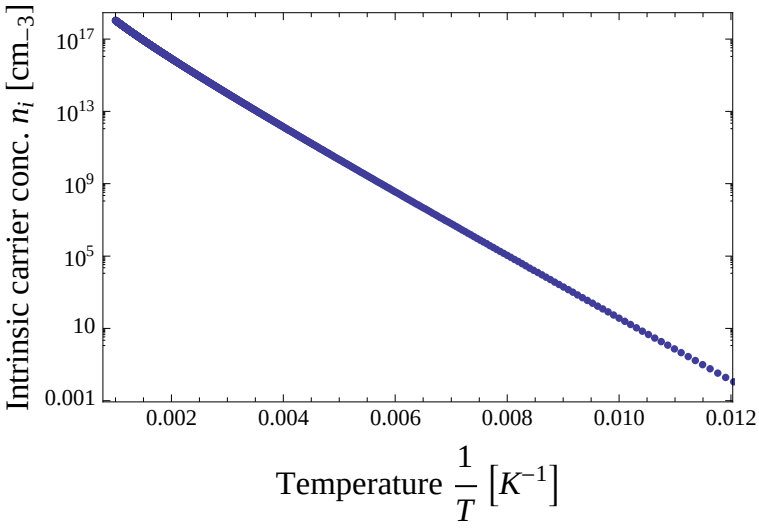

Figure 3.2: *The intrinsic carrier concentration $n_i(T)$ plotted for germanium with respect to the temperature T.*

3. Cooling with liquid argon

The AGATA-triple-clusters are cooled with liquid nitrogen which is hosted in a dewar (see fig. 3.5). The dewar itself is linked by a cooling finger with the germanium crystals, as they have a temperature about $-190\,°\mathrm{C}$ when being cooled. This temperature is in a region where the intrinsic carrier concentration is marginal (see fig. 3.2) and thus does not contribute to the concentration of charges which are created by radiation. In order to keep this temperature at a constant level the crystals environment needs to be evacuated. Otherwise the gas between the crystals and the endcap causes a thermal contact to the outside environment of the cryostat which leads to a heating of the crystals.

3.1.2 Working under vacuum

All AGATA-detector-systems are operated under high vacuum ($p \approx 7{\cdot}10^{-7}\,\mathrm{mbar}$), which means the crystals and electronics inside the cold part are evacuated. Operating the cluster under such a vacuum has two main aspects:

i) The radiation detection only works if the germanium crystals are kept at a low temperature and therefore a thermal contact between them and the cryostat needs to be avoided.

ii) If the cluster is not operated under vacuum, spontaneous discharges may occur and cause a severe damage of the electronics inside the cold part.

The second aspect is related to the **Paschen-law** which is displayed in fig. 3.3. If a voltage is applied to two electrodes in a gaseous environment, free electrons get accelerated and scatter with the gas molecules.This scattering causes an ionization or excitation of the molecules which leads to more free electrons [Rai99]. These free electrons can ionize further molecules. Whether this chain reaction stops or causes an avalanche of free electrons depends on the pressure p of the gas, the distance d between the electrodes and the applied voltage U. In case of an avalanche of free electrons, a current may occur which may cause a severe damage of an electrical system. The relation between the

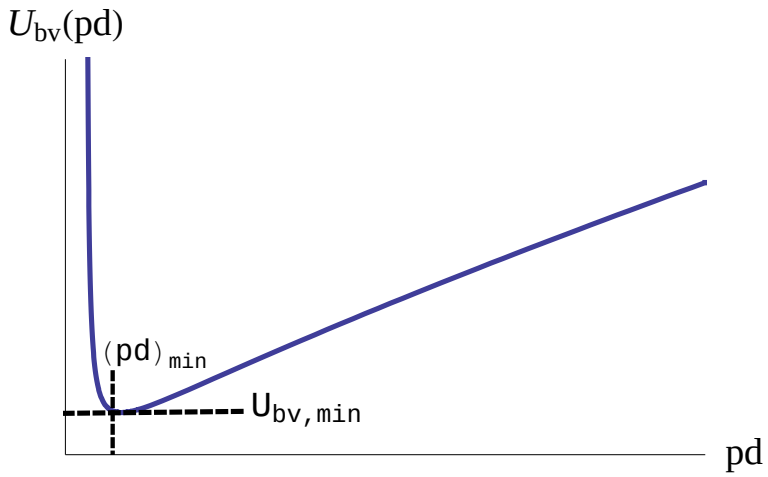

Figure 3.3: *Paschen-curve of the breakdown $U_{bv}(pd)$ with respect to the product of pressure and distance pd. The minimum voltage $U_{bv,min}$ is indicated by the black dashed lines.*

breakdown voltage U_{bv} which causes the severe current and the product of p and d was found by Friedrich Paschen [pas09]:

$$U_{bv} = \frac{c_1 \cdot pd}{\log[c_2 pd] - \log[\log[1 + \gamma^{-1}]]} \tag{3.6}$$

The constants c_1 and c_2 depend on the gas between the electrodes and the electrode material itself. γ is called the Townsend-coefficient [Rai99] and determines whether an avalanche is formed or not. The breakdown voltage is minimal if the product of pressure and distance takes the value $(pd)_{min}$ (see fig. 3.3). If $pd < (pd)_{min}$, the gas pressure is too low and the distance between the electrodes too short the probability for a scattering between the free electrons and gas molecules decreases. Thus a higher voltage for creating avalanches is needed.For values which are larger than $(pd)_{min}$ (see fig. 3.3) the breakdown voltage depends linear on the product of pressure and distance [Rai99]:

$$U_{bv} \sim pd, \;\; pd > (pd)_{min} \tag{3.7}$$

High pressure forces the electrons to scatter with the molecules before they have enough energy to ionize or excite them. Large distances between the electrodes will cause a weak electrical field if the voltage is not increased. Thus the electrons gain not enough energy to ionize the gas molecules. Fig. 3.4 shows three different Paschen-curves for three different gases, e.g air with a pressure of 10 Torr $\approx$ 13 mbar and a distance of 1 cm causes a break down voltage of $U_{bv} \approx 10^3$ V. This value is crucial for any AGATA-detector since the operational voltage is $4 - 5$kV. In order to achieve a high breakdown voltage which is not in the range of the operational voltage, a low pressure or high vacuum is needed. A special feature of the AGATA-cryostats are the getter inside them which have the ability to bind gas molecules [Rot79]. The getter used in AGATA-cryostats work in a low temperature environment, which can be reached by using LN_2. The getter start binding gas molecules when a certain (low) temperature T_l is reached which happens during a cooling-in-process of the cryostat. When the pressure of 10^{-7} mbar is reached it will remain inside the cryostat as long as the temperature T inside the cryostat is:

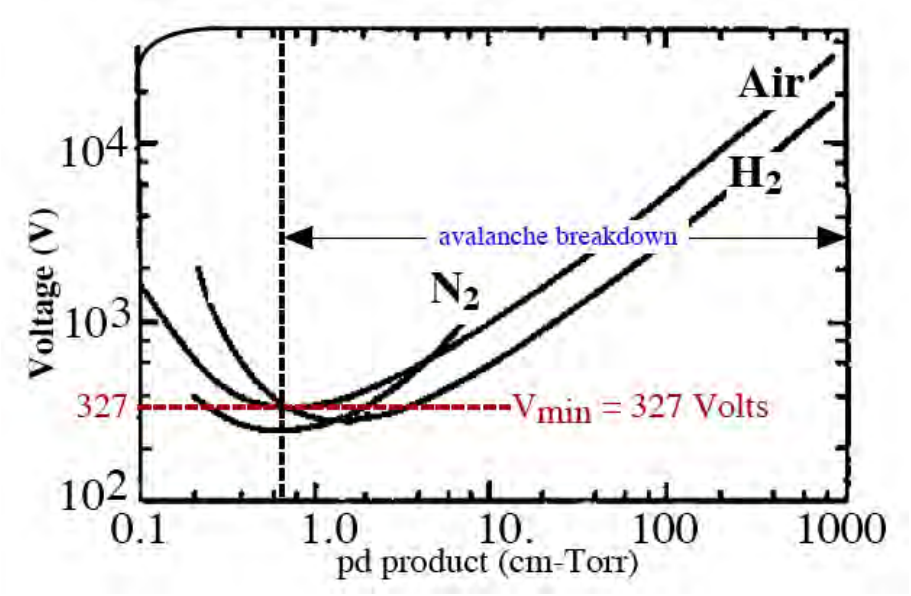

Figure 3.4: *Plot of equation 3.5 for three different gases: air, N_2 and H_2 [Cob41].*

$T < T_l$. When the temperature inside the cryostat is above T_l the getter start gasing out immediately and the pressure increases. According to Paschen's law a spontaneous discharge may occur and damage the electronics. Thus there is a need for constant cooling and a stable monitoring of the LN_2-level inside the dewar. In the following sections two oportunities of temperature- / LN_2-monitoring will be discussed.

3.1.3 The AGATA-dewar

Figure 3.5 shows an AGATA-triple-cryostat and a schematic drawing of an AGATA dewar where the liquid nitrogen is hosted. The germanium crystals are in thermal contact with the dewar through a copper cooling finger. An AGATA dewar is able to host 4.5 l of liquid nitrogen which is roughly the half of the dewars volume.The dewar has a total length of $l = 38\,\text{cm}$ and an outer diameter $d = 25\,\text{cm}$ and is equipped with a pressure control valve which opens automatically if the pressure inside the dewar is about 10 bar. A possibility to check the LN_2-level inside the dewar is to open the valve and measure the filling-level manually. But this method is too inefficient because the AGATA-array consists of 60 triple cluster which have different positions inside the array and no digital data produced to be used on a PC.

3.2 Temperature-monitoring

The LN_2 filling level can be indirectly checked by monitoring the temperature inside the dewar and the temperature of the germanium crystals. If the crystals are not cooled anymore their temperature will increase.

3.2.1 The PT-100-sensor

A most common possibility of monitoring the temperature inside the dewar is using a PT-100 sensor. Such a sensor consists of a PT-resistance $R(T)$, which

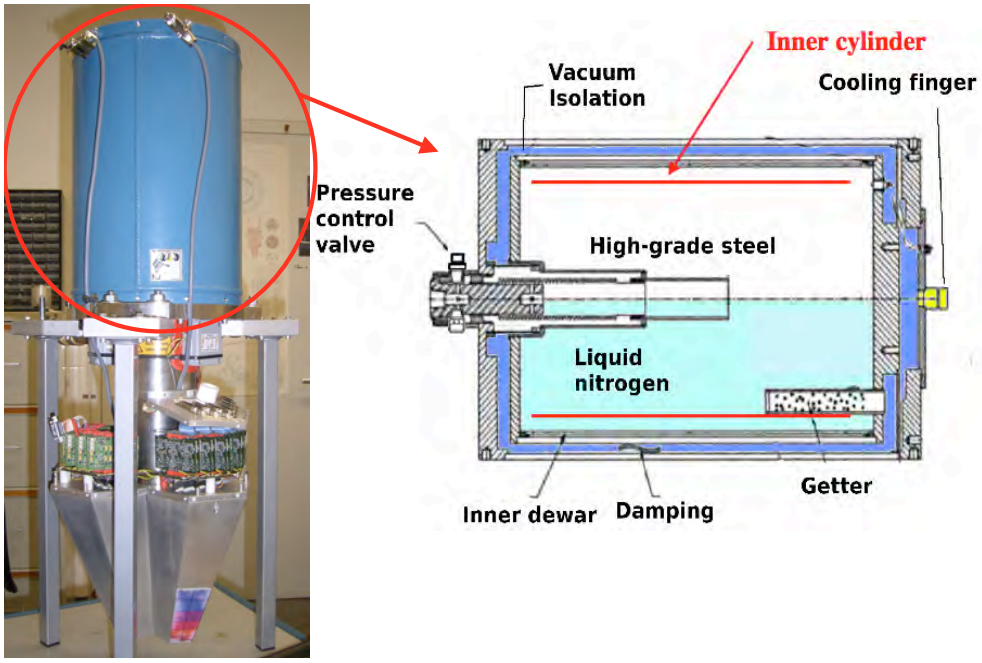

Figure 3.5: **Left:** *AGATA-Triple-cryostat at IKP-Cologne. The blue part on top is the dewar where the liquid nitrogen is hosted.* **Right:** *Schematic drawing of a dewar used for AGATA. The dewar is linked to the crystals by a cooling finger. A getter is mounted inside the dewar to hold the pressure low. The interior of the dewar is separated from the exterior by a damping and a vacuum isolation as the vacuum region inside the dewar is indicated in dark blue.The inner metallic cylinder (indicated by the red lines) is used for the* LN_2*-monitoring. The filling nozzle extends about one half into the inside of the dewar. Thus the maximum filling height is limited by the length of the filling nozzle.*

varies as function of the temperature T. For low temperatures $T \leq 0°C$ the resistivity is described by [pt1]:

$$R(T) = R_0 \cdot [1 + a \cdot T + b \cdot T^2 + c \cdot (T - 100\,°C) \cdot T^3] \tag{3.8}$$

With the coefficients: $a = 3,9 \cdot 10^{-3} \frac{1}{°C}$, $b = -5,8 \cdot 10^{-7} \frac{1}{°C^2}$ and $c = -4,2 \cdot 10^{-12} \frac{1}{°C^4}$. The ouput of the sensor for $T = 0\,°C$ is defined as: $R_0 = R(T = 0\,°C) = 100\,\Omega$.

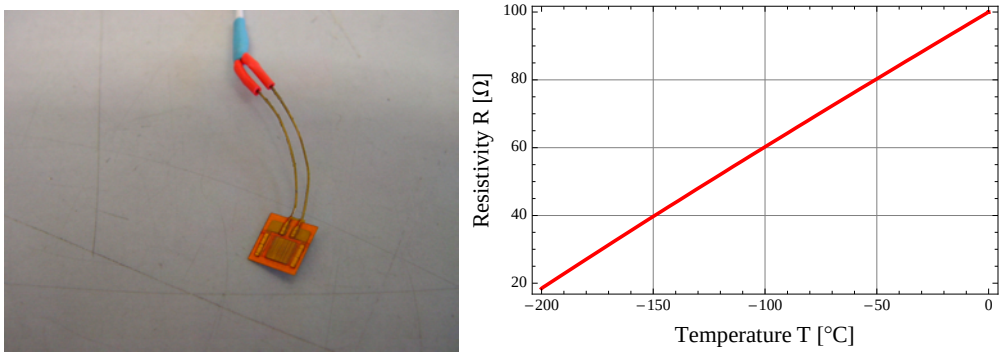

Figure 3.6: **Left:** *Typical PT-100 sensor, used for the AGATA-detectors.* **Right:** *Plot of the PT100-resistivity $R(T)$ for low temperatures $T \leq 0\,°C$.*

The PT-100-sensors used for AGATA-detectors (figure 3.6 left) are fixed at two positions: the first is inside the cryostat on the copper rod of the dewar. The second PT100 is on the crystal-surface itself. Figure 3.7 shows the PT100-read-out of an cooling-in-process as the measured resistance has been translated into a temperature. For this reason equation 3.7 has been approximated by the following linear function:

$$R(T \leq 0\,°C) \approx \mathrm{R}_0 \cdot (1 + 4.02 \cdot \frac{10^{-3}}{°C} \cdot \mathrm{T}) \tag{3.9}$$

The temperature decreases when liquid nitrogen is filled inside the dewar. After one hour the temperature has reached a minimum of $-193\,°C$. However the fluctuations in the measured curve are caused by frequently filling of liquid nitrogen. During the cooling-in-process the dewar and its temperature are not in a steady state as the temperature is changing quickly with any amount of LN_2 filled in. The red curve in figure 3.7 is a fit to the measured temperature $T(t)$ as a function of time:

$$T(t) = a \cdot \exp[-b \cdot t] + c \tag{3.10}$$

Fitting this equation to the measured data leads to the following coefficients: $a = (246 \pm 1)\,°C$, $b = (3.80 \pm 0.04)\,\frac{1}{h}$ and $c = (-194.2 \pm 0.3)\,°C$. The fluctuations are disregarded because they depend on the amount of liquid nitrogen filled in and are absolutely randomly. Except the fluctuations the data is fitted well by equation 3.8. Thus the temperature seems to decrease exponential during a cooling-in-process.

3.2.2 The Bias-shut-down

The critical temperature of the detector-system is about $T_C \approx -160°C$, which is equivalent to a resistivity of $R(T_C) \approx 35\,\Omega$ on the crystal's surface.

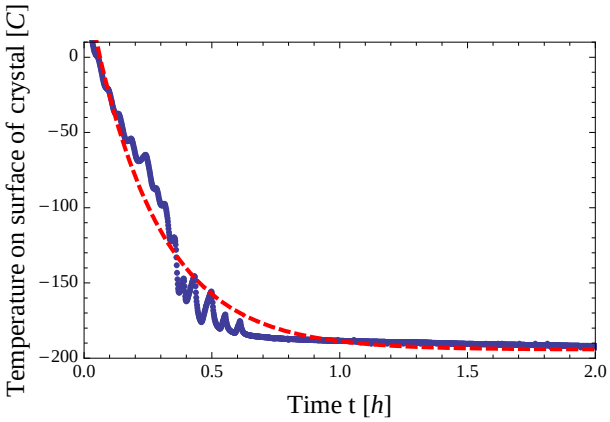

Figure 3.7: *Temperature of the crystal's surface during a cooling-in-process. By using equation 3.8 the temperature has been calculated from the measured resistance of the PT100-sensor. The red curve is an exponential fit to the measured temperature:* $T(t) = a \cdot e^{-b} + c$ *with coefficients* a, b *and* c.

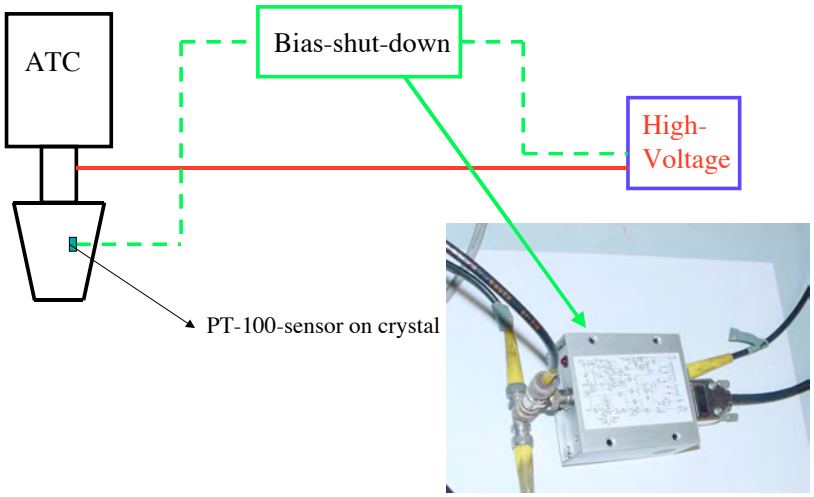

Figure 3.8: *Schematic drawing and photograph of the bias-shut-down. The PT-100-signal is linked with the shut-down-system (right side on photograph), which is linked to the high-voltage power supply (left side on foto). For* $R \simeq 30\Omega$ *the shut-down-function is activated and ramps down the high-voltage immediately.*

By reaching T_C the getter will start gasing out and the breakdown voltage increases. Moreover the leakage current over the crystal's surface increases and may damage it. Thus the high voltage needs to be shut down, in order to protect the detector-electronics and the crystals. This can be achieved by a bias-shut-down, which is linked between the PT-100-sensor and the high-voltage-supply (fig. 3.8). If the PT-100 has a resistance of $R \simeq 30\,\Omega$ ($T \geq -170\,^{\circ}\mathrm{C}$), the bias-shut-down will ramp down the high-voltage.

The sensor is fixed on the crystals surface and the crystal is linked through the cooling finger with the dewar. The cooling finger is made of copper, which has good thermal conduction. This means: If the dewar is getting warm and the getter starts gasing out already, the crystal will remain cold for a while due to its own and the cooling fingers' heat capacity. Hence the PT-100-sensor will not alarm the cryogenic filling system at the right time (before the getter starts gasing out). Therefore the only possibility for preventing damages of the detector-system is to release the bias shut down by the PT-100-sensor.

An other aspect of this monitoring-method is that the detector is not operational after a bias shut down since its temperature and the condition of its electronics need to be checked. The worst case is the separation of a detector unit from the array which is not trivial at all considering the few space between each detector (about 0.5 mm space between the endcap of each detector). Therefore a shut down of a detector unit causes an expenditure of time, a lack of the measurement period and extra costs. These problems can be overcome by a direct read out of the LN_2-level and provides an additional safety in operating such delicate detector systems.

3.3 The capacitive LN_2-read-out (I)

The LN_2-filling-level can be directly checked by measuring the capacity inside the dewar. For that reason a metallic cylinder has been mounted inside the inner dewar (red line in fig.3.5 left). The dielectric constant of liquid nitrogen is $\epsilon_{LN_2} = 1.4$ [APG] whereas the dielectric constant of nitrogen is $\epsilon \approx 1$. Thus a change in the filling level causes a change of the capacity C between the inner cylinder and inner dewar.

3.3.1 The steady state and vertical dewar-postion

Figure 3.9 shows a schematic drawing of a dewar in vertical position which is filled up to the height h with liquid nitrogen. Considering the gas phase of the nitrogen (indicated by N_2(g) and the liquid-phase (indicated by N_2(g)) being in thermal equilibrium a classical cylindrical capacitor may be used to describe the electrical properties of the dewar (see right hand side of fig. 3.9). Using the equivalent circuit diagram (see fig. 3.9) leads to the average dielectric constant $\langle\epsilon_r\rangle$ of the whole dewar:

$$\langle\epsilon_r\rangle = \frac{1}{h_0}\cdot[(h_0 - h) + \epsilon_{r,l}\cdot h] \Leftrightarrow \tag{3.11}$$

$$\langle\epsilon_r\rangle = \frac{1}{h_0}\cdot[h_0 + (\epsilon_{r,l} - 1)\cdot h] \Leftrightarrow \tag{3.12}$$

$$\langle\epsilon_r\rangle = 1 + 0.4\cdot\frac{h}{h_0} \tag{3.13}$$

As the dielectric constant for gasious nitrogen is equal to 1 and the dielectric constant for liquid nitrogen is 1.4 then the total capacity C of the dewar is given by:

$$C = 2\pi\epsilon_0\cdot\frac{h_0\cdot\langle\epsilon_r\rangle}{\ln\left(\frac{r_2}{r_1}\right)} \Rightarrow \tag{3.14}$$

$$\boxed{C(h) = \frac{2\pi\epsilon_0}{\ln\left(\frac{r_2}{r_1}\right)}\cdot\Big(h_0 + 0.4h\Big)} \tag{3.15}$$

For the dewar in a vertical position the measuring capacity C is a linear function of the filling level h. Figure 3.10 shows a simulation of the filling capacity $C(h)$ as a function of the filling level h when the liquid nitrogen level inside

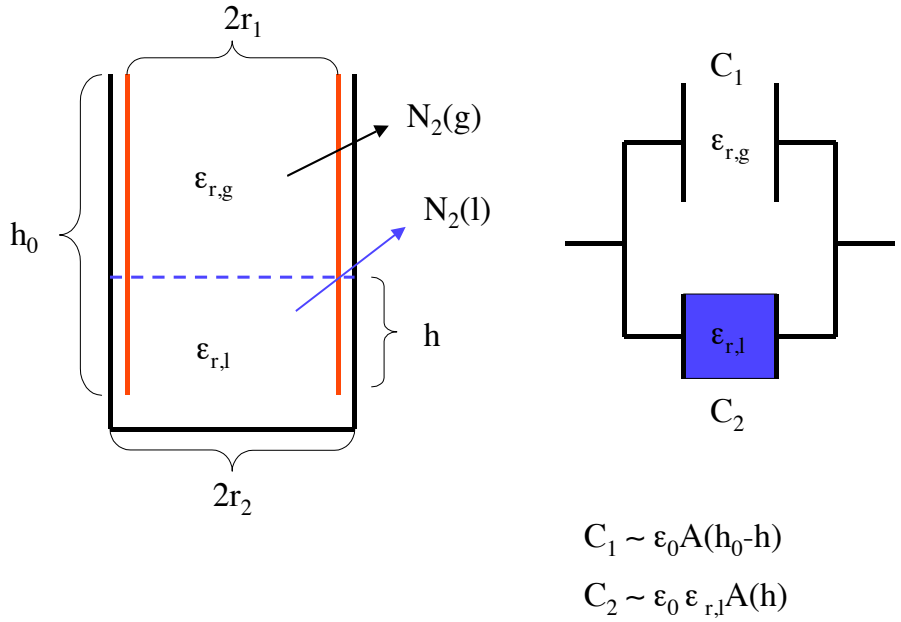

Figure 3.9: **Left:** *Schematic representation of the dewar as a cylinder capacitor.The red line indicates the inner cylinder with radius r_1. The inner dewar's radius is r_2. The dewar has the total height h_0 and is filled up to h with liquid nitrogen. Because the system is in thermal equilibrium, this part can be represented by the dielectric constant $\epsilon_{r,l} = 1.4$ of LN_2. The upper part contains gasious nitrogen $N_2(g)$, which has the dielectric constant $\epsilon_{r,g} = 1$.* **Right:** *Equivalent circuit diagram of a dewar which is filled with LN_2. The capacity C_1 depends on ϵ_0 and the area $A(h_0 - h)$ whereas the capacity C_2 depends on the electrical constant $\epsilon_{r,l}$ of liquid nitrogen and the area $A(h)$. Both capacities add up to the measured capacity $C = C_1 + C_2$.*

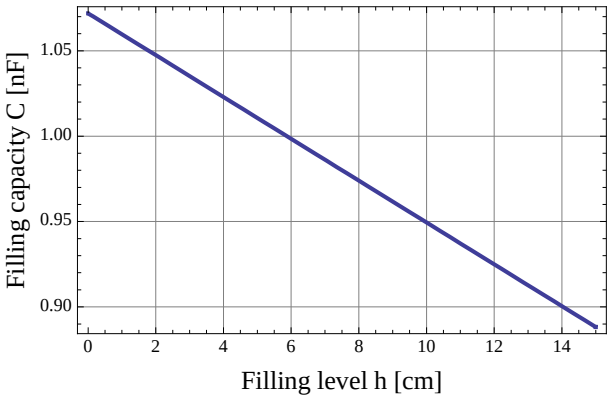

Figure 3.10: *Simulation of the filling capacity C as a linear function of the filling level h. The simulation has been done for an ideal dewar with total height $h_0 = 29\,\text{cm}$, radius $r_2 = 10\,\text{cm}$ and $r_1 = 9.82\,\text{cm}$.*

the dewar is decreasing. The expected values for the measuring capacities are a few nF. Considering this simulation, the variation between the maximum capacity $C(h = 0\,\text{cm})$ and the minimum capacity $C(h = 15\,\text{cm})$ varies about 21 % which is considerably low.

3.3.2 Measuring device (I)

The capacity inside a dewar is read out through a BNC-connector (figure 3.11 left), which has been connected to a multimeter. The first capacitive measurements were done this way. Additionally, the multimeter has a digital output and is connected to a laptop (figure 3.11 right).

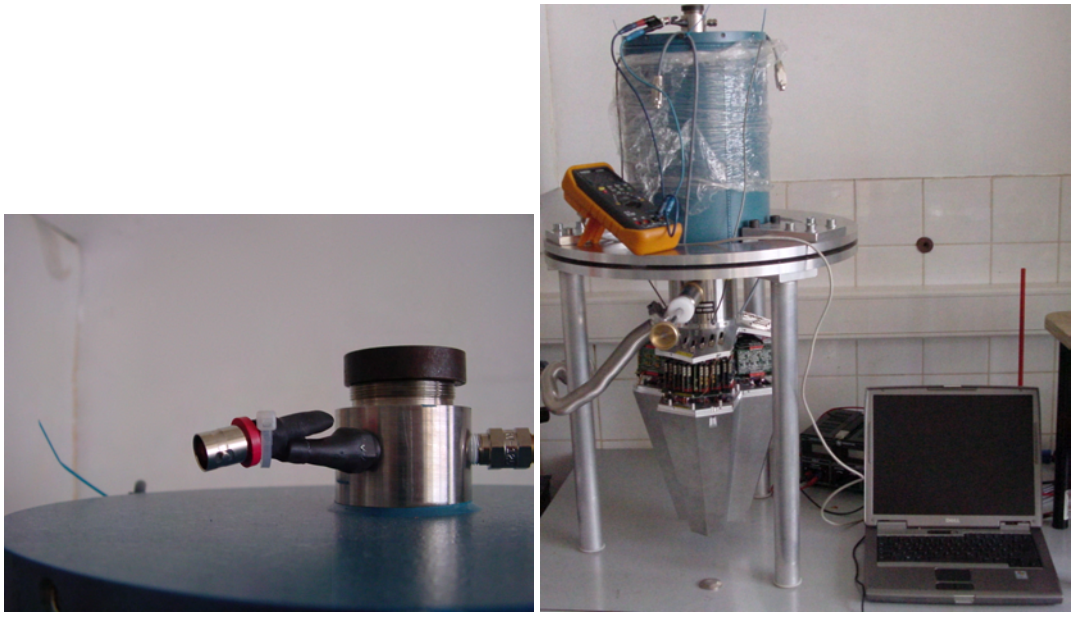

Figure 3.11: **Left:** *BNC-connector for reading out the capacity.* **Right:** *Multimeter with digital-output, connected to a laptop.*

First measurements and results

First of all, the capacity was measured with respect to the LN_2-filling level. This was done at ATC(1) (fig. 3.12 a)) and repeated for ATC(3) (fig. 3.12 b)) later. The capacity C was measured with a multimeter and the filling-level h was read out analogously. The red curves in fig. 3.12 are linear regressions: $C(h) = m \cdot h + C_0$. Using this and equation 3.12 leads to:

$$\frac{m}{b} = \frac{1}{h_0} \cdot [\epsilon_{r,l} - 1] \Leftrightarrow \tag{3.16}$$

$$\epsilon_{r,l} = \frac{m}{C_0} \cdot h_0 + 1 \tag{3.17}$$

With $h_0 = (29 \pm 1)\,\text{cm}$, the value of $\epsilon_{r,l}$ results in:

$$ATC(1) : \epsilon_{r,l} = (1.29 \pm 0.02) \tag{3.18}$$

$$ATC(3) : \epsilon_{r,l} = (1.31 \pm 0.01) \tag{3.19}$$

These values are not consistent with the true value of $\epsilon_{r,l} = 1.4$. The measured capacity C depends strongly on the adjusted measuring-range of the multimeter. Thus the determination of $\epsilon_{r,l}$ is less precise. Figure 3.13 represents the

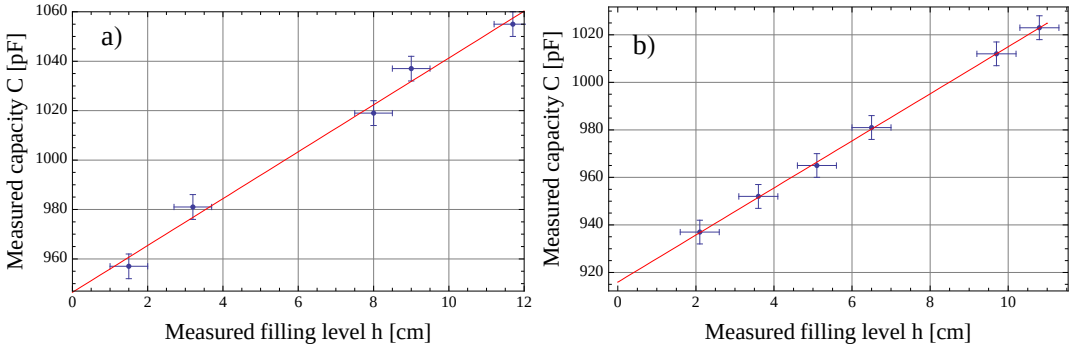

Figure 3.12: **a)** *First capacitive read-out at ATC(1). The capacity C was measured with respect to the filling level h. The red curve is a linear regression $C(h)$ through the measured data:* $C(h) = (9.48 \pm 0.59)\frac{\mathrm{pF}}{\mathrm{cm}} \cdot h + (947 \pm 5)\,\mathrm{pF}$. **b)** *The measurement was repeated for ATC(3) as the measured data was regressed by:* $C(h) = (9.91 \pm 0.11)\frac{\mathrm{pF}}{\mathrm{cm}} \cdot h + (916 \pm 1)\,\mathrm{pF}$. *The errors of the measured capacities are related to the multimeter and assumed as* $\Delta C = 5\,\mathrm{pF}$. *The errors of the measured filling height h are assumed to be* $0.5\,\mathrm{cm}$.

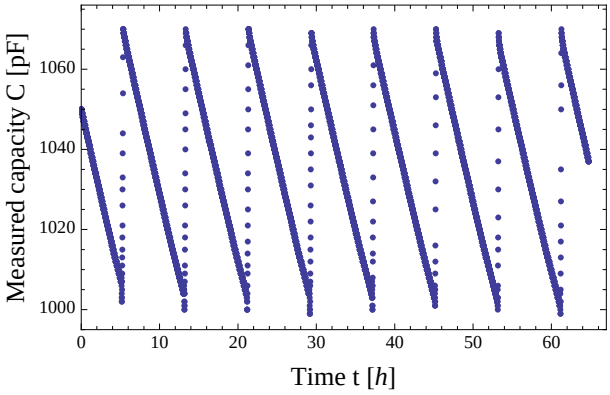

Figure 3.13: *Over-weekend-measurement at ATC(2) during a filling-cycle. ATC(2) was connected to an automatic filling system, which refilled the detector with LN_2 every 8 hours.*

results of an over-weekend-measurement of $C(h)$. It perfectly reflects the linear behaviour of $C(h)$, as C was measured with respect to the time and not to the filling height. The maximum capacity is $C_{max} \approx 1070\,\text{pF}$. The minimum capacity C_{min} of an empty dewar was not measured because the dewar has been refilled every 8 h. The lowest capacity which can be observed in fig. 3.13 is $C \approx 1000\,\text{pF}$. The minimum capacity of a dewar C_{min} is referring to an empty where no liquid nitrogen is inside. But the dewar is still cold and the getter is not gasing out.

3.3.3 Cooling-in- and warming-up-process

Considering a cooling-in or warming-up-process, the liquid phase N_2(l) and the gas phase N_2(g) are not in thermal equilibrium and therefore equation 3.14 is not valid anymore. The mean dielectric constant of the dewar is now strongly time-dependent. Figure 3.14 (left)shows that the liquid nitrogen is boiling

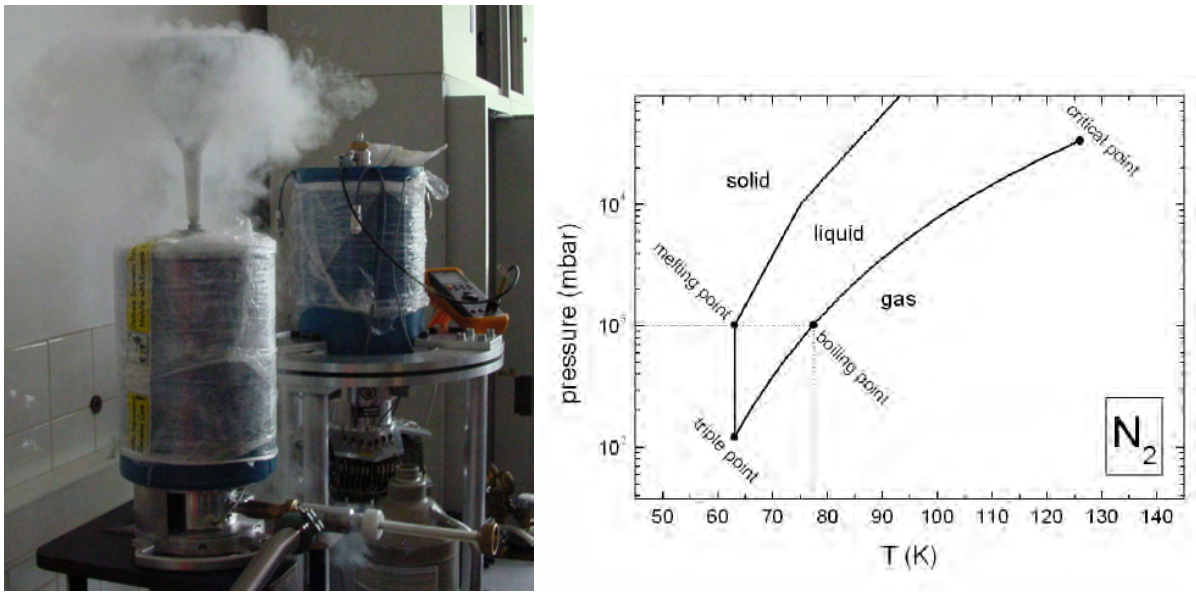

Figure 3.14: **Left:** *Cooling in of an AGATA-single-cryostat. The* LN_2 *is boiling at room temperature.* **Right:** *Phase diagram of liquid nitrogen [Thr08].*

under pressure and steam development while a cryostat is cooled in. The right hand side of fig. 3.14 displays the phase diagram of liquid nitrogen. Since the liquid nitrogen is filled into the dewar at room temperature and normal pressure, the phase of the LN_2 is far away from the critical point. Thus the liquid phase and the gas phase of nitrogen are co-existing.

Cooling in an AGATA-triple-cryostat

The data during a cooling-in-process are shown in figure 3.15 where two structures are striking: the first one is visible in diagram a) of fig. 3.15. The second one is a minimum of the measured capacity at $t \approx 15\,\text{min}$. The expansion of this diagram (see fig. 3.15 b)) points out several peaks which have already appeared in fig. 3.7. When liquid nitrogen is filled into the dewar for the first time, the whole material is working under thermal contraction. As the temperature of the whole system is not constant, the dewar is getting warm immediately, as long as no LN_2 is filled in. The material starts to expand.

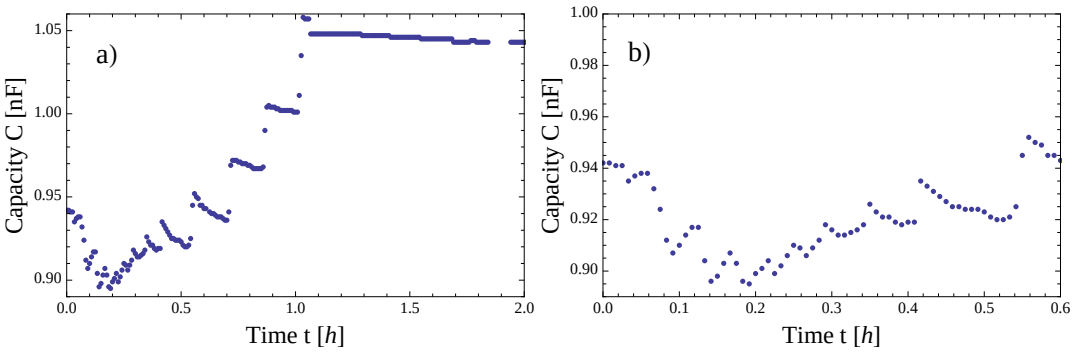

Figure 3.15: **a)** *Cooling-in-Process of an AGATA-triple-cryostat.* **b)** *Expansion of the left figure. The measured capacity C decreases in the first* 15 min *but increases after that point. The thermal equilibrium is reached approximately after one hour, because $C(t)$ is linear as a function of time.*

When LN_2 is filled in again the temperature decreases rapidly and the dewar-material is contracting. This process, namely the expansion and contraction of

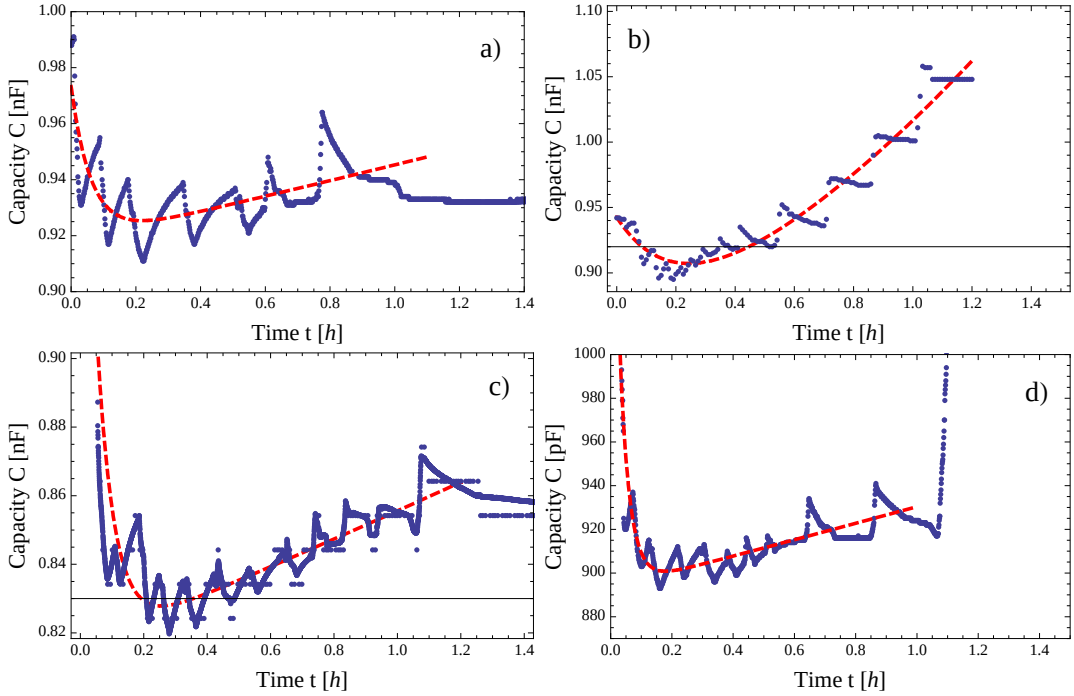

Figure 3.16: *Comparison of the function $C_R(t)$ (red curve) within the measured data during several cooling-in-processes.* **a)** *Cooling-in-process of ATC(2).* **b)** *Cooling-in-process of ATC(4).* **c)** *and* **d)** *Cooling-in-process of ATC(3).*

the dewar (including the rest of the cryostat), will repeat itself until the temperature of the system is in equilibrium. The liquid nitrogen inside the dewar strongly boils until the cryostat is cooled down to $-190\,°C$ and the filling level and the dielectric constant behave in an irregular way. These considerations may be reasonable for the peaks of the measured capacity which are displayed in diagram b). Moreover the height and width of each peak depends strongly on the amount of liquid nitrogen filled in during a cooling-in-process. Taking a closer look at diagram a) again points out that the measured capacity decreases in the first 15 min of the cooling-in-process. After that the capacity increases as a function of the filling height. Figure 3.16 shows the measured

data during four-cooling-in-processes. The red curve in each diagram is a fit $C_R(t)$ to the measured data which only considers the thermal contracting of the dewar. Diagram a) of fig 3.17 shows the variation of the factor $\ln\left(\frac{r_2}{r_1}\right)^{-1}$ as a function of the distance $\Delta r = r_2 - r_2$, as r_1 is the radius of the inner cylinder and r_2 the radius of the inner dewar respectively. The distance Δr between the inner cylinder and inner dewar is 5 mm when the cryostat is at room temperature. Diagram a) points out that even small variations of Δr lead to considerable high variations of the factor $\ln\left(\frac{r_2}{r_1}\right)^{-1}$ which affects the measuring capacity C (see equation 3.14). Due to the thermal contraction of the dewar during a cooling-in-process the radius r_2 and r_1 depend on the temperature T of the system:

$$\ln\left(\frac{r_2}{r_1}\right) = \ln\left(\frac{r_2(T)}{r_1(T)}\right) \tag{3.20}$$

The temperature dependence of a solid with length l is given by [Dem04]:

$$l(\Delta T) = l_0 \cdot (1 + \alpha \cdot \Delta T) \tag{3.21}$$

l_0 is the length at room-temperature and ΔT the change in temperature. The coefficient α is called the **coefficient of expansion** and is material specific constant. Considering the temperature-measurement discussed in section 3.2.1 it is shown that the temperature decreases exponentially:

$$T(t) = a \cdot e^{-bt} + c \tag{3.22}$$

Assuming that the derivative $\frac{dT}{dt}$ can be approximated by $\frac{\Delta T}{\Delta t}$ and that Δt is a constant time interval (e.g. the measuring time) leads to:

$$\Delta T = \kappa \cdot e^{-b \cdot t} \tag{3.23}$$

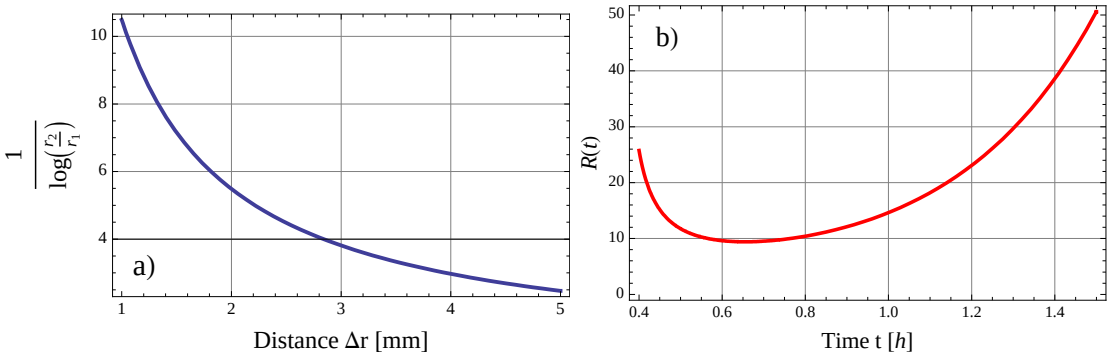

Figure 3.17: **a)** *Variation of* $\ln\left(\frac{r_2}{r_1}\right)^{-1}$ *as a function of the distance* $\Delta r = r_2 - r_1$ *between the inner cylinder and the inner dewar.* **b)** *Plot of the contraction function* $R(t)$ *as a function of time with arbitrary parameters:* $\frac{r_{0,2}}{r_{0,1}} = 1$, $c_2 = 2$, $b_2 = 3$, $c_1 = 4$ *and* $b_1 = 5$.

Using this for equation 3.20 results in:

$$r(t)_i = r_{0,i} \cdot \left[1 + c_i \cdot e^{-b_i t}\right], \; c_i = \alpha \cdot \kappa_i, \; i = 1, 2 \tag{3.24}$$

$r_{0,2}$ is the radius for the inner dewar in case of constant temperature and $r_{0,1}$ the radius for the inner cylinder respectively. Considering the thermal coupling, thickness and fixing inside the dewar, the inner cylinder and inner dewar should behave slightly different during a cooling-in-process and therefore the coefficients b_i and c_i are for each radius different. This leads to the following function:

$$R(t) := \left\{ \ln \left[\frac{r_{0,2}}{r_{0,1}} \cdot \frac{(1 + c_2 e^{-b_2 t})}{(1 + c_1 e^{-b_1 t})} \right] \right\}^{-1} \tag{3.25}$$

$R(t)$ shall be called the **contraction function**. A plot of $R(t)$ as a function of time is shown in diagram b) of figure 3.17. Comparing this simulation and the capacity measurement shown in figure 3.15 point out a similar structure. For a first consideration of the capacity C during the cooling-in-process, the average dielectric constant $\langle \epsilon_r \rangle$ inside the dewar has been approximated as: $\langle \epsilon_r \rangle \approx 1$. Thus the capacity C during a cooling-in-process is approximated by the capacity C_R:

$$\boxed{C(t) \approx C_R(t) = 2\pi\epsilon_0 h_0 \cdot R(t)} \tag{3.26}$$

The fits of $C_R(t)$ to the measured data is not very accurate for the cooling-in-process of ATC(2) (see fig. 3.16), whereas the measured capacity C of ATC(3) and ATC(4) is approximated very well by $C_R(t)$. Thus the decrease of the measured capacity during the first 15 min of a cooling-in-process and the increasing of C after that time are related to the thermal contraction of the dewar.

Describing the peaks of C is not trivial because they depend on the amount

Cryostat	c_1	c_2	b_1[1/h]	b_2[1/h]
ATC(2)	17.11 ± 0.79	16.03 ± 0.74	-15.98 ± 1.35	-15.98 ± 1.35
ATC(4)	7.93 ± 0.54	7.38 ± 0.51	-4.78 ± 0.63	-4.79 ± 0.63
ATC(3), c)	3.66 ± 0.03	3.4 ± 0.03	-18.52 ± 0.25	-15.98 ± 1.35
ATC(3), d)	0.0695 ± 0.0001	0.0177 ± 0.0002	0.042 ± 0.002	-29.4 ± 0.7

Table 3.1: *Fit-paramters c_1, c_2, b_1 and b_2 of the function $C_R(t)$ which is shown in fig. 3.16. The ratio $\frac{r_{0,2}}{r_{0,1}}$ has been set as 1.*

of liquid nitrogen which is filled into the dewar. Table 3.1 shows the fit-parameters of $C_R(t)$. The coefficient pairs c_1, c_2 and b_1, b_2 for one cryostat do not differ very much from each other. This is not surprising, since the inner cylinder and inner dewar are made of the same material and effects like thermal coupling should not have any significant effect. Comparing the coefficients of

the third and fourth row of table 3.1, shows a discrepancy while the cryostat is the same.This discrepancy between the coefficients is related to the experimental conditions, like the amount of LN_2 filled in, which were not accounted for. The experimental conditions are also reasonable for the complexity of an exact fit of $C(t)$ during a cooling-in-process.

Warming-up-process

The warming-up-process is another process in which the thermal equilibrium is not valid after a certain time. In principle $R(t)$ with different parameters is applicable to describe $C(t)$ during this process but this will not be treated in this section. One important aspect of measuring $C(t)$ during a warming-up-process is the determination of C_{min} and C_{max}. C_{min} is the capacity of the dewar when no liquid nitrogen is inside, but the dewar is still cold and the getter does not start gasing out. C_{max} is the capacity in case of a completely

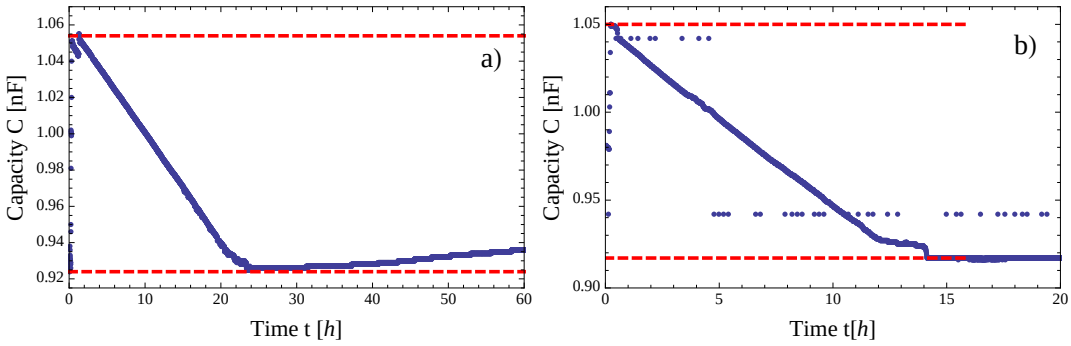

Figure 3.18: **a)** *Warming-up-process of ATC(4).* **b)** *Warming-up-process of ATC(3). The red dashed lines indicate C_{min} and C_{max}.*

filled dewar. The capacity $C(t)$ was measured as a function of time during two warming-up-processes for two different triple clusters. The results of these measurements are displayed in fig. 3.18. The measurements were done with ATC(4) and ATC(3) (further warming-up-processes are shown in appendix A). The red lines in both diagrams indicate the minimum capacity C_{min} and the maximum capacity C_{max}. The measured values are listed in table 3.2. The

Cryostat	C_{min}[pF]	C_{max}[pF]	$\Delta C = C_{max} - C_{min}$[%]
ATC(4)	924 ± 5	1054 ± 5	12.3 ± 0.6
ATC(3)	917 ± 5	1050 ± 5	12.7 ± 0.6

Table 3.2: *Measured minimum capacity C_{min} and maximum capacity C_{max} for ATC(3) and ATC(4). The difference capacity $\Delta C = C_{max} - C_{min}$ is evaluated in %.*

difference between a full and empty dewar is about 14%. The left diagram in fig. 3.18 also reveals a behaviour of $C(t)$ opposite to the cooling in process. At first, $C(t)$ decreases nearly linearly (see equation 3.15). When the

LN_2-reservoir is exhausted, the non-equilibrium-environment starts and the contraction function is not constant anymore. Thus the inner cylinder and inner dewar start to expand slowly and the capacity increases over a long time period until the whole dewar is at room temperature. The measurement with ATC(4) was stopped after 60 hours, whereas the warming-up-process itself was not completed at that time.
Another interesting aspect is the consumption of liquid nitrogen, which is slightly different for each cryostat and depends on whether the cryostat is fully equipped with detectors, the preamplifier stage is under operation and whether high voltage is applied. By looking again at fig. 3.18, a considerable difference between the LN_2-consumption of the two cryostats is visible. ATC(4) (see fig. 3.18 left) is not equipped with electronics and detectors, whereas ATC(3) is fully equipped (but not biased). However the empty cryostat of ATC(4) lasts 22 h; a huge difference of 8 h compared to the LN_2-consumption of ATC(3).

Chapter 4

LN_2-consumption-measurements

The LN_2-consumption is the important feature for operating the AGATA detector-cryostat. Consumption-measurements were performed with the following three AGATA triple clusters: ATC(2), ATC(3) and ATC(4). All capacitive measurements were performed with measuring device (I) which has been discussed in chapter 3.

4.1 LN_2-consumption of ATC(2)

The consumption-measurement performed with ATC(2) shows how the consumption ν is influenced by applying high / low voltage and the room temperature. Furthermore, the direct read out by measuring the LN_2 filling height and the capacitive read out shall be compared.

4.1.1 Setting up ATC(2)

The consumption-measurements of ATC(2) were done over four days. The dewar was filled manually each day and the measurement started 30 min after that, so there was enough time for the filled in LN_2 inside the dewar to settle down.The capacity and LN_2-filling-height have been checked every hour. The LN_2-consumption of ATC(2) has been measured under three different conditions:

- ATC(2) being operated with high and low voltage
- ATC(2) being operated without any voltage
- ATC(2) being operated with low voltage and high voltage which was ramped up slowly. Moreover, the XIA-electronics was running[1]

In order to provide equal conditions for each measurement, the pressure inside the dewar and the amount of liquid nitrogen at the beginning of each measurement were kept constant. Figure 4.1 shows several closings for the AGATA-dewar. ATC(2) was closed with a lead piece with a hole in the middle (closing d)) which has the advantage that the pressure inside the dewar is always in balance with the pressure of the environment. The lead piece has also no valve which might freeze up (like closing d) in fig. 4.1) and cause a built up pressure inside the dewar. Since the pressure inside the dewar is still

[1] If the XIA-electronics is running the room temperature increases apreciably which might influence the consumption.

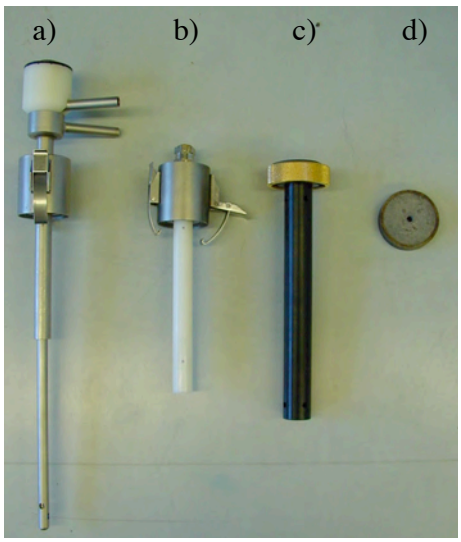

Figure 4.1: *Four different closings for an AGATA-triple-cryostat.* **a)** *filling nozzle for connecting the detector to the automatic filling system.* **b)** *dewar closing with valve (on top) which opens at an internal pressure of one bar.* **c)** *dewar closing without any valve.* **d)** *lead piece with a* 2 mm *hole in the middle to avoid build up pressure.*

high after a first filling, a re-opening would cause a burst of liquid nitrogen and therefore the filling height $h(t = 0\text{h})$ could not be determined.

4.1.2 Results: ATC(2)

The results of the capacity measurements under different conditions are displayed in fig. 4.2. Diagram a) shows a plot of the measured capacities related to time, where all curves show a linear dependency between the measuring capacity C and the time t. The blue (high and low voltage) and black curve (low and high voltage and xia-electronics running) have the same gradient but different axis-intercept which is related to (slightly) different filling heights at the beginning of each measurement. The green curve (no high and low voltage) has a different slope than the others which indicates a lower LN_2-consumption. Diagram b) displays the same data, as the blue curve has been shifted by the difference δC between the maximum capacity $C(t = 0)$ of the black and blue curve. This diagram points out that there is no severe difference between the slopes of the blue and black curve. Thus **the LN_2-consumption predominantly depends on the applied low voltage**. Diagram c) and d) show the measured filling height h which has been measured with respect to the time t (The measured filling heights are displayed in appendix B.). The measured capacity and the filling-height are strictly linear in time and thus can be described by:

$$C(t) = m_C \cdot t + b_C \tag{4.1}$$

$$h(t) = m_h \cdot t + b_h \tag{4.2}$$

m_C, b_C, m_h and b_h are fit-parameters. A fit of equation 4.2 to the measured filling heights is shown by the red curve in diagram c) and d) and therefore

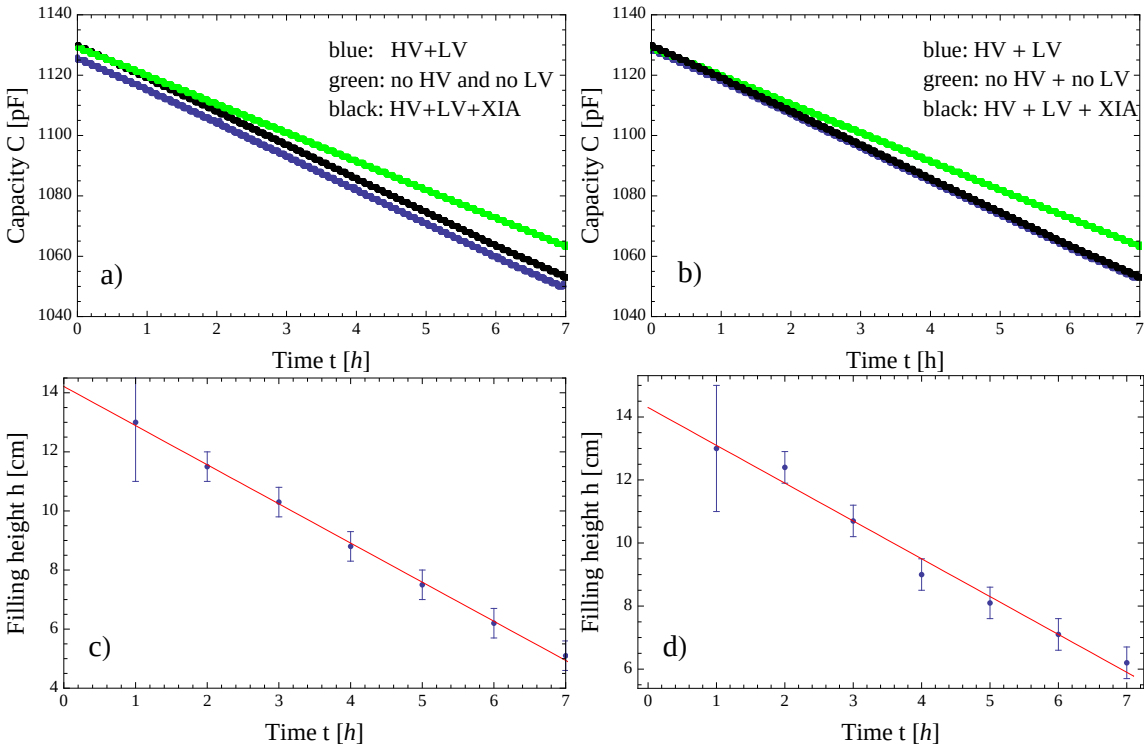

Figure 4.2: **a)** *Measured* LN_2*-consumption for ATC(2) under different conditions (HV = high voltage, LV = low voltage).* **b)** *The blue curve has been shifted by the constant value* $\delta C = 3\,\mathrm{pF}$ *which compensates the indifferent filling height at the beginning of each measurement. Thus they are overlapping now.* **c)** *Measured* LN_2*-filling-level for ATC(2) which has been operated with high and low voltage. The red curve is a linear regression* $h(t) = (-1.33 \pm 0.02)\frac{\mathrm{cm}}{\mathrm{h}} \cdot t + (14.2 \pm 0.1)\,\mathrm{cm}$. **d)** *Measured* LN_2*-filling-level for ATC(2) without any voltage applied. The function of the fitted curve here is given by:* $h(t) = (-1.2 \pm 0.07)\frac{\mathrm{cm}}{\mathrm{h}} \cdot t + (14.3 \pm 0.1)\mathrm{cm}$.

the LN_2-consumption ν and operation time τ are given by:

$$\nu = \frac{m_h}{b_h} \cdot 4.5\,\mathrm{l} \tag{4.3}$$

$$h(\tau) = 0 \Leftrightarrow \tau = \frac{b_h}{m_h} \tag{4.4}$$

The factor 4.5 l is equal to the maximum amount of liquid nitrogen which can be hosted inside the dewar being in vertical position. The operation time of a detector depends on the different system-conditions, before the liquid nitrogen reservoir is completely consumed. Table 4.1 summarises the measured

Low voltage	$\nu\left[\frac{\mathrm{ml}}{\mathrm{h}}\right]$	ν_W[W]	τ[h]
ON	419 ± 19	18.65 ± 0.85	11 ± 0.5
OFF	378 ± 23	16.83 ± 1.02	12 ± 0.7

Table 4.1: *Summary of the consumption measurements at ATC(2). τ is the operation time of the detector-system under two different conditions: low voltage on or off.*

consumption of liquid nitrogen and operation time. The operation time varies up to one our between operating the system with low voltage turned on or off. The evaporation heat ΔQ_V and density ρ_{LN_2} of liquid nitrogen are: $\Delta Q_V = 198.6\frac{\mathrm{kJ}}{\mathrm{kg}}$ and $\rho_{LN_2} = 0.807\frac{\mathrm{kg}}{\mathrm{l}}$. Thus the LN_2-consumption ν_W expressed in Watt is given by: $\nu_W = \nu \cdot \Delta Q_V \cdot \rho$. The values for ν_W are also listed in table 4.1. Considering them, the applied low voltage is equivalent to an extra heat loss about 2 W which is related to the heat loss of the FETs (20 mW per channel, as each triple-cluster consists of 111 channels) in the cold part [JE08].

4.2 LN_2-consumption of ATC(3): The capton-cable-test

Two different sets of cables inside the cold part of ATC(3) have been tested for this consumption-measurement. The FETs in the cold part are linked through a cable harness with the feedthroughs to the warm part. The first set of cabling is used in all AGATA-triple-clusters and single cryostats so far. The characteristics of these cables are a low thermal conductivity but a rather high electrical conductivity. The second set of cabling consists of copper wires which are coated with capton (seef ig. 4.3). This new

Figure 4.3: *Second set of cable harness: copper wires which are coated with capton.*

cabling is considered to be more robust and reproduceable in production, in comparison to the old cabling. To see the different influence of the old or new cabling, the following issue has to be considered, namely: how does the new cabling influence the cooling of the detectors and their LN_2-consumption. The results related to this issue are described in the following section.

4.2.1 Setting up ATC(3)

The setup of ATC(3) was similar to the one of ATC(2), whereas a dewar closing with valve (see fig. 4.1) was used instead of a lead piece. ATC(3) was operated with preamplifier-voltage on. The first consumption-measurement has been performed with the old cabling for all three crystals, whereas the second measurement was done with the capton-cabling for all three crystals.

4.2.2 Results: ATC(3)

The results of both capacitive measurements are displayed in diagram a) of fig. 4.4. Both curves have a different maximum capacity $C(t = 0)$ which is related to a different filling height at the beginning of each measurement. For that reason the orange curve has been shifted by $\delta C = 14\,\mathrm{pF}$ with respect to the y-axis (see diagram b) in fig. 4.4). Both curves have a different gradient, caused by a higher LN_2-consumption of the capton cable harness. The measured data

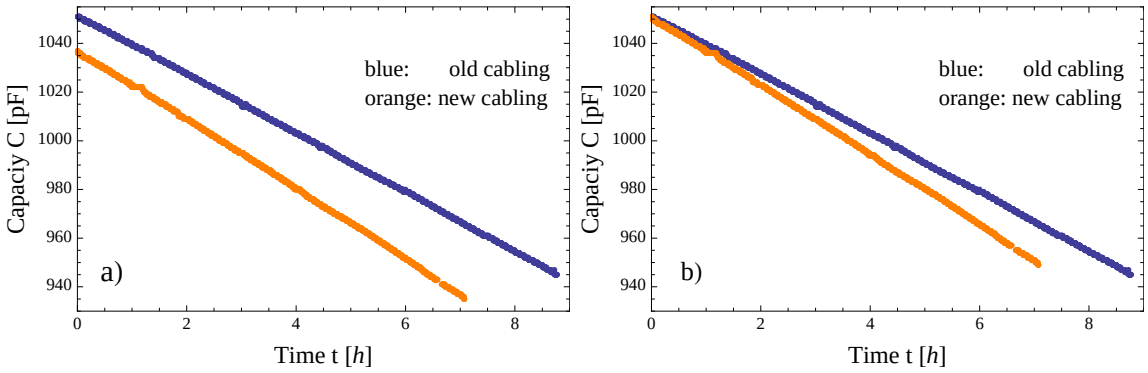

Figure 4.4: *Measured LN_2-consumption for ATC(3).* **a)** *Measured capacity C for the new and old cabling.* **b)** *The orange curve is shifted by $\delta C = 14\,\mathrm{pF}$ with respect to the y-axis.*

is fitted equation 4.1[2] and therefore the consumption is given by:

$$\nu = m_C \cdot \frac{4.5\,\mathrm{l}}{\Delta C} \tag{4.5}$$

ΔC is the difference between the maximum and minimum capacity of the dewar. This was already determined in chapter 3 to be: $\Delta C = (133 \pm 5)\,\mathrm{pF}$. The operation time τ can be determined by using:

$$\tau = \frac{4.5\,\mathrm{l}}{\nu} = \frac{\Delta C}{m_C} \tag{4.6}$$

[2]The measured filling heights and a linear regression of them are shown in appendix B

Cabling	ν_C[ml/h]	ν_W[W]	τ[h]
old cabling	414 ± 16	18.43 ± 0.71	10.9 ± 0.4
Capton	489 ± 19	21.77 ± 0.85	9.2 ± 0.4

Table 4.2: *Consumption value ν, ν_W and operation time τ for the two different cabling-setups.*

Table 4.2 shows the measured consumption values for the two different cabling-sets. The measured operation time for ATC(3) being equipped with the old cabling is consistent with the measured operation time of ATC(2) being operated with low voltage. Considering the 2 W heat loss due to operating the FETs, points out that the capton cabling causes an extra heat loss of 3.34 W.

4.2.3 Vacuum-leak in ATC(3)

Further tests with ATC(3) being equipped with the capton-cabeling inside could not be done because the detector got warm. Fortunately the LN_2-consumption was measured before the warm up, as the detector was linked to the filling system and a filling period of 8 hours was used. Diagram a) of figure 4.5 shows the measured capacity $C(t)$ as a function of time. The slope of each curve is changing by time which is only reasonable for an indifferent consumption of liquid nitrogen.

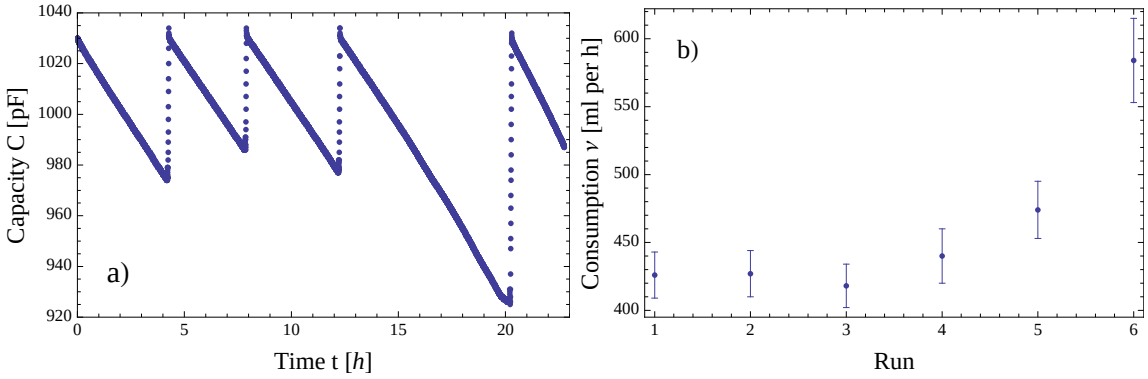

Figure 4.5: **a)** *Measurement of the capacity C of ATC(3) equipped with capton-cabeling. The slopes of the curves differ as a function of time, indicating a change in the* LN_2*-consumption.*

Each slope has been fitted by equation 4.1 and the consumption was calculated by using equation 4.5. The results of this procedure are displayed in diagram b) of fig. 4.5, where ν is plotted with respect to each measuring run. The consumption varies slightly around 425 $\frac{\text{ml}}{\text{h}}$ during the first three runs, but increases after the third run up to 585 $\frac{\text{ml}}{\text{h}}$. Thus an instability of the consumption appeared during the measurement which caused a variation of ν about 38 %.

What happened?

An increased consumption value is in most cases related to a thermal contact between endcap and the interior of the detector or to a vacuum leak, such as a broken feedthrough, which actually happened to ATC(3). As a consequence the pressure inside the cryostat and the consumption of LN_2 increased. Furthermore, the outer endcap was cooled and its temperature fell below the dew point and therefore the whole detector got wet at the surface (see fig. 4.6). The pressure inside the cryostat increased due to the broken feedthrough from

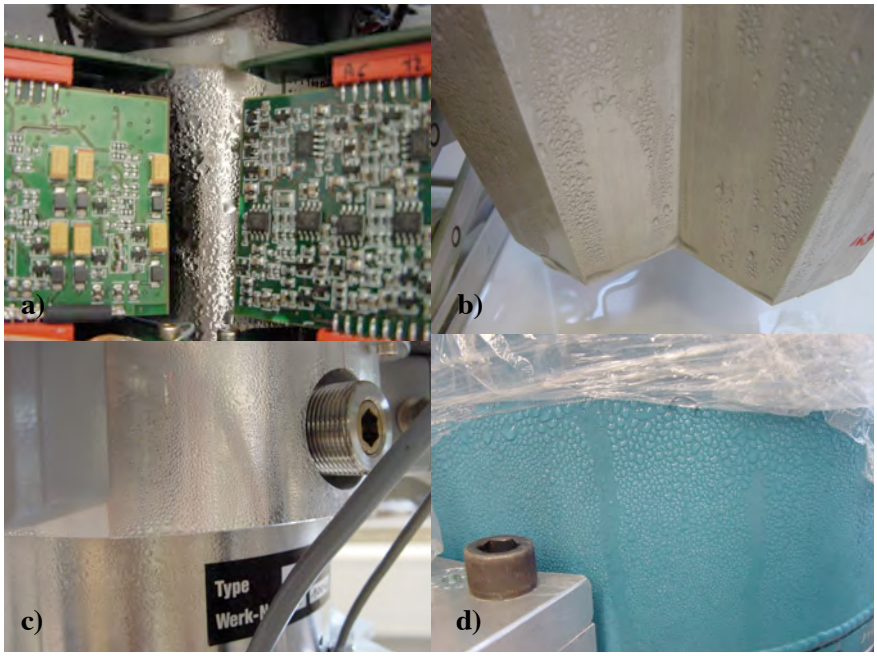

Figure 4.6: *Status of ATC(3) after the vacuum broke.* **a)** *Flange near the warm preamplifier is covered with water.* **b)** *The endcap is totally wet. A temperature of* 12 °C *(which is below the dew point) has been measured in some regions.* **c)** *The flange near the high voltage feedthrough got also wet.* **d)** *The dewar was covered with water and had a temperature of* 14 °C.

10^{-7} mbar to 10^{-4} mbar. As a consequence, the cabling has been changed back to the old cabling and the broken feedthroughs were repaired.

4.3 LN_2-consumption of ATC(4)

Considering the results gained in the previous sections, the question arose, how the consumption ν of the cryostats reacts to different loads (e.g. low voltage, different cabeling, change in electronics). The change in the LN_2-volume is given by:

$$V(t) = -\nu \cdot t + V_0 \tag{4.7}$$

$\nu \cdot t$ is the amount of liquid nitrogen which is needed to keep the detector at a certain temperature at the time t. Figure 4.7 shows the schematic drawing of an AGATA-cryostat which is treated as ideal for simplicity. A heat loss through the copper-rod or thermal coupling with the environment are neglected. The crystal with temperature T_1 is linked by the copper-rod with the LN_2-reservoir with temperature T_2. The system reaches a steady state after a certain time, so

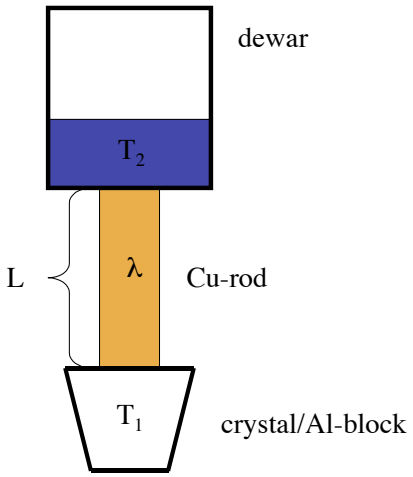

Figure 4.7: *Schematic drawing of an AGATA-cryostat. The dewar is linked by a copper-rod (cooling finger) with the Ge-crystal, or Aluminium-block in the case of ATC(4). The dewar with liquid nitrogen inside has the temperature T_2, whereas the crystal/Al-block has the temperature $T_1 > T_2$. The copper-rod has the length L and thermal conductivity λ.*

that a constant amount of heat is floating through the rod from the crystal to the dewar [Dem04]. Despite the temperature difference $T_1 - T_2$, this heat flow depends on the length L, the sectional area A and the thermal conductivity λ of the copper rod [Dem04]:

$$\frac{dQ}{dt} = (T_1 - T_2) \cdot \frac{\lambda \cdot A}{L} \tag{4.8}$$

As the LN_2-reservoir is constantly heated by $\frac{dQ}{dt}$, the consumed amount of liquid nitrogen per time is given by:

$$\Delta Q_V \cdot \rho_{LN_2} \cdot \nu = \frac{dQ}{dt} \Leftrightarrow \nu = (T_1 - T_2) \cdot \frac{\lambda \cdot A}{\Delta Q_V L \rho_{LN_2}} \tag{4.9}$$

As ρ_{LN_2} is the density, ΔQ_V the evaporation heat and ν the consumption of liquid nitrogen. In this simplified model the consumption of liquid nitrogen depends on the temperature T_1 of the crystals and the characteristics of the cooling finger. Since $\frac{dQ}{dt}$ is constant, the amount of heat P_{in} which is induced into the cooling finger is equal to equation 4.8. Thus the consumption of liquid nitrogen is given by:

$$\boxed{\nu = \frac{1}{\Delta Q_V \rho} \cdot P_{in}} \tag{4.10}$$

4.3.1 Setting up ATC(4)

For the purposes mentioned above, the cryostat of ATC(4) (picture a) fig. 4.8) has been equipped with three aluminium blocks (picture b) fig. 4.8) and a caddock (picture c) fig. 4.8). In principal a caddock is a resistor which creates heat when voltage is applied. A caddock is used for annealing a cryostat which needs to be done when the getter is saturated after several cooling-in-processes or a long operation-time. The getter is heated by the caddock and starts gasing

out. Hence the cryostat has to be pumped in order to get the gas molecules out of the system. If P is the heating power of the caddock, the injected heat per time yields for:

$$P_{in} = \kappa \cdot (P + P_0) \tag{4.11}$$

The factor κ determines how much heat radiation produced by the caddock is injected into the cooling-finger and heats the LN_2-reservoir. κ depends on the heat-conductivity of the copper rod and the surrounding material, such as the aluminium blocks, the attachment for the crystals etc. P_0 is the amount of heat which is frequently emitted by the material attached at the cooling finger. Thus the liquid nitrogen consumption as a function of the applied heating power is given by:

$$\nu(P) = m \cdot P + \nu_0 \tag{4.12}$$

As $m = \frac{\kappa}{\Delta Q_V \cdot \rho}$ and $\nu_0 = \frac{\kappa P_0}{\Delta Q_V \rho}$. The caddock has been fixed directly on the cooling finger (picture d) fig. 4.8) in order to measure the influence of the applied heating power on the consumption. Apart from the aluminium blocks

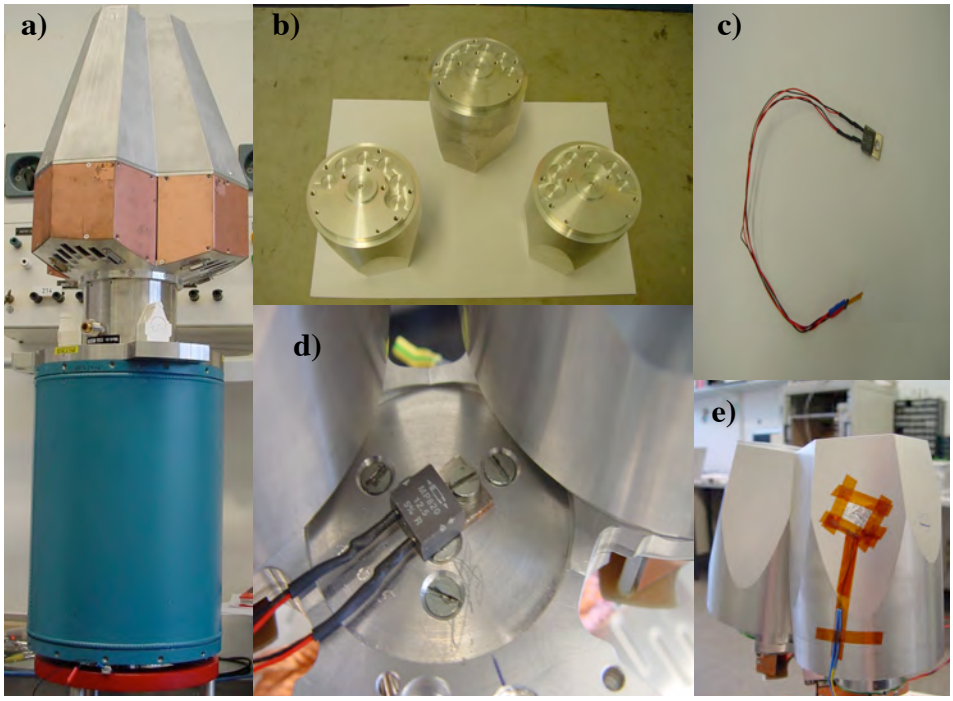

Figure 4.8: **a)** *The cryostat of ATC(4), equipped with no crystals and no electronics inside.* **b)** *Three asymmetrical aluminium blocks of A, B and C-type. Each block has a mass of* $m_{block} = 1.6\,\text{kg}$. **c)** *Caddock with a resistance of* $R = 13\,\Omega$. **d)** *The caddock been mounted directly onto the cooling finger and between the aluminium blocks.* **e)** *In order to check the temperature a PT100-sensor has been fixed on the outside of a block.*

and the caddock a PT100-sensor has also been fixed on one block (picture e) fig. 4.8) so that the temperature inside the cryostat could be checked. Again the capacity has been read out with measuring device I. The caddock was biased with a standart power supply unit, which can be seen in fig. 4.9.

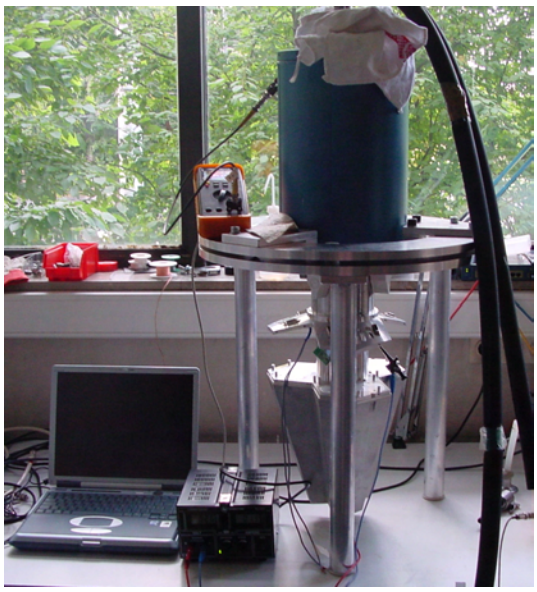

Figure 4.9: *The cryostat of ATC(4) is equipped with aluminium blocks inside and plugged to the automatic filling system. The caddock is linked to an external power supply unit (black box) and the capacity is read out by using measuring device I.*

4.3.2 Cooling-in ATC(4)

After preparing the system for the consumption-measurement, the cryostat was cooled in and directly linked to the automatic filling system. The consumption was measured over two filling periods. Figure 4.10 shows the results of this measurement. Diagram a) displays the measured capacity as a function of time. The slope of $C(t)$ is changing by time which indicates a change of the consumption ν. Diagram b) of fig. 4.10 displays the measured consump-

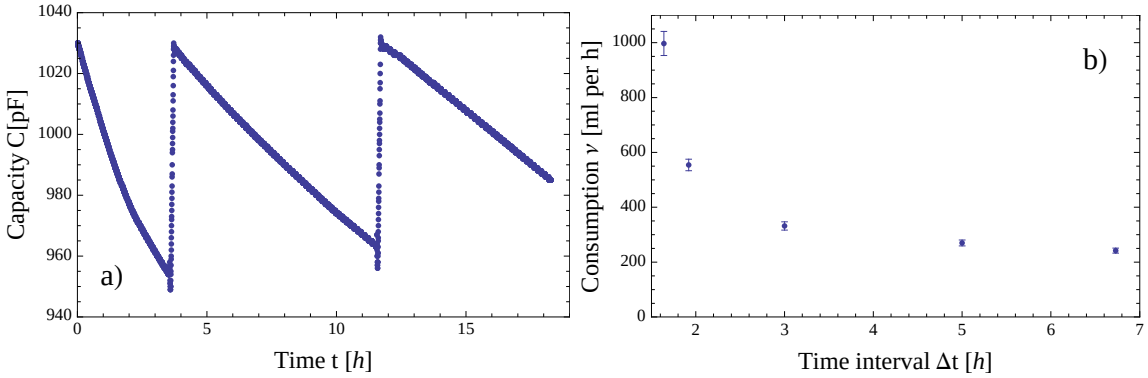

Figure 4.10: **a)** *Measured capacity $C(t)$ as a function of time during one filling cycle. The curves are changing within one period of 8hours.* **b)** *Measured LN_2-consumption after cooling in ATC(4) as a function of the time intervals in which the consumption did not change.*

tion ν of liquid nitrogen as a function of time. According to equation 4.9 the consumption of liquid nitrogen is direct proportional to the difference $T_1 - T_2$ between the temperature T_2 inside the dewar and the temperature T_1 of the whole material which is attached at the cooling finger. The temperature T_2 is constant, whereas T_1 is changing by time after cooling in. Thus the consumption ν changes as long as T_1 is not constant. Considering a one dimensional

heat flow inside the copper rod, the change of T_1 as a function of time is given by [Dem04]:

$$\frac{\partial T_1}{\partial t} = \frac{\lambda}{c \cdot \rho_{rod}} \cdot \frac{\partial^2 T_1}{\partial x^2} \tag{4.13}$$

λ is the heat conductivity, ρ_{rod} the density and c the heat capacity of the copper rod. Thus the temperature T_1 changes as longs as the temperature gradient inside the cooling finger is not constant. The condition $\frac{\partial T_1}{\partial t} = 0$ (steady state) is prerequisite for equation 4.8.

4.3.3 Results of the consumption tests

The capacity has been measured during one filling-cycle (see section 4.3.1) and each measurement lasted 22 h. The heating power was changed for each measurement by biasing the caddock with different voltages. One run is shown in fig. 4.11 where the heating power is $P = 2W$. Each curve has been fitted by

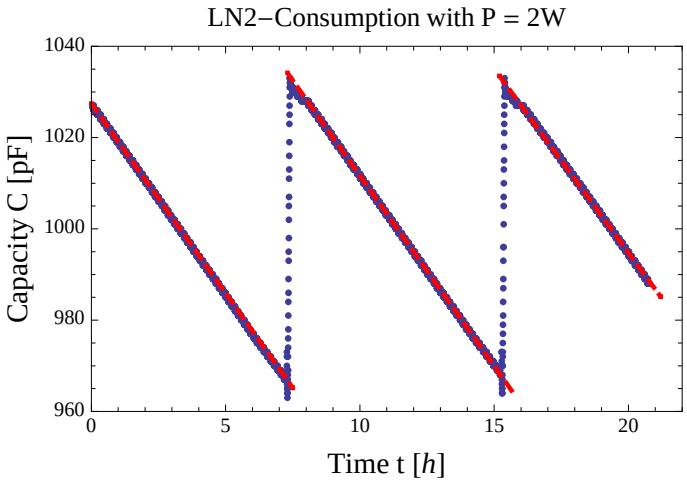

Figure 4.11: *LN_2-consumption for $P = 2W$. The three slopes result from the filling-system, which fills the detector every 8h. The red dashed lines indicate the linear fit to each curve.*

a linear regression: $C = m_C \cdot t + b_C$ therefore three values of $m_{i,C}$ are obtained with an average:

$$\bar{m}_C = \frac{1}{3} \cdot \sum_{i=1}^{3} m_{i,C} \tag{4.14}$$

and its standard deviation. This causes the consumption:

$$\nu = \frac{\bar{m}_C}{\Delta C} \cdot 4.5l \tag{4.15}$$

for one P-value. This has been repeated for several heating powers. At first the power was increased in 0.5 W-steps until 3 W and after that in 1 W-steps until a maximum of 7 W. The curves of the other measurements are listed in appendix B. The measured consumption as a function of the applied heating loss is displayed in figure 4.12. As expected from equation 4.12, the consumption $\nu(P)$ is strictly linear in P. The fitted function was found as:

$$\nu(P) = (27.66 \pm 1.05) \cdot 10^{-3} \frac{l}{Wh} \cdot P + (0.241 \pm 0.004) \frac{l}{h} \tag{4.16}$$

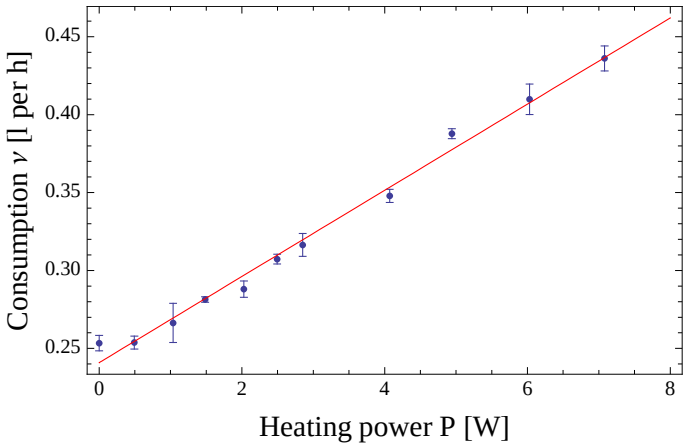

Figure 4.12: *Results of the consumption-measurement with ATC(4). The consumption $\nu(P)$ is a linear function of the applied heating loss P.*

The axis intercept $\nu_0 = 0.241\frac{l}{h}$ is related to the cryostat with aluminium blocks inside but without any extra heating power applied. The consumption ν_0 differs for each detector system, when the configuration of the cold part (e.g. cabeling, amount of crystals etc.) is different. Multiplying equation 4.16 with $\Delta Q_V \cdot \rho_{LN_2}$ leads to the consumption ν_W expresses in Watt:

$$\underline{\nu_W(P) = (1.23 \pm 0.05) \cdot P + (10.73 \pm 0.18)\,\mathrm{W}} \tag{4.17}$$

According to equation 4.10 and 4.11, the consumption ν_W is given by: $\nu_W = \kappa \cdot (P + P_0)$. Thus the factor κ measured in this experiment is given by: $\kappa = (1.23 \pm 0.05)$. This result is surprising, since κ is larger than 1 which means more heating power than produced by the caddock is injected into the cooling finger. This is only reasonable if a thermal radiation emitted from another source inside the cryostat is considered.

Chapter 5

The LN_2-read-out (II): A capacitive preamplifier

Up to now all capacitive measurements were performed by measuring the filling capacity directly with a multimeter which was read out by a PC. Since the variations of the measured capacities are of 12 %, a high accuracy of the read out is needed. This implies that the read-out-device itself does not influence the measuring capacity. Measuring device (I) however does not fulfill this condition, because the BNC-cable which links the multimeter with the capacitive read-out of the dewar has an own capacity $C_{BNC} = 150\,\text{pF}$. This capacity is in the same range as the variation between C_{min} and C_{max}. Moreover the measured capacity is shifted by C_{BNC} with respect to the „real“filling capacity of the system. Apart from this, the measured capacity is also influenced by the adjusted measuring-range of the multimeter. Figure 5.1 shows a capacitve measurement which has been performed with measuring device (I). The two horizontal lines (marked by red circles) refer to capacity values which have not been measured but written by the program which reads out the multimeter. Thus all measured data which has been taken with device (I) has to be corrected by those unwanted values.

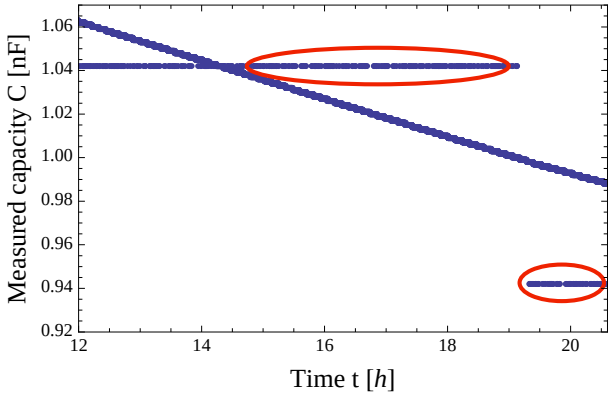

Figure 5.1: *Result of a capacitive measurement with ATC(2). The measured capacity C runs linear with respect to the time t. The horizontal data-points which are marked with red circles do not refer to the measured capacity, as they result from the PC-read-out-software. The program wrote frequently some extra capacity values of $C = 1042\,\text{pF}$ and $C = 942\,\text{pF}$ into the measured data.*

In order to avoid all these problems a LN_2-read-out-device is needed which meets the following conditions:

- Measuring the capacity C and amplifying it
- Converting the measuring capacity into a signal which can be easily read

out and is independent of further read-out-devices (e.g. BNC-cabling, range of multimeter)

- Sensitive to capacity changes in the range of 12 %
- Compact in size
- The device should be supplied with the warm and cold amplifier's low voltage
- A DC-operator, such that the detector electronics is not disturbed by measuring the capacity C

Such a device has been developed by Gheorghe Pascovici and is realised by a capacitive preamplifier.

5.1 The capacitive preamplifier

The basic principle of the LN_2-read-out-device (II) is measuring the difference ΔC between the measuring capacity C_m and a fixed reference capacity C_r, instead of measuring the filling capacity C_m over the full range of 1000 pF. Thus this device is more sensitive to small changes of C_m which are typically about 12 %. The reference capacity C_r has been set to $C_r = \frac{1}{2} \cdot (C_{m,max} + C_{m,min})$, as $C_{m,max}$ is the measured maximum filling capacity and $C_{m,min}$ the minimum capacity respectively.

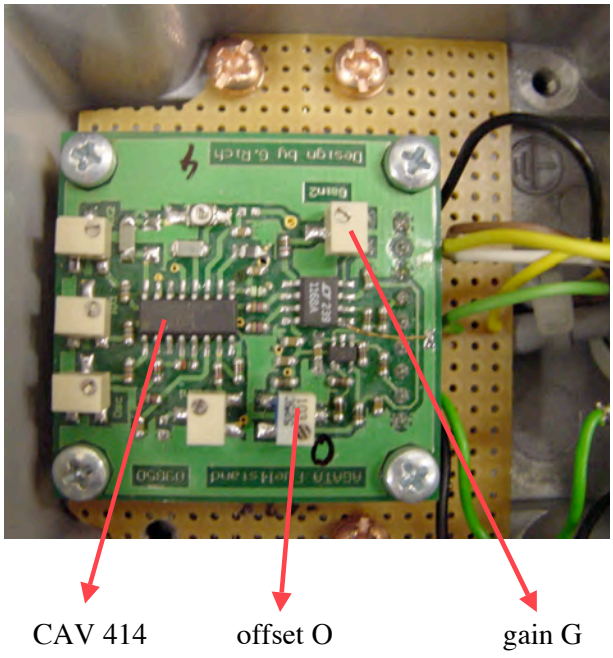

Figure 5.2: *Capacitive* LN_2*-read-out-device developed by the electronic workshop at IKP Cologne. The CAV 414 converts the measuring capacity into a voltage. The gain G and offset O of the final output signal are adjustable.*

The output signal of the LN_2-read-out-device is a direct-voltage signal which can be manipulated by an adjustable gain G and offset O (see fig. 5.2) and therefore set to defined values. Figure 5.2 shows a photograph of the LN_2-read-out-device which converts the measuring capacity C_m into a voltage U_m. The circuit diagram of this device is displayed in fig. 5.3. The conversion of the filling capacity into a DC-voltage is predominantly done by an analogue measuring device called CAV414 (developed by Analog Microelectronics). The working principle of this device can be seen on [Gmb08] in detail. But the main and basic aspects are discussed in the following section.

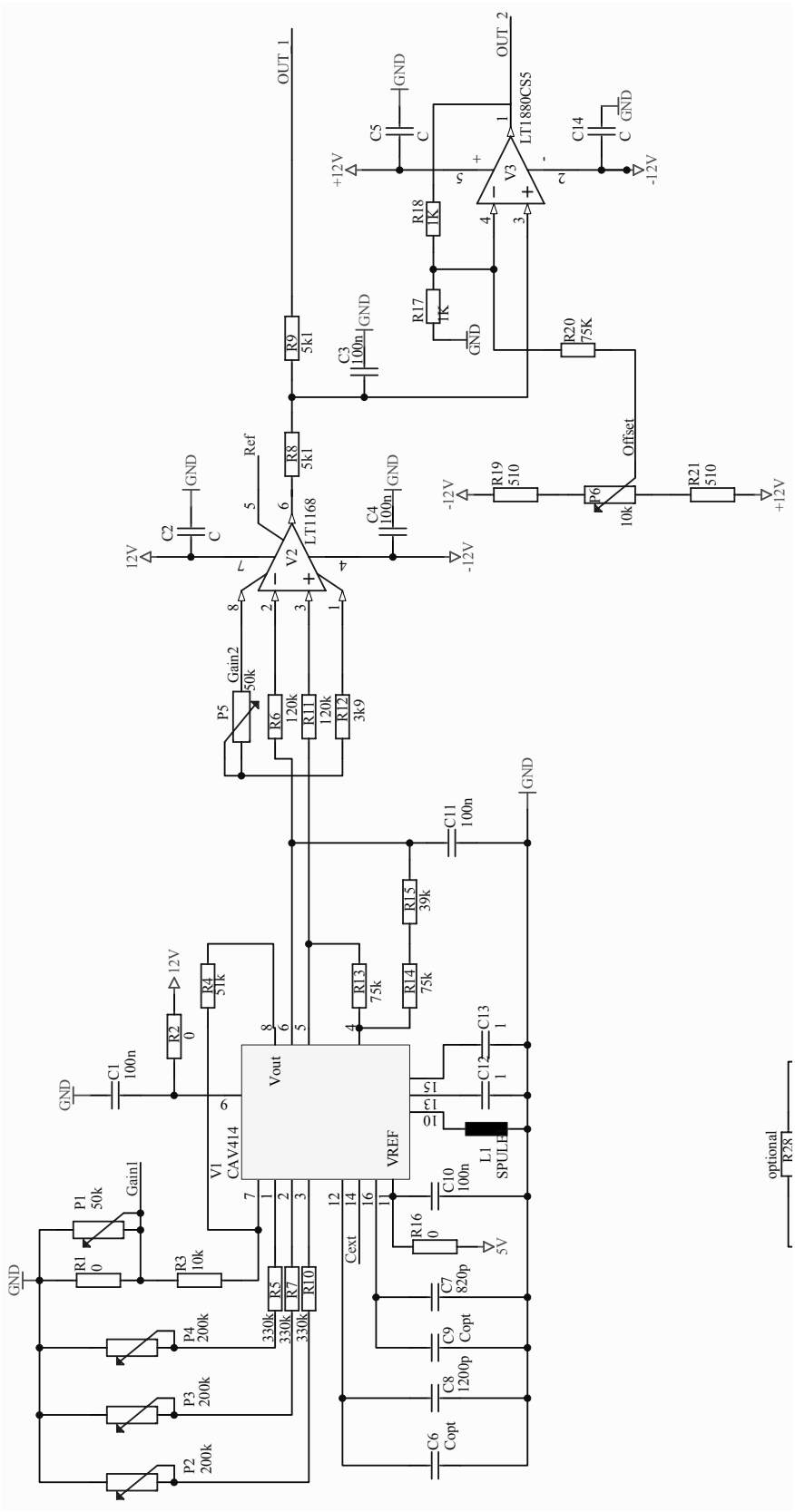

Figure 5.3: *Circuit diagram of the* LN_2*-read-out-device designed at IKP Cologne. The potentiometer P5 (Gain 2) and P6 (Offset) are the adjustable gain and offset as shown in fig. 5.2.*

5.1.1 The CAV414

The CAV414 is a capacity/voltage transducer with an adjustable output voltage. A reference oscillator drives two identical integrators, as one is equipped with the reference capacity C_r and the other one with the measuring capacity C_m respectively (see fig. 5.4). The output signals of each integrator are subtracted from each other, as their amplitude depends on C_r and C_m respectively. This difference signal is filtered and amplified several times so that the output signal is a DC voltage which is proportional to $\Delta C = C_m - C_r$ [Gmb08]. A triangular wave oscillator is in principle realised by the combination of a

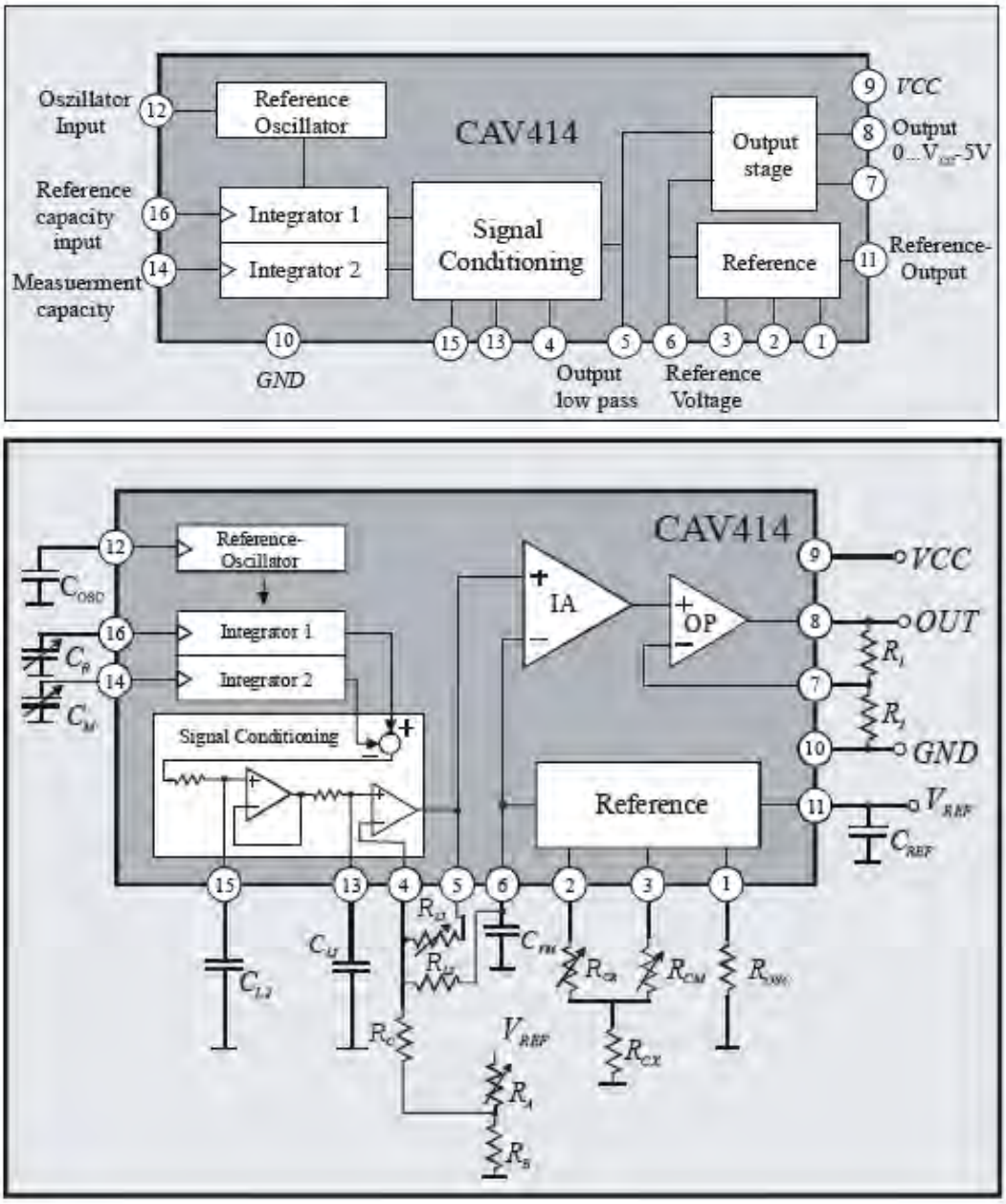

Figure 5.4: **Top:** *Working principle of the CAV414 [Gmb08].* **Bottom:** *Functional diagram of the CAV414 for a constant oscillator frequency $f_{osc} = const$ [Gmb08].*

Schmitt Trigger and an Integrator. Since the filling capacity C_m is measured with respect to the cryostats ground, this method is not favourable. For this reason the oscillator used here consists of a constant current source which

charges/ discharges a grounded capacitor C by the constant currents $+I/\ -I$ (see fig. 5.5). If the capacitor is directly charged by the constant current $-I$

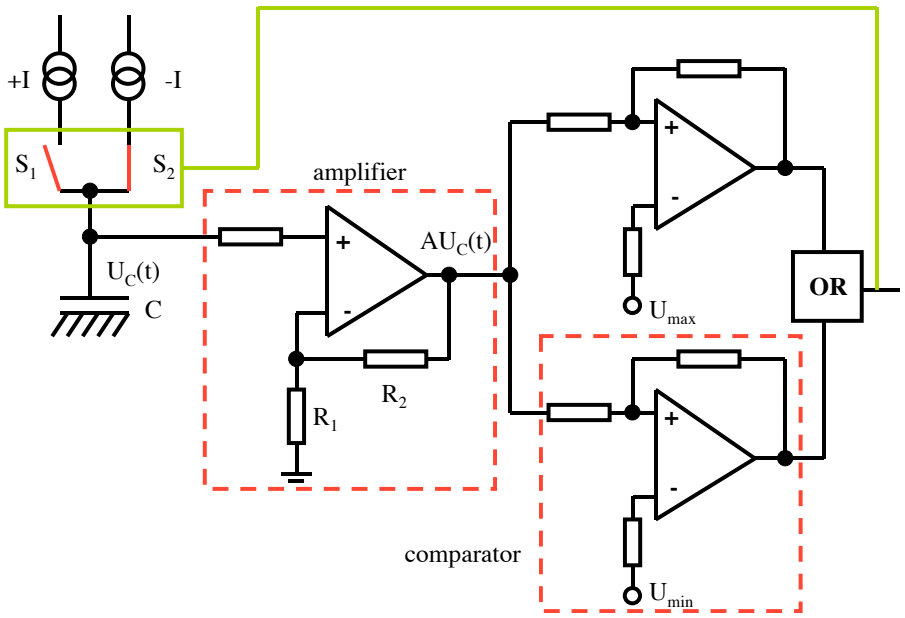

Figure 5.5: *Simplified circuit-diagram of an oscillator (design by G.Pascovici).*

for example, the voltage $U_C(t)$ after a time t at the capacitor is given by:

$$U_C(t) = \frac{1}{C} \cdot Q(t) = -\frac{1}{C} \cdot I \cdot t \tag{5.1}$$

The voltage decreases linearly as a function of time t. This voltage signal passes a non-inverting amplifier and is amplified by the factor $A = \left(1 + \frac{R_2}{R_1}\right)$. The output $A \cdot U(t)$ is injected into two identical comparators with different threshold-voltages U_{min} and U_{max}. A comparator switches between two fixed voltages $\pm U_0$ depending on the polarity of the difference-signal $U_{in} - U_{trsh}$ as U_{trsh} is the threshold-voltage. A positive polarity of $U_{in} - U_{trsh}$ leads to $+U_0$ whereas a negative polarity leads to $-U_0$ [EH05]. The lower comparator in fig. 5.5 switches if the input voltage is $AU_C(t) < U_{min}$, whereas the upper comparator switches for $AU_C(t) > U_{max}$. Both comparator signals drive through an OR-gatter the switches S_1 and S_2. Considering the example displayed in fig. 5.5, switch S_2 opens if $AU_C(t)$ is below U_{min} and the switch S_1 is closed. The capacitor is now charged by $+I$. If $U_C(t)$ exceeds U_{max}, switch S_1 is opened and S_2 closed respectively. The output signal of such a device is a triangular wave (see diagram a) of figure 5.6). The frequency of this signal is found by using equation 5.1:

$$U_{max} = \frac{1}{C} \cdot I \cdot \frac{T}{2} + U_{min} \Leftrightarrow \tag{5.2}$$

$$f = \frac{I}{2 \cdot (U_{max} - U_{min}) \cdot C} \tag{5.3}$$

Thus the frequency f_{osc} of the reference oscillator is determined by its capacity C_{osc} and the constant current I_{osc}. The two integrators are working in much the same way as the reference oscillator (see fig. 5.5), whereas the integrators are not equipped with two comparators (like the oscillator in fig. 5.5). The

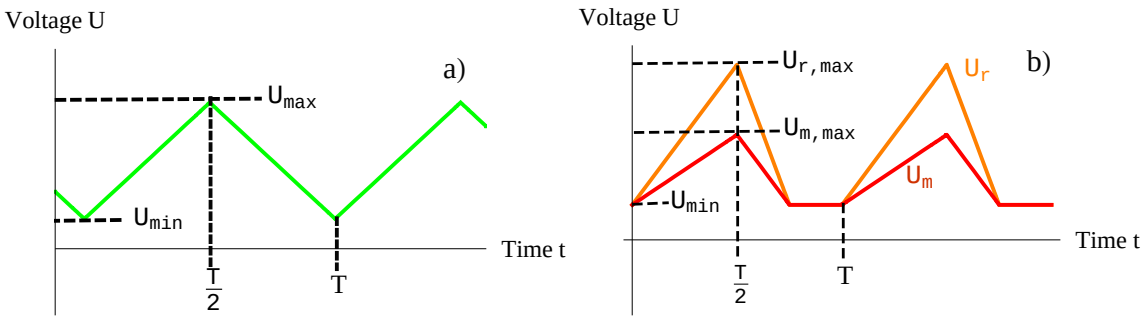

Figure 5.6: **a)** *Output signal of the reference oscillator with period T, maximum amplitude U_{max} and minimum amplitude U_{min}.* **b)** *Output signals U_r and U_m of the two integrators which have the same period T as the reference oscillator.*

constant current sources of each integrator is driven phase locked and clock synchronised by the reference oscillator instead [Gmb08]. This feature ensures that the output signals of both integrators are not shifted to each other and have exactly the same frequency. Another characteristic of the integrators is that the discharging current is twice of the charging current. Thus the ratio between the charging time t_{charge} and discharging time $t_{discharge}$ of the capacitor is given by: $t_{charge} = 2 \cdot t_{discharge}$ [Gmb08]. The minimum voltage of each integrator is set to a fixed value of $U_{min} = 1.2\,\mathrm{V}$ [Gmb08]. The maximum output voltages of both integrators are given by:

$$U_{m,max} = \frac{I_m}{2 \cdot f_{osc} \cdot C_m} \tag{5.4}$$

$$U_{r,max} = \frac{I_r}{2 \cdot f_{osc} \cdot C_r} \tag{5.5}$$

I_m is the charging current of the integrator with capacity C_m and I_r the charging current of the integrator with C_r respectively. Diagram b) of fig. 5.6 displays the output signals of the integrators. In a next step both triangular signals U_r and U_m are subtracted from each other which leads to the difference signal $\Delta U_{rm} = U_r - U_m$. This signal is filtered by an active lowpass and amplified (see fig. 5.4) which leads to the DC-signal U_{LPOUT} at pin no. 5 [Gmb08]:

$$U_{LPOUT} = \left(1 + \frac{R_{L1}}{R_{L2}}\right) \cdot \frac{3}{8} \cdot \Delta U_{rm,filtered} \tag{5.6}$$

The DC-voltage U_M at pin 6 (pin out of the CAV414 see appendix C) is subtracted from equation 5.6: $U_{LPOUT} - U_M$. This signal is amplified by an instrumentation and operational amplifier (see functional diagram in fig. 5.4). The instrumental amplifier has a fixed gain $G = 5$, whereas the gain of the operational amplifier is determined by the two resistors R_1 and R_2. This leads to the output voltage [Gmb08]:

$$U_{out} = 5 \cdot \left(1 + \frac{R_1}{R_2}\right) \cdot \left[U_{LPout} - U_M\right] \propto C_m - C_r \tag{5.7}$$

The resistors R_1, R_2, R_{L1} and R_{L2} are adjustable and change the amplitude of U_{out}. U_M is an adjustable DC-potential. Considering the circuit diagram shown in fig. 5.3 the resistors R_{L1} and R_{L2} are realised by $R_{L1} = 75\,\mathrm{k\Omega}$ and $R_{L2} = (75 + 39)\,\mathrm{k\Omega}$. The amplification through the resistors R_1 and R_2 is

realised in the circuit diagram by the potentiometer P1, the resistor $R3$ and $R4$.
The CAV414 might be operated in two different configurations [Gmb08]:

1. The load currents I_r and I_m are selected as constant, thus the oscillator frequency f_{osc} has to be adjusted.

2. The oscillator frequency f_{osc} is constant and the load currents I_r and I_m are functions of the resistors R_{CM} and R_{CR}.

The second method is realised in the LN_2-read-out-device, since the potentiometers P2, P3 and P4 are used for adjusting the currents I_r, I_m and I_{osc}.

5.1.2 Further signal processing

The circuit diagram in fig. 5.3 shows that the output voltage U_{out} of the CAV414 is connected to pin 7 (as indicated by the functional diagram) but not read out. Instead of that, the voltages U_{LPOUT} and U_M are plugged into an instrumentation amplifier namely LT1168. The pin out of this device is shown in fig. 5.7. The voltages U_{LPOUT} and U_M are connected to pin 2 and 3. The resistor R_G is realised by the resistor $R12$ and the potentiometer P5 (Gain 2) as shown in the circuit diagram.The final output gain is given by [Tec00]: $G = (49.4\,\mathrm{k\Omega}/\mathrm{R_G}) + 1 = (49.4\,\mathrm{k\Omega}/(\mathrm{R12} + \mathrm{R_{P5}}) + 1$. This adjustable gain is indicated by the black circle in fig. 5.2. In a last step, the output voltage of the LT1168 is connected to a non-inverting amplifier (LT1880CS5). The inverting input of this device is connected to an adjustable offset-voltage (potentiometer P6 in fig. 5.3). This adjustable offset is also indicated by a black circle in fig. 5.2. The final output voltage of the LN_2-read-out-device is taken at the output OUT 2 and is a function of the measuring capacity C_m, the gain G (adjusted by potentiometer P5) and the offset O (potentiometer P6).

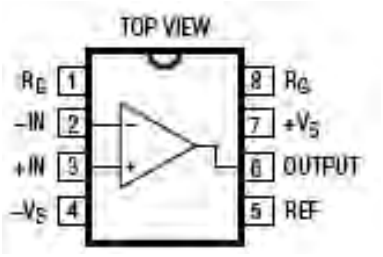

Figure 5.7: *Pin out of the LT1168 instrumentation amplifier. The output gain of this amplifier is determined by only one external resistor R_G [Tec00].*

5.1.3 First tests with the prototype

A first prototype of a LN_2-read-out-device (see fig. 5.8) has been tested at ATC(4) being in vertical position. The results of this measurement are displayed in diagram a) of fig. 5.8. The slope of the measured curve is not linear in time as expected. The capacity C_{BNC} of the BNC-cable was not considered when adjusting the measuring range of the prototype therefore the device is not detecting the filling capacity in a proper way. Nevertheless the LN_2-read-out-device is working since the curve in diagram a) is linear for capacities which are in the range of $780 - 880\,\mathrm{pF}$. Diagram b) in fig. 5.8 shows a plot of the device-output versus the filling capacity which has been corrected by C_{BNC}. The red curve in this diagram is a linear regression $U(C) = m \cdot C + b$ through the data points. The prototype was also used for a position-dependent

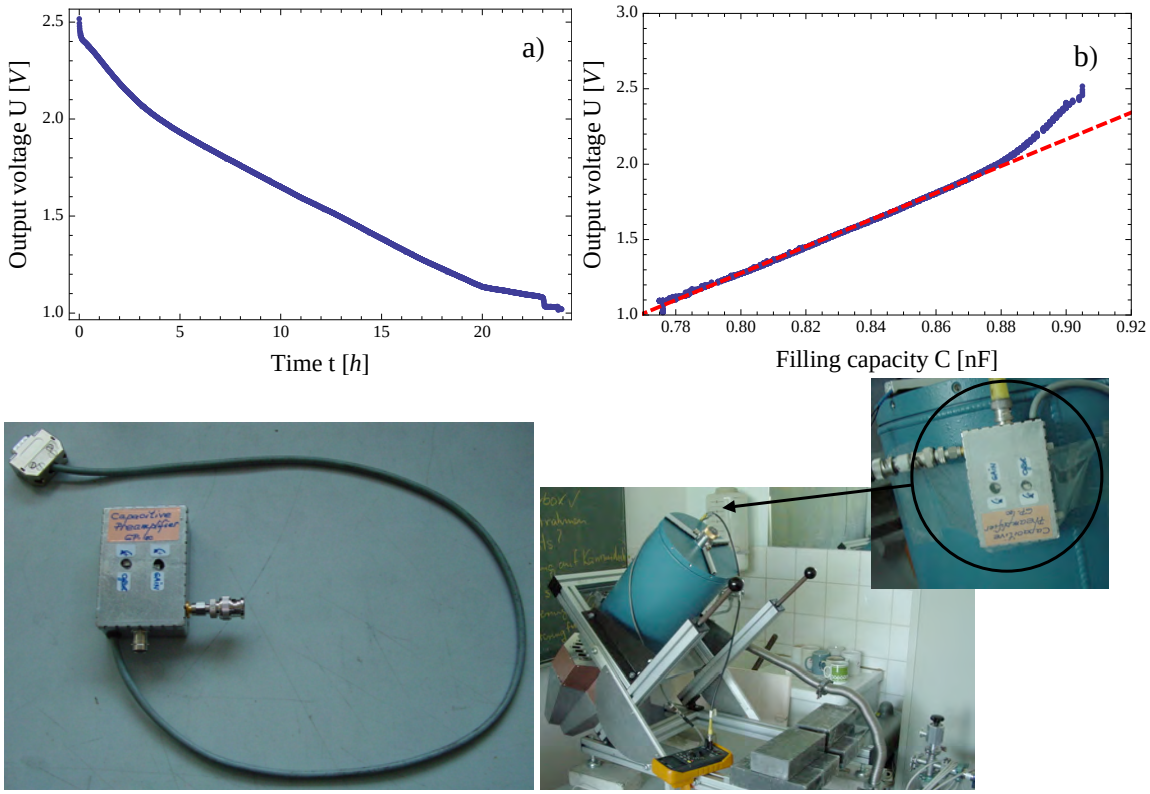

Figure 5.8: **a)** *Results of the filling capacity measurement at ATC(4) performed with a prototype of the* LN_2*-read-out device.* **b)** *Plot of the devices output U versus the measuring capacity C of ATC(4). The red line is a linear regression* $U(C) = mC + b$ *through the measured data.* **Down left:** *Photo of the prototype which is equipped with an BNC-input, an SMB-outbut and a voltage supply. Gain and offset of the device are adjustable by two potentiometers.* **Down right:** *ATC(4) inclined by the angle* $\theta = 45\,^{\circ}$*. The read-out-device is fixed onto the dewar. The results of this measurement are shown and discussed in chapter 6.*

capacity measurement as displayed in fig. 5.8. The results of this measurement will be discussed in chapter 6.

5.2 The LN_2-read-out-box

After testing the prototype successfully another four read-out-devices (boxes) were produced (see fig. 5.9). One of the four devices is shown in fig. 5.9. Each device has an SMA-input for reading in the measuring capacity and a BNC-ouput for reading out the voltage. The boxes are supplied by the preamplifier-low-voltage. Every box has two potentiometers (see fig. 5.2) for adjusting the gain G and offset O of the output signal. The offset can be varied in a range of $0 - 10\,\mathrm{V}$. The influence of these two parameters on the output-signal of a

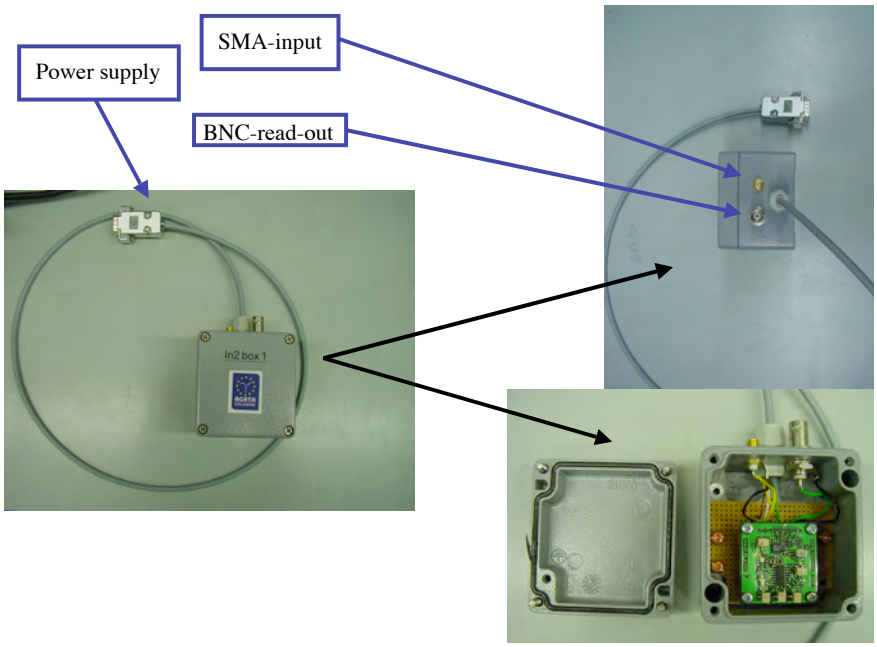

Figure 5.9: LN_2*-read-out-box. The housing is very robust and water resistent. This feature is important, because it will protect the electronics inside against an unwanted contact with liquid nitrogen.The whole electronics of this device can be seen in the down right corner of this figure.*

LN_2-read-out-device is briefly discussed in the following section.

5.2.1 Characterising the LN_2-read-out

The output of each device depends on the measuring capacity C (The index m is neglected for simplicity.) and the two parameters gain G and offset O namely (see fig. 5.10). Therefore it is convenient to calibrate each device on the basis of a defined basic setting, such as $G = 1$ and $O = 0$. This setting leads to the output voltage:

$$U(G = 1, O = 0, C) := m_0 \cdot C + b_0 = U_0 \tag{5.8}$$

Diagram a) of fig. 5.13 displays the output voltage U_0 of box no.2. This measurement was done by using a capacitive dummy which is able to simulate test-capacities from 888 pF to 1030 pF. A change of gain and offset leads to

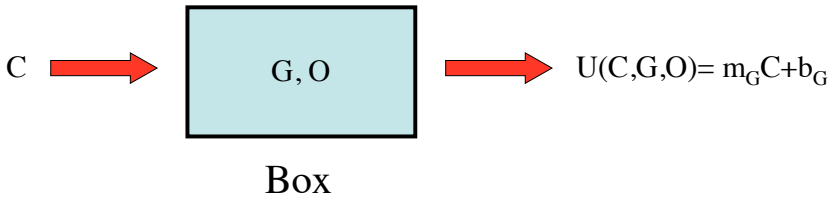

Figure 5.10: *Schematic drawing of a read-out-device. The output voltage $U(C, G, O)$ is a function of the adjustable gain G, offset O and the input capacity C.*

a change of the output from U_0 to $U(G \neq 1, O \neq 0, C)$. Moreover, the order of adjusting the gain and offset is important, which is shown by the following equations:

$$U'(C) = G' \cdot U_0 + O \tag{5.9}$$
$$U(C) = G \cdot [U_0 + O] \tag{5.10}$$

Adjusting the gain first and the offset after that is described by equation 5.9, whereas the reverse case is described by equation 5.10. The relation between G and G' is given by:

$$G' = \left(\frac{O}{U_0} + 1\right) \cdot G + \frac{O}{U_0} \tag{5.11}$$

This equation simplifies if $O = 0$. All calibrations of the boxes were done by considering equation 5.10. Thus the output voltage of a box with adjusted gain G and offset O is given by:

$$U = G \cdot [U_0 + O] = m_G C + b_G \tag{5.12}$$

Introducing the ratios $\alpha := \frac{m_G}{m_0}$ and $\gamma := \frac{b_G}{b_0+O}$ leads to the following expression for the gain:

$$\boxed{G(C, \alpha, \gamma, O) = \frac{U_G}{U_0+O} = \alpha + (\gamma - \alpha) \cdot \frac{b_0+O}{U_0(C)+O}} \tag{5.13}$$

This equation points out, that the gain is decreasing for an increasing capacity. If the measuring capacity reaches the critical value C_{crit} at $U_0(C_{crit}) + O = 0$ the gain of a box will be nearly infinite. Solving this equation leads to the critical capacity:

$$C_{crit} = -\frac{b_0 + O}{m_0} \tag{5.14}$$

Diagram a) of fig. 5.11 displays how the gain changes for different adjustments of the offset. The gain decreases for an increasing offset and the critical capacity shifts to the right with respect to the x-axis. The codomain of the gain $G(C)$ is influenced by the parameter α. Solving the equation $\frac{dG}{dC} = 0$ leads to:

$$\alpha_{crit} = \gamma \tag{5.15}$$

If the adjusted parameter α is smaller than α_{crit}, the codomain of $G(C)$ changes from positive to negative (see blue curve in diagram b) of fig. 5.11). If α exceeds α_{crit}, the codomain of $G(C)$ changes from negative to positive (see red

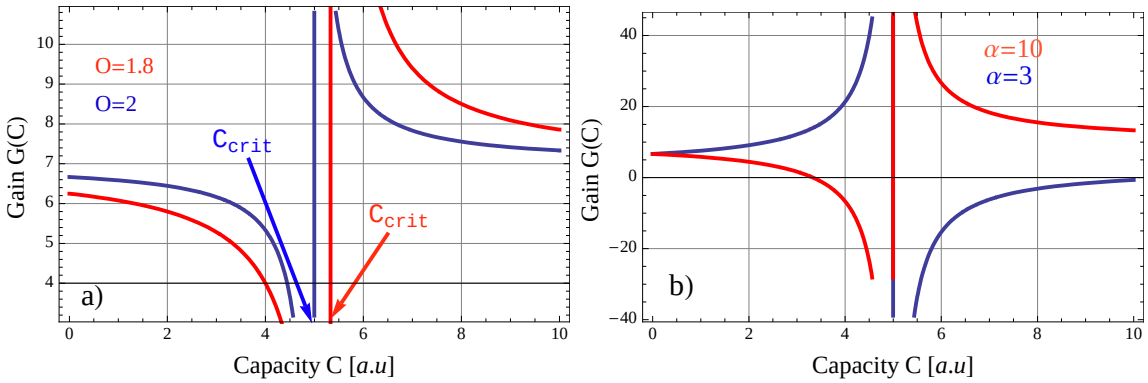

Figure 5.11: **a)** *Plot of the gain $G(C)$ as a function of the measuring capacity for two different offsets.* **b)** *Plot of $G(C)$ for two different parameters α as the critical value α_{crit} is: $\alpha_{crit} = 4$.*

curve in diagram b)). The critical capacity C is not affected by changes of α. Considering two different gains $G_1(C, \alpha_1, \gamma_1, O))$ and $G_2(C, \alpha_2, \gamma_2, O)$ with one common offset O and demanding $G_1 = n \cdot G_2$ for $n \in \mathbf{R}$ leads to the following relation between the parameters α_1, γ_1, α_2 and γ_2:

$$\frac{\alpha_1}{\gamma_1} = \frac{\alpha_2}{\gamma_2} \tag{5.16}$$

This relation is needed for calibrating each box, which is discussed in the following section.

5.2.2 Calibrating the LN_2-read-out

The calibrated output U_{cal} and calibrated gain G_{cal} of each box are given by:

$$U_{cal} = m_{cal} \cdot C + b_{cal} \tag{5.17}$$

$$G_{cal} = \frac{U_{cal}}{U_0 + O} = \alpha_{cal} + (\gamma_{cal} - \alpha_{cal}) \cdot \frac{b_0 + O_{cal}}{U_0(C) + O_{cal}} \tag{5.18}$$

Figure 5.12 displays the calibrating procedure for the LN_2-read-out-devices: first the test-capacities of the capacitive dummy were measured with no gain $G = 1$ and no offset $O = 0$, which leads to the output U_0 with parameters m_0 and b_0. After that the gain has been increased to its maximum G_{max} which leads to the output voltage U_{max}:

$$U_{max} = m_{max} \cdot C + b_{max} \tag{5.19}$$

$$G_{max} = \alpha_{max} + (\gamma_{max} - \alpha_{max}) \cdot \frac{b_0}{U_0} \tag{5.20}$$

and the test-capacities were measured again. Diagram b) and c) of fig. 5.13 display the maximum gain G_{max} and the output U_{max} of box 2 as function of the measured test-capacity C. The relation between the measured parameters α_{max}, γ_{max} of the maximum gain G_{max} and the unknown parameters α_{cal} and

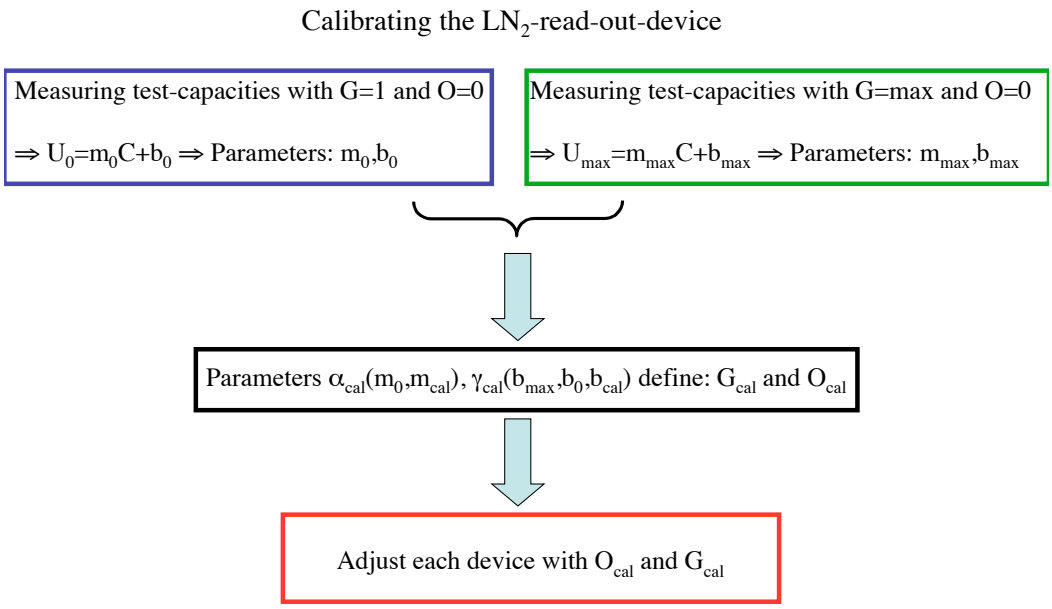

Figure 5.12: *Schematic drawing of the calibrating-procedure of each device.*

γ_{cal} of the calibrated gain G_{cal}, is given by equation 5.16:

$$\alpha_{cal} = \frac{m_{cal}}{m_0} \tag{5.21}$$

$$\gamma_{cal} = \frac{\alpha_{cal}}{\alpha_{max}} \cdot \gamma_{max} = \frac{m_{cal}}{m_{max}} \cdot \frac{b_{max}}{b_0} \tag{5.22}$$

$$O_{cal} = \frac{b_{cal}}{\gamma_{cal}} - b_0 \tag{5.23}$$

Thus the calibrated offset O_{cal} and the calibrated gain G_{cal} are determined by the measured quantities m_0, m_{max}, b_0 and b_{max}. Table 5.1 displays the measured parameters of the maximum gain G_{max} and the calibrated values for each box.

Box Nr.	α_{max}	$\gamma_{max}/\alpha_{crit}$	C_{crit}[pF]	$m_{cal}[10^{-3}\,\frac{\mathrm{V}}{\mathrm{pF}}]$	b_{cal}[V]
1	7.13 ± 0.28	6.12 ± 0.26	964 ± 37	38.29 ± 0.97	-30.47 ± 0.95
2	7.3 ± 0.26	6.21 ± 0.25	986 ± 29	39.1 ± 1.11	-31.27 ± 1.08
3	7 ± 0.2	6.25 ± 0.19	1000 ± 31	39.71 ± 0.73	-31.72 ± 0.71
4	7.06 ± 0.25	6.09 ± 0.24	971 ± 25	39.11 ± 1.19	-31.3 ± 1.16

Table 5.1: *Measured parameters α_{max}, γ_{max} and C_{crit} for all four boxes. The adjusted parameters m_{set} and b_{set} define the output U_{out} of each box.*

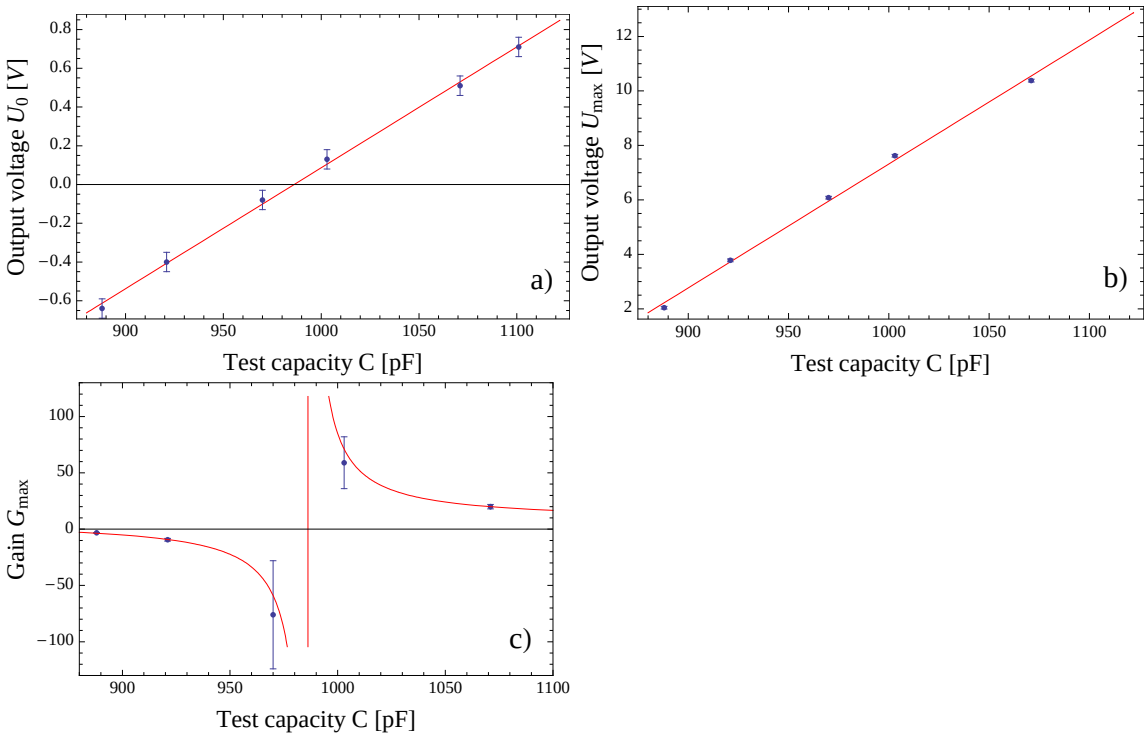

Figure 5.13: **a)** *Measured output U_0 of box 2 as gain and offset have been set to $G = 1$ and $O = 0\,\mathrm{V}$.* **b)** *Measured output U_{max} of box 2 for a maximum gain and no offset.* **c)** *Plot of the measured maximum gain G_{max} of box 2 with respect to the input capacity. The measured outputs U_0, U_{max} and the gain G_{max} of all other boxes are displayed in appendix C.*

The output voltages for C_{min} and C_{max} are defined for an AGATA-dewar in vertical position:

$$U_{cal}(C_{min}) = 5\,\mathrm{V} \tag{5.24}$$

$$U_{cal}(C_{max}) = 10\,\mathrm{V} \tag{5.25}$$

These equations determine the calibrated output U_{cal}. The adjusted output voltages of all boxes are displayed in diagram a) of figure 5.14. Only two curves are visible since the curves of box 1,2 and 4 are overlapping. The orange curve is slightly shifted with respect to the y-axis. Diagram b) shows the results of a capacitive measurement which was performed with all boxes at ATC(4). Except for box 3 all other boxes are working identically, since the orange curve is shifted. The missing capacity of the BNC-cable has been compensated by an extra capacity of 150 pF which was fixed at the input of each box. All curves in diagram b) are strictly linear in time and show that all read out devices are performing well. The red lines in diagram b) indicate the defined values 5 V and 10 V which are met quite well by the measured data. The following chapters will focus on the issue how an inclination or axial rotation of a cryostat influences the filling capacity. The LN_2-read-out-devices discussed here will be used for these position-dependent measurements.

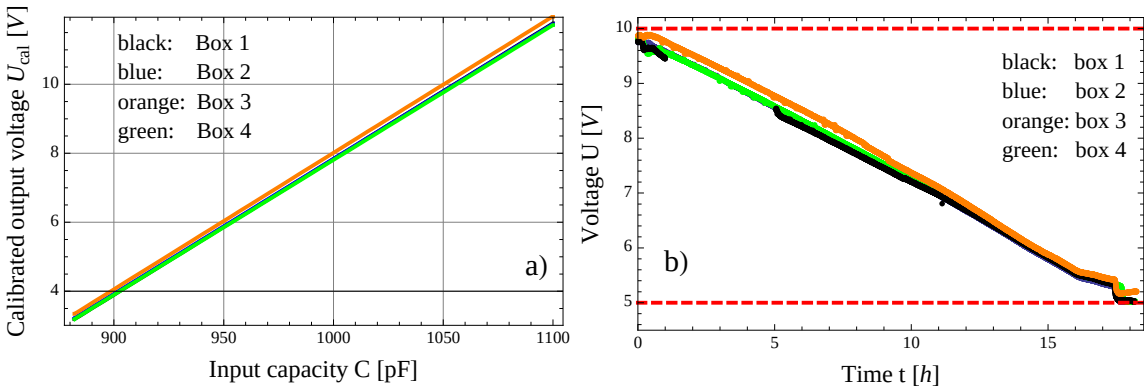

Figure 5.14: **a)** *Plot of $U_{out}(C) = m_{set} \cdot C + b_{set}$ fo all four boxes. The curves of Box 1,2 and 4 are overlapping whereas the curve of box 3 is slightly shifted with respect to the y-axis.* **b)** *Results of measuring the filling capacity C of ATC(4) in vertical position with each box. The red lines indicate $U_{min} = 5\,\mathrm{V}$ and $U_{max} = 10\,\mathrm{V}$.*

Chapter 6

Position-dependence of the LN_2-monitoring

Each AGATA-detector in the array takes a different position (see fig. 6.1) which has an effect on the time dependent capacity. Thus the angle dependence of the filling capacity has to be analysed. Moreover, it will be discussed how the consumption of liquid nitrogen depends on the inclination. Figure 6.1

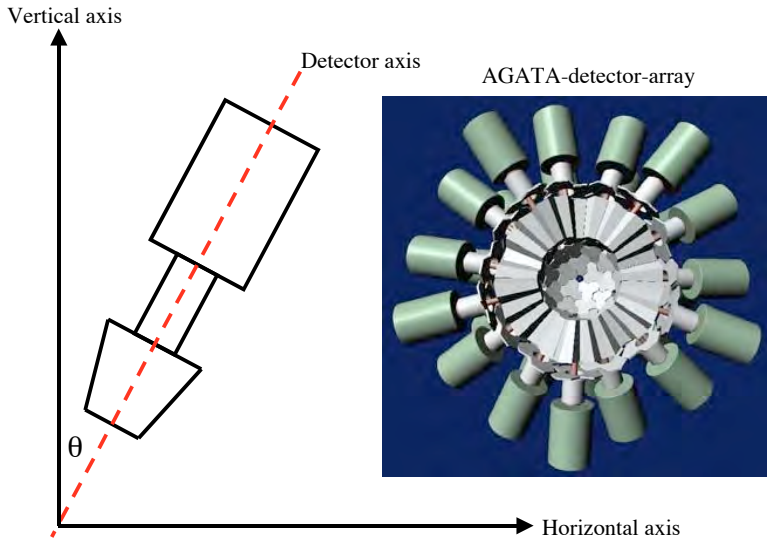

Figure 6.1: *AGATA-detector-array. Each triple-cluster in the array has its inclination angle θ between the vertical axis and the detector axis.*

shows a CAD-drawing of the AGATA-detector-array and a schematic drawing indicating the definition of the inclination angle θ. A detector is in vertical position for $\theta = 0\,^\circ$ and in horizontal position for $\theta = 90\,^\circ$.
The position of a triple-cluster in the array is not only determined by the inclination angle θ but by the rotation around its own axis as well, which is not shown in fig. 6.1. The rotation around the detector axis shall be described by the angle β, so that each detector position inside the array is given by a pair of these two angles (θ, β). The position $(90\,^\circ, 120\,^\circ)$ for example describes a detector which is in horizontal position and rotated $120\,^\circ$ around its axis with respect to a fixed position.

6.1 Influence of horizontal inclination and axial rotations

The first position dependent measurements were performed by Heinz Georg Thomas with a triple cluster.The measurements were performed in such a way that the cryostat was filled once with liquid nitrogen and inclined stepwise after that. The filling capacity has been measured for each inclination and for different filling heights. The results of these measurements are plotted in

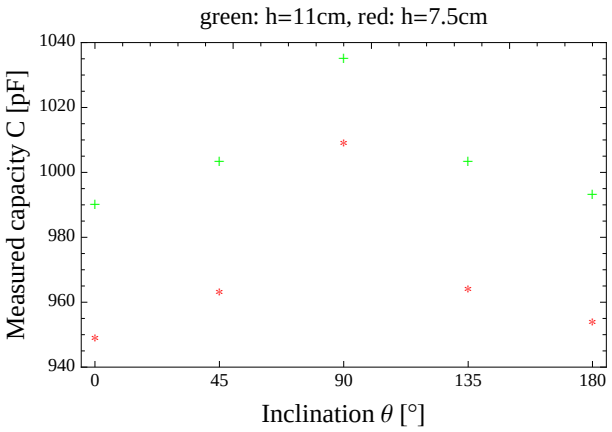

Figure 6.2: *Results of the first position-dependend measurement done by Heinz Georg Thomas. The measured capacity is plotted versus the inclination angle. The green markers represent the measurement done with a filling height h of $h = 11\,\mathrm{cm}$ whereas the red markers represent a measurement performed with a filling height $h = 7.5\,\mathrm{cm}$.*

fig. 6.2 for two different filling heights (11 cm and 7.5 cm measured in vertical position). Both measurements show that the capacity has a maximum at $\theta = 90\,^\circ$ and a minimum at $\theta = 0\,^\circ$ and $\theta = 180\,^\circ$. Therefore the filling capacity measurements are inclination-dependent.
For the purpose of understanding and describing the inclination-dependency of the measuring capacity C, the relation $C \sim (h_0 + 0.4h)$ is not adequate because it is only valid for a detector in vertical position. Hence a parameterisation of C as a function of inclination is needed. The capacity C between the inner and outer cylinder inside the dewar depends on the volume $vol(\theta)$ of liquid nitrogen between them. Since the distance Δr between the two cylinders is small compared to the radius $r_{0,1}$ of the inner cylinder, the volume between the cylinders can be approximated by the surface $S(\theta)$ which is covered by the liquid nitrogen: $vol(\theta) \cong \Delta r \cdot S(\theta)$. Like in chapter 3 the dewar is divided in two sections: one with liquid nitrogen and one without. This is shown in fig. 6.3. The calculations for the capacity C considering the surface $S(\theta)$ are similar to those in chapter 3. The average dielectric constant is given by:

$$\langle \epsilon_r \rangle(S) = \frac{1}{S_0} \cdot [\epsilon_{r,g} \cdot (S_0 - S) + \epsilon_{r,l} \cdot S] \Leftrightarrow \tag{6.1}$$

$$\langle \epsilon_r \rangle(S) = \frac{1}{S_0} \cdot [\epsilon_{r,g} S_0 + (\epsilon_{r,l} - \epsilon_{r,g}) \cdot S] \Leftrightarrow \tag{6.2}$$

$$\langle \epsilon_r \rangle(S) = 1 + 0.4 \cdot \frac{S}{S_0} \Rightarrow \tag{6.3}$$

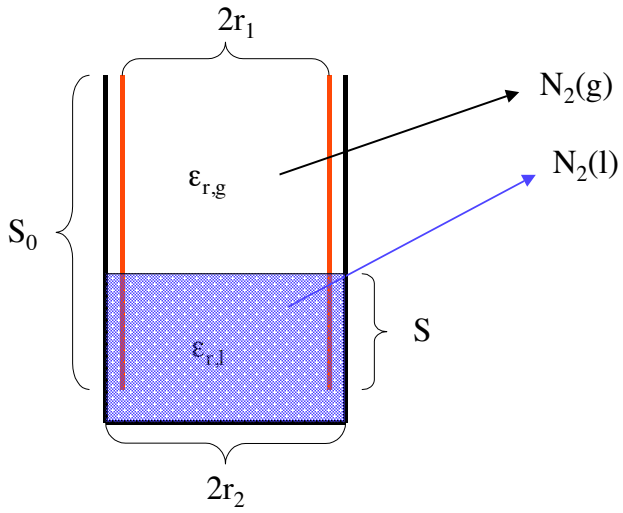

Figure 6.3: *Schematic drawing of a dewar, like in fig. 3.9. The filling height h has been replaced by the surface S covered with liquid nitrogen. The total surface of the inner cylinder is described by $S_0 = 2\pi r_2 \cdot h_0$.*

$$\boxed{C \sim S(\theta)} \tag{6.4}$$

As the capacity C is always measured with respect to the time t a further parameterisation of t as a function of the angle θ is needed. The volume $V(\theta, t)$ (not to be mistaken with $vol(\theta)$) of liquid nitrogen inside the dewar at a certain time is linked through equation 4.7 with the time:

$$V(\theta, t) = V_0(\theta) - \nu(\theta) \cdot t \tag{6.5}$$

ν is the consumption of LN_2 and $V_0(\theta)$ the volume of liquid nitrogen at the beginning of each measurement. Understanding how an inclination θ effects the surface S and the volume V of liquid nitrogen inside the dewar is related to the question, how volume and surface of a liquid inside an ideal cylinder changes as a function of the inclination θ.

6.1.1 Calculations of $S(\theta)$ and $V(\theta)$ of a liquid inside a cylinder for different inclination θ.

The mathematics used and discussed in this section is taken from *Horst Stocker* and *John W. Harris* [Wei09a]. Figure 6.4 shows a liquid inside a cylinder at different inclination. In case of no inclination the liquid has a cylindrical shape with a surface $S = 2\pi Rh$ and volume $V = \pi R^2 h$ as R is the radius of the cylinder and h the filling height of the liquid. If the cylinder is slightly inclined, the shape of the liquid changes to a cylindrical segment (see fig 6.5) which „[...]is the solid cut from a circular cylinder by two (or more) planes.[...]“ [Wei09a, p.1].

The surface S_{seg} and volume V_{seg} of a cylindrical segment are:

$$S_{seg}(\theta) = \pi R(h_1 + h_2) \tag{6.6}$$

$$V_{seg}(\theta) = \frac{1}{2}\pi R^2(h_1 + h_2) \tag{6.7}$$

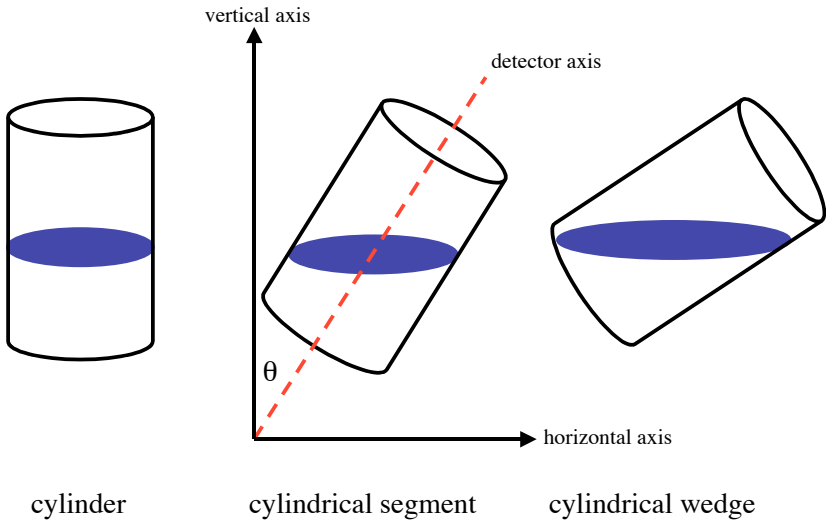

Figure 6.4: *Schematic drawing of an ideal cylinder which is filled with a liquid (indicated by dark blue coloured area). The geometrical shape which is formed by the liquid changes with respect to the inclination θ.*

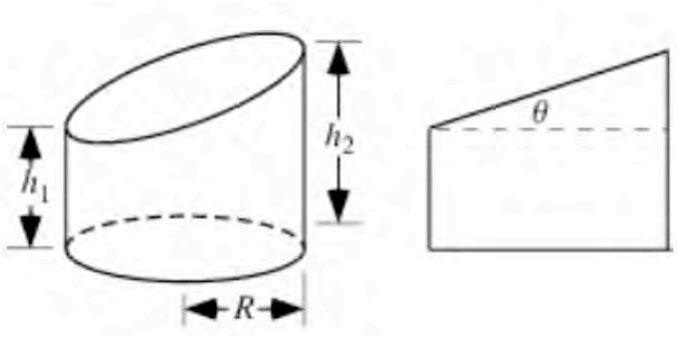

Figure 6.5: *Cylindrical segment with inclination angle θ [Wei09a]. The relation between height h_1 and h_2 is given by: $h_2 = h_1 + 2R\tan\theta$.*

As long as $0 < h_1 < h_2$ the filling height h can be written as $2h = h_1 + h_2$. This leads to:

$$S_{seg}(\theta) = 2\pi Rh \tag{6.8}$$
$$V_{seg}(\theta) = \pi R^2 h \tag{6.9}$$

Both quantities do not depend on θ, thus they are constant for a given filling height h. If this is not the case and h_1 or h_2 is negative, the cylindrical segment changes to a cylindrical wedge. „A wedge is cut from a cylinder by slicing a plane that intersects the base of the cylinder. [...]“ [Wei09b, p.1].

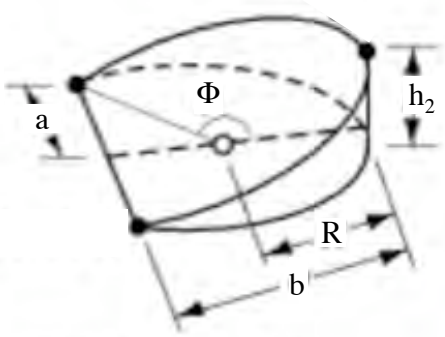

Figure 6.6: *A cylindrical wedge with base length $b > R$ and height $h_2 = b\tan\theta$ [Wei09b]. The parameters a and Φ which are shown in this drawing depend on h_2 and θ.*

The results of a detailed derivation of $S_{wdg}(\theta)$ and $V_{wdg}(\theta)$ for the cylindrical wedge are [Wei09b]:

$$S_{wdg}(h_2,\theta) = 2R\tan\theta \cdot [a(h_2,\theta) + (h_2/\tan\theta - R)\cdot\Phi(h_2,\theta)] \tag{6.10}$$
$$V_{wdg}(h_2,\theta) = \frac{1}{2}R\cdot S_{wdg}(h_2,\theta) - \frac{1}{3}a(h_2,\theta)^3\cdot\tan\theta \tag{6.11}$$

As a and Φ are the parameters shown in fig. 6.6 and given by [Wei09b]:

$$\Phi = \frac{1}{2}\pi + \arctan\left(\frac{b-R}{a}\right) \tag{6.12}$$
$$a = \sqrt{2bR^2 - R^2} \tag{6.13}$$

In order to describe the surface $S(\theta)$ and volume $V(\theta)$ over the full range of the inclination θ both expressions of surface and volume for a wedge and segment have to be combined. The shape of a cylindrical segment turns into the shape of a cylindrical wedge when the height h_1 is equal to zero: $h_1 = 0 \Leftrightarrow h_2 = R\cdot\tan\theta$. Using this condition and the step-function Θ leads to the following formula:

$$S(\theta) = S_{wdg}\cdot\Theta(k) + S_{seg}\cdot\Theta(-k) \tag{6.14}$$
$$V(\theta) = V_{wdg}\cdot\Theta(k) + V_{seg}\cdot\Theta(-k) \tag{6.15}$$

The parameter k is given by $k = 2R\tan\theta - h_2$. Equation 6.14 and 6.15 are invalid if the inclination exceeds a certain angle namely θ_{crit}. Figure 6.7 shows a two dimensional cut through a cylinder which is filled with a liquid inside. The volume and surface of the liquid change for $\theta > \theta_{crit}$ in such a way that they can not be described by V_{wdg} and S_{wdg} anymore because these expressions

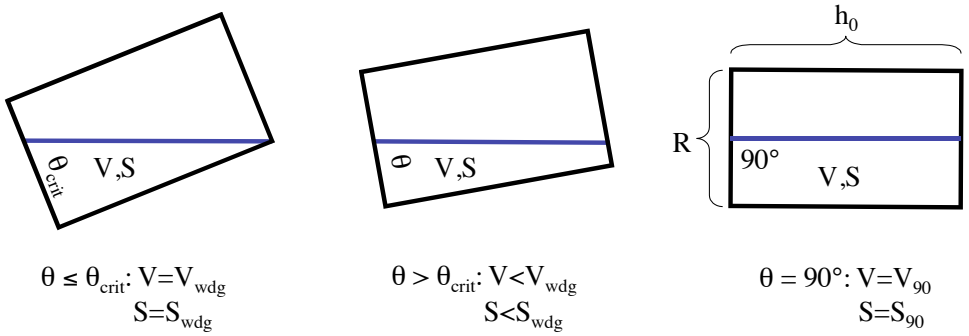

Figure 6.7: *Two dimensional drawing for three different inclination: $\theta_{crit} < \theta < 90\,^\circ$ of a cylinder with radius R and total height h_0 which is filled with a liquid (indicated by dark blue line). The inclination θ_{crit} represents the angle for which the liquids shape can still be described by V_{wdg} and S_{wdg}. In the case that $\theta > \theta_{crit}$ the volume and surface of the liquid inside the cylinder can not be described by V_{wdg} and S_{wdg} anymore. Inclining the cylinder up to $90\,^\circ$ will change the geometrical shape of the liquid to a horizontal segment with volume V_{90} and surface S_{90}.*

predict larger values than it is in reality the case. This problem can be solved by introducing two correction-terms called δV_{wdg} and δS_{wdg} which are negative and correct equation 6.14 and 6.15 for $\theta > \theta_{crit}$.
The last case to discuss is a horizontal inclination of the cylinder (see fig. 6.7). In this configuration the liquid inside the cylinder is shaped like a horizontal segment with volume V_{90} and surface S_{90} (see fig. 6.8). The formulas for these expressions are given by [Wei09a]:

$$S_{90}(h) = 2 \cdot \arccos\left[\frac{R-h}{R}\right] \cdot Rh_0 \tag{6.16}$$

$$V_{90}(h) = h_0 \cdot \left(R^2 \cdot \arccos\left[\frac{R-h}{R}\right] - (R-h) \cdot \sqrt{2Rh-h^2}\right) \tag{6.17}$$

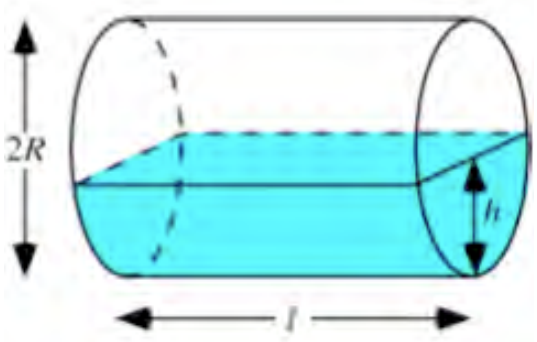

Figure 6.8: *Schematic drawing of a cylinder in horizontal position which is half filled with a liquid [Wei09a]. The total length l in this picture corresponds to the total height h_0 of the cylinder.*

The volume $V(\theta)$ and surface $S(\theta)$ of a liquid inside a cylinder with height h_0 and radius R over the full range of inclination $0\,^\circ - 90\,^\circ$ can be found by

combining equations 6.14 to 6.17. This leads to:

$$S(\theta) = \begin{cases} S_{wdg}\Theta(k) + S_{seg}\Theta(-k) - \delta S_{wdg}\Theta(\theta_{crit} - \theta), & \theta < 90\,^\circ \\ S_{90}, & \theta = 90\,^\circ \end{cases} \quad (6.18)$$

$$V(\theta) = \begin{cases} V_{wdg}\Theta(k) + V_{seg}\Theta(-k) - \delta V_{wdg}\Theta(\theta_{crit} - \theta), & \theta < 90\,^\circ \\ V_{90}, & \theta = 90\,^\circ \end{cases} \quad (6.19)$$

In order to simulate the volume and surface of a liquid inside an inclined cylinder with radius R and height h_0, a model is needed which has two main features:

- Equations 6.18 and 6.19 shall be part of it, so that $V(\theta)$ and $S(\theta)$ can be predicted for all angles between $0\,^\circ$ and $90\,^\circ$.
- The theoretical values of $V(\theta)$ have to be inclination independent for a given filling height h (conservation of the LN_2-mass).

The second feature is not trivial to realise. The model used[1] here considers an ideal cylinder with an imaginary filling-nozzle with length $l_f = h_0 - h$ and a varying diameter $d(\theta)$, so that the volume of the liquid remains constant for each inclination θ. Figure 6.9 shows a simulation of the volume and surface

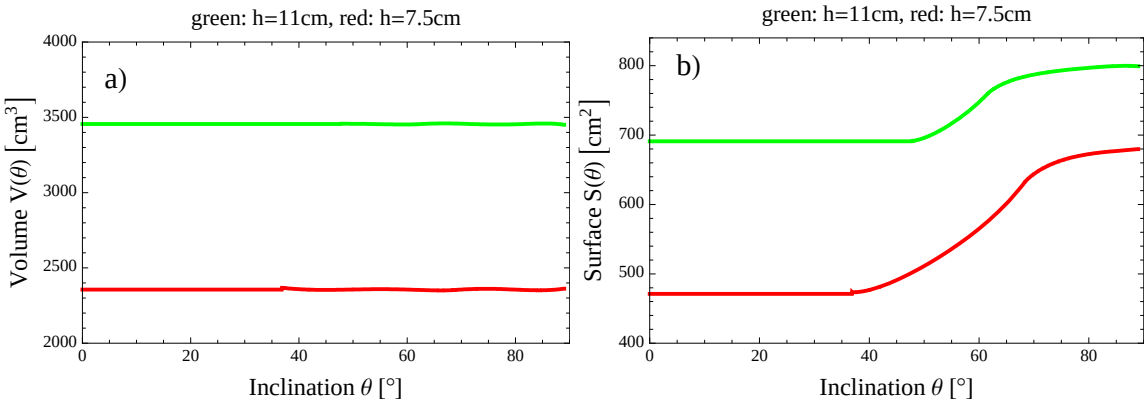

Figure 6.9: *Simulation of the volume $V(\theta)$ and surface $S(\theta)$ of liquid inside a cylinder with radius $R = 10\,\text{cm}$ and height $h_0 = 29\,\text{cm}$ for different inclination angle θ and filling height h.* **a)** *Simulation of $V(\theta)$ for two filling heights $h = 11\,\text{cm}$ and $h = 7.5\,\text{cm}$.* **b)** *Simulation of $S(\theta)$ for the same two filling heights. All curves in both diagrams are not perfectly shaped which is related to the model that was used for these simulations.*

of a liquid inside a cylinder. The curves of $V(\theta)$ are nearly straight lines as expected. The deviation of each curve from an ideal straight line is related to the working precision of the model which was used for these simulations. The curves of $S(\theta)$ show some small deviations too, but their order of magnitude is low, thus the are negligible. Since the measuring capacity C is proportional to the surface $S(\theta)$, the simulations point out that **the measuring capacity changes with respect to an inclination even though the amount of liquid nitrogen is constant**. This statement meets perfectly with the results of the position-dependend measurements which are shown in fig. 6.2. The experimental data shows that the measuring capacity has its maximum at

[1] A detailed description of this model and the calculations of $S(\theta)$ and $V(\theta)$ are shown in appendix D.

$\theta = 90\,°$ and its minimum at $\theta = 0\,°$, whereas the difference between these two values depends on the filling height.These two observations are also reflected by the simulation of $S(\theta)$. One aspect which is not considered by the model used here, is the fact that the inner cylinder inside the dewar does not reach until the dewars ground and therefore the correlation between volume and surface of the liquid nitrogen inside the dewar is different to the correlation between volume and surface of a liquid inside an ideal cylinder.

6.1.2 Influence of the dewars geometry

The geometry of a dewar differs from an ideal cylinder in such a way that the dewar is equipped with a filling nozzle which has a length l_f and a diameter d. Figure 6.10 (left) shows a schematic drawing of a dewar with a filling-nozzle.

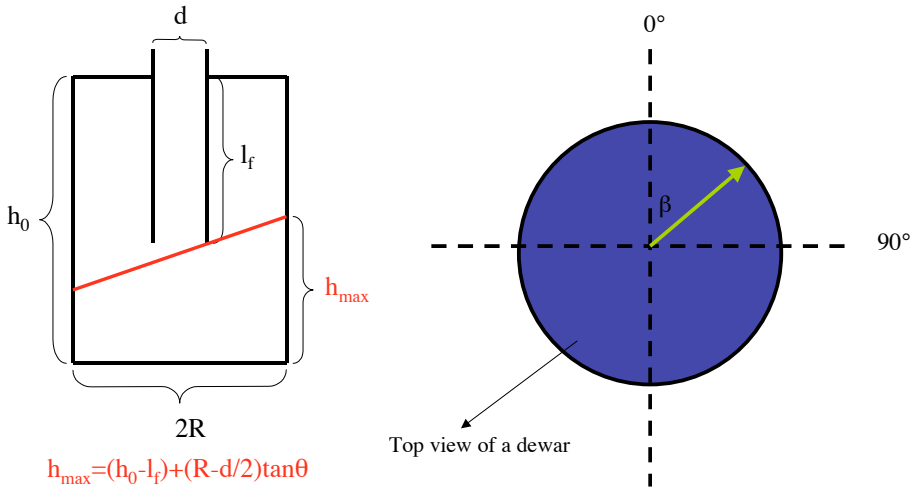

Figure 6.10: **Left:** *Schematic drawing of a dewar with radius R, total height h_0 and a filling-nozzle which has a length l_f and a diameter d. The red line in this drawing indicates the filling level of a liquid inside the dewar.* **Right:** *Top view of a dewar. The axial rotation is defined by the angle β.*

As long as the dewar is not completely filled with liquid nitrogen, the filling-nozzle should have no influence on the calculations of $V(\theta)$ and $S(\theta)$ however.

6.1.3 Axial rotations

Apart from inclining the system, the detector might also be rotated around its own axis which is shown on the right hand side of fig. 6.10. The axial rotations are described by the angle β. Considering an ideal dewar the axial rotations should have no effect on the measuring capacity. The inner and outer cylinder of a real dewar might not have a perfect cylindrical shape which causes an asymmetry between them. This might have an effect on the measuring capacity if the dewar is inclined and rotated around its own axis.

6.1.4 Simulating the time behaviour of the capacity $C(t)$

The model which was introduced in section 6.1.1 shall now be used for simulating the capacity of a dewar which is filled with liquid nitrogen. The relation

between surface $S(\theta)$ and capacity C is shown by equation 5.2 and leads to:

$$C(\theta) = \frac{\epsilon_0}{R \cdot \ln\left(\frac{R}{R-\Delta r}\right)} \cdot [S_0 + 0.4 \cdot S(\theta)] \tag{6.20}$$

As Δr is the distance between the inner and outer cylinder. The relation between volume $V(\theta)$ and time t is given by equation 6.5. In an intuitive picture the consumption ν of liquid nitrogen should not depend on an inclination θ thus ν is assumed to be inclination-independent. Solving equation 6.5 for t and considering a constant consumption leads to:

$$t(\theta) = \frac{V(\theta) - V_0(\theta)}{|\nu|} \tag{6.21}$$

$V_0(\theta)$ is the maximum amount of LN_2 which can be filled into the dewar with inclination θ. Due to the dewars geometry this amount is assumed to be inclination dependent. Figure 6.11 shows four simulations of the measuring capacity $C(t)$ as a function of time for an ideal dewar which is filled with liquid nitrogen. Furthermore the ideal dewar is equipped with a filling-nozzle. Diagram a) and b) in fig. 6.11 show the case of a partially filled dewar. Both simulations reflect the observations which have already been made and discussed in section 6.1.1. The filling-nozzle has no effect on $C(t)$ until the dewar is completely filled. The simulation of a completely filled dewar for each inclination is displayed in diagram c) of fig. 6.11. The liquid nitrogen inside the dewar seems to last longer when the cryostat is in horizontal position, as the filling nozzle limits the maximum filling height in vertical position. Considering a finite diameter of the filling-nozzle leads to the simulation shown in diagram d). The operation time and the maximum capacity $C(t = 0)$ are different for each curve. Nevertheless the simulations shown in diagram c) and d) imply that the liquid nitrogen is exactly filled until the beginning of the filling-nozzle. This condition is difficult to realise in a real experiment, hence it is not clear how the filling-nozzle effects the measuring capacity in a real experiment.

6.2 Position-dependent measurements (I)

The first position-dependend measurements were performed with the setup shown in fig. 6.12 and an empty cryostat (ATC(4)). The results of these measurements are shown in fig. 6.13. The position in which the capacity was measured is indicated by a pair (inclination θ, axial rotation β). Diagram a) shows the measured capacity for the two positions $(0\,^\circ, 0\,^\circ)$ and $(90\,^\circ, 0\,^\circ)$. Both measured curves are shaped as predicted by the simulation of $C(t)$ shown in section 6.1.3. The results of measuring $C(t)$ under the influence of axial rotations can be seen in diagram b) of fig. 6.13. All curves are again shaped as predicted by the simulation of $C(t)$ and have a common minimum at $C = 924\,\mathrm{pF}$. The curves in diagram b) are not unique which is also revealed by the measured operation times τ (see table 6.1). The difference between the operation time of position $(0\,^\circ, 0\,^\circ)$ and position $(90\,^\circ, 0\,^\circ)$ is about one hour. This might be related to the length of the dewars filling nozzle as simulated in diagram c) of fig 6.11. The difference between the operation times which are indicated by the blue, red and green curve are striking. Table 6.1 shows that

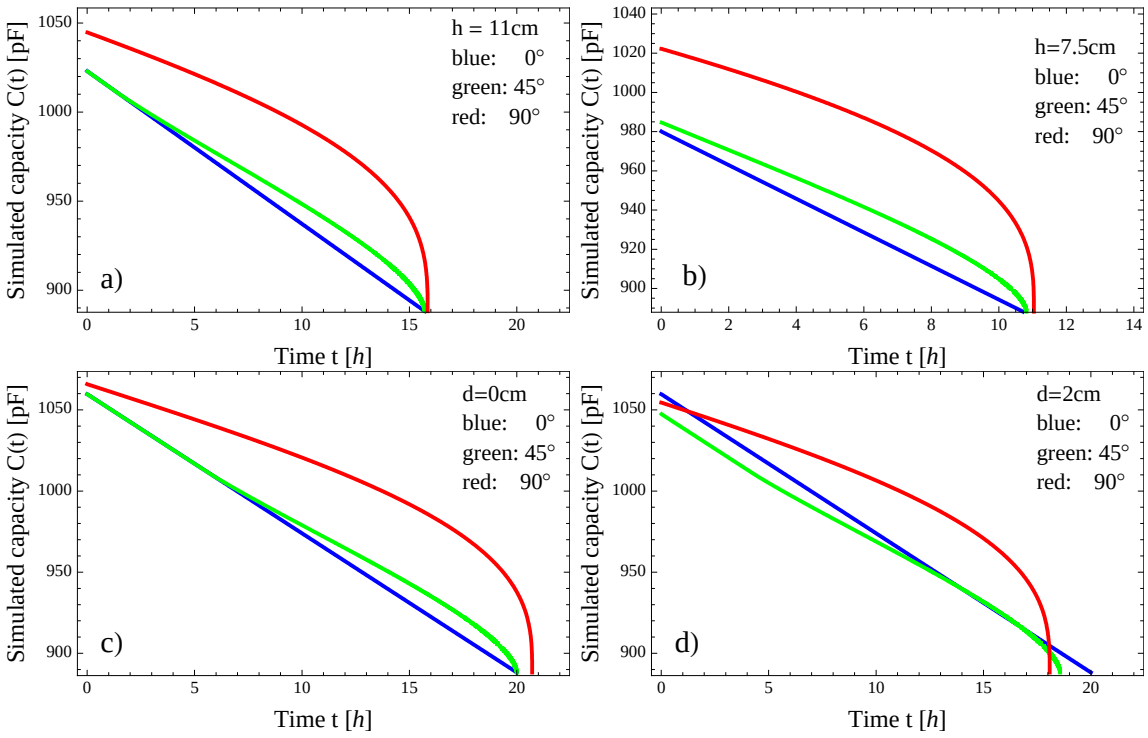

Figure 6.11: *Simulations of the measuring capacity $C(t)$ as a function of time for an ideal dewar with filling-nozzle. The dewars radius and total height are: $R = 10\,\mathrm{cm}$, $h_0 = 29\,\mathrm{cm}$. The distance Δr between inner and outer cylinder has been chosen as $\Delta r = 0.18\,\mathrm{cm}$. The nozzles length is $l_f = 15\,\mathrm{cm}$. The inclination angles which have been chosen for these simulation are: $0\,^\circ$, $45\,^\circ$ and $90\,^\circ$. The consumption of the system was set to the constant value $\nu = 220\frac{\mathrm{ml}}{\mathrm{h}}$.* **a)** *Simulation of $C(t)$ for a filling height $h = 11\,\mathrm{cm}$.* **b)** *Simulation of $C(t)$ for a filling height $h = 7.5\,\mathrm{cm}$.* **c)** *Simulation of $C(t)$ considering the filling-nozzle with a diameter which is here $d = 0\,\mathrm{cm}$.* **d)** *Simulation of $C(t)$ for a nozzle with diameter $d = 2\,\mathrm{cm}$.*

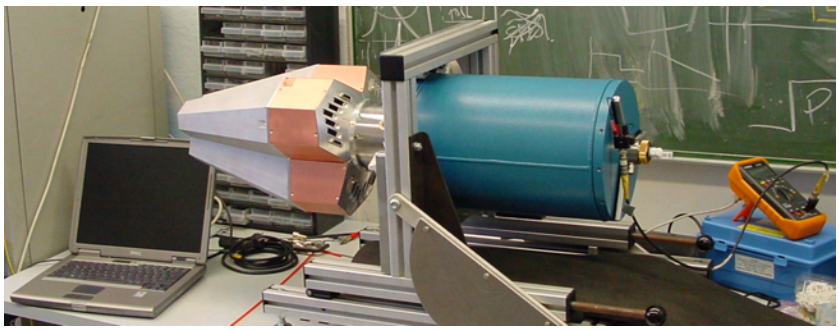

Figure 6.12: *Experimental setup for measuring the filling capacity of ATC(4) being in horizontal position. The cryostat is mounted in a special frame with adjustable inclination. The capacity was measured with device (I). The dewar has been completely filled with liquid nitrogen before the measurement was started.*

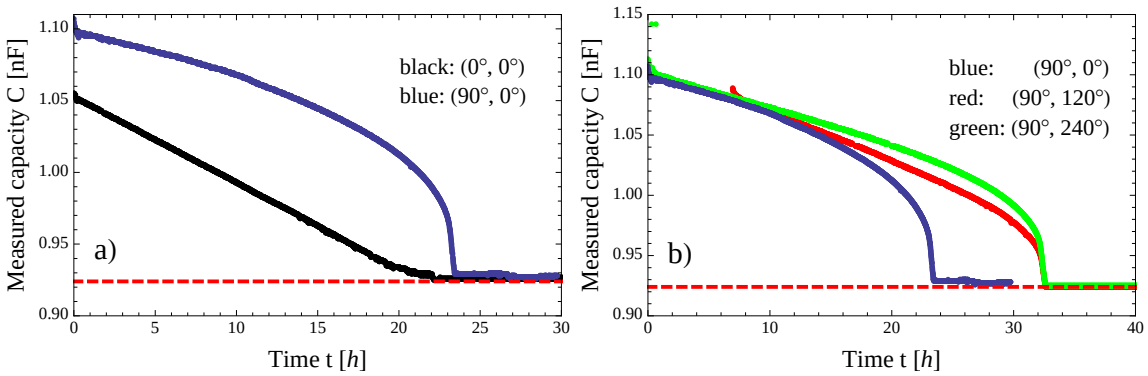

Figure 6.13: **a)** *Measured capacity for* $\theta = 0\,^\circ$ *and* $\theta = 90\,^\circ$. **b)** *Measured capacity for* $\theta = 90\,^\circ$. *The cryostat has been rotated during this measurement around its own axis in* $120\,^\circ$*-steps. The red dashed line indicates the common minimum capacity* $C_{min} = 924\,\mathrm{pF}$ *of all curves.*

the amount of liquid nitrogen inside the dewar being in position $(90\,^\circ, 120\,^\circ)$ lasts nearly 9 h longer than for the dewar being in position $(90\,^\circ, 0\,^\circ)$. This discrepancy can not be explained by the dewars properties (e.g. the filling-nozzle or asymmetries between the inner and outer cylinder). The second

Position	$(0\,^\circ, 0\,^\circ)$	$(90\,^\circ, 0\,^\circ)$	$(90\,^\circ, 120\,^\circ)$	$(90\,^\circ, 240\,^\circ)$
τ[h]	22.1 ± 0.3	23.4 ± 0.3	32.5 ± 0.3	32.5 ± 0.3

Table 6.1: *Measured operation time* τ *of ATC(4) in four different positions.*

position-dependent measurements were performed with ATC(4) again in which the inclination was changed to $\theta = 45\,^\circ$ and the capacity was read out for the first time with the prototype of the C/V-transcenducer. Figure 6.14 shows the experimental setup of the measurement. The LN_2-read-out-box was fixed at the outside of the dewar and read out by a multimeter which was itself connected to a laptop. The results of these measurements are shown in fig. 6.15. The slight deformation of the measured curves in fig. 6.15 are related to the missing capacity of the BNC-cable as discussed in chapter 5. Apart from the deformation the measured curves show for each position a different operation time (see table 6.2). Comparing them with the data shown in table 6.1 points out that the operation times ot ATC(4) are not unique. The blue curve in diagram b) of fig. 6.2 has a larger maximum $U(t = 0)$ than the red and green one. Neglecting all measurements with an operation time longer than 23 h points out that τ varies up to one hour with changing inclination from $0\,^\circ$ to $90\,^\circ$. These variation in time might be caused by a variation of the pressure and filling level inside the dewar. Hence further investigation needs to be done in order to determine the influence of inclination θ or axial rotation β on the liquid nitrogen consumption ν.

Figure 6.14: *ATC(4) with inclination $\theta = 45\,°$. The capacity was read out with a C/V-transcenducer which was fixed on the site of the dewar.*

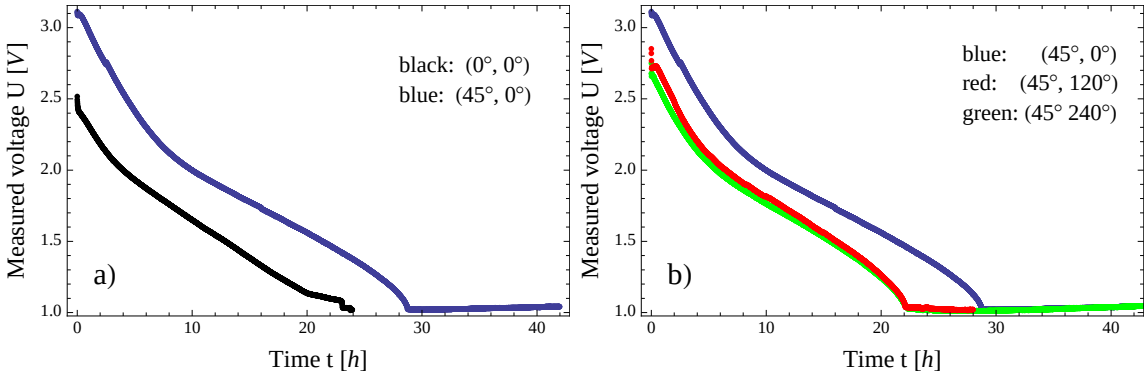

Figure 6.15: **a)** *Measured voltage U as a function of time for $\theta = 0\,°$ and $\theta = 45\,°$.* **b)** *Measured voltage for $\theta = 45\,°$. The cryostat has been rotated during this measurement around its own axis in $120\,°$-steps. All curves have a common minimum at $U = 1\,\mathrm{V}$. Gain and offset of the C/V-transcenducer were not adjusted.*

Position	$(0\,°, 0\,°)$	$(45\,°, 0\,°)$	$(45\,°, 120\,°)$	$(45\,°, 240\,°)$
τ[h]	23.1 ± 0.3	28.8 ± 0.3	22 ± 0.3	22 ± 0.3

Table 6.2: *Measured operation time τ of ATC(4) in four different positions.*

6.3 Position-dependent measurements (II)

The third iteration of position-dependent LN_2-measurements was performed with four LN_2-read-out-devices (called box for short) which have been discussed in chapter five in detail. This iteration aimed for the following issues:

- Testing the performance of each read-out-device. Ideally all devices should work identically.
- Measuring the capacity and hopefully achieving a consistent picture about the influence of inclination and axial rotations on the consumption of liquid nitrogen.

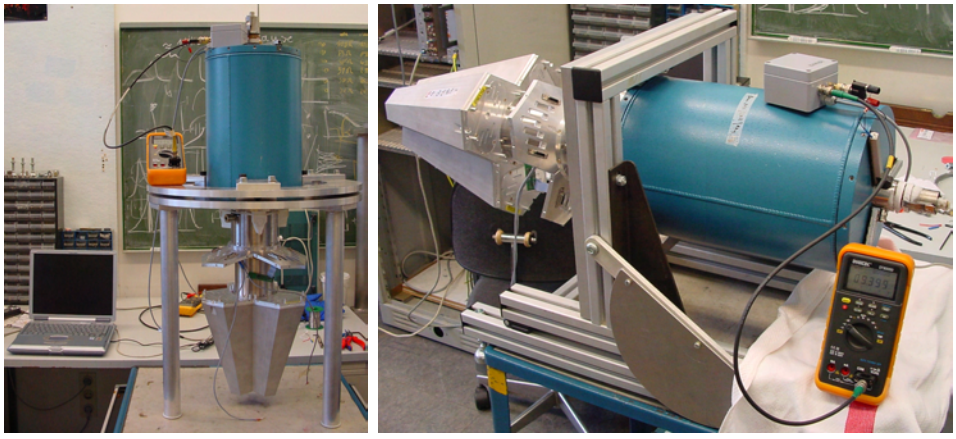

Figure 6.16: **Left:** *ATC(4) in vertical position with a* LN_2*-read-out-device on top.* **Right:** *ATC(4) in horizontal position; the* LN_2*-read-out-device is standing on the dewar.*

In order to compensate the missing capacity of the BNC-cabling, the capacity-read-out of the dewar was equipped with an extra capacity of 150 pF. The experimental setup for the measurements in horizontal and vertical position is shown in figure 6.16. All measurements were performed with ATC(4) which was equipped this time with three aluminium blocks. In order to provide stabile and reliable measurement-conditions a dewar-closing with an overpressure protection valve has been used. Furthermore the dewar has been completely filled with LN_2 for each position-measurement and the filling-capacity has been measured with all four boxes one after another in each position. All results of the position-dependent measurement (II) are shown in diagram a)-d) of figure 6.17. The deformation which appeared in the measurements discussed in the section before is not present anymore, as the extra capacity of 150 pF has been added. All curves are perfectly shaped as predicted by the simulation of $C(t)$. The red lines in each diagram indicate the range of 5 V between the minimum voltage $U_{min} = 5\,\mathrm{V}$ and the maximum voltage $U_{max} = 10\,\mathrm{V}$. The black curve (box 1) shown in diagram a) is interrupted between $t = 1\,\mathrm{h}$ and $t = 5\,\mathrm{h}$ for a period of four hours due to a power failure. The orange curve (box 3) in diagram a) is a bit shifted with respect to the other curves, whereas the blue (box 2) and green curve (box 4) are overlapping. Thus box 2 and 4 are working identically. After readjusting box 3 the capacity-measurements have been repeated with inclination $\theta = 45\,^\circ$ as the data of this measurement

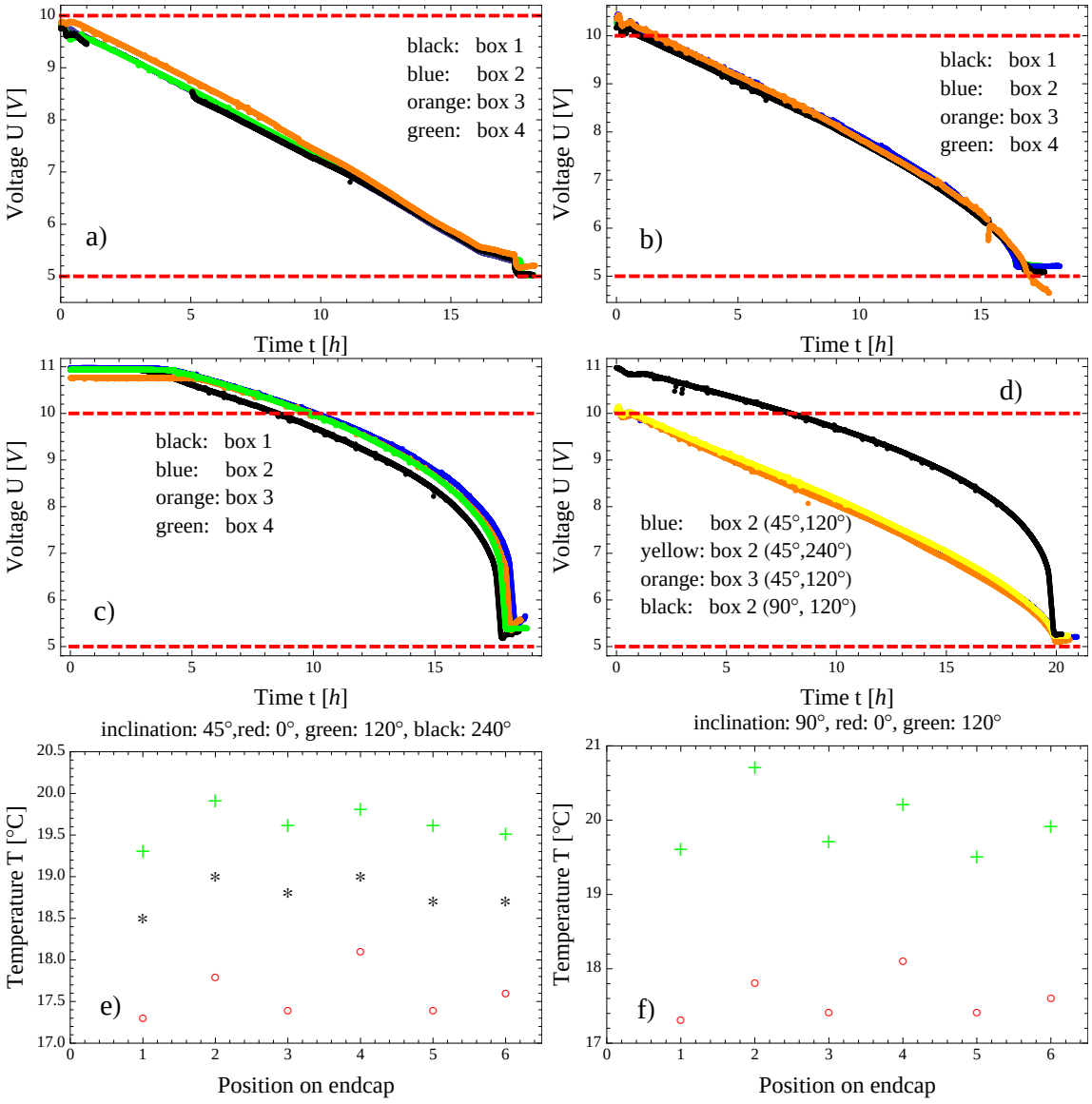

Figure 6.17: *Measured voltage with inclination* **a)** $\theta = 0\,°$, **b)** $\theta = 45\,°$ *and* **c)** $\theta = 90\,°$. *The red, dashed lines indicate the minimum voltage* $U_{min} = 5\,\mathrm{V}$ *and the maximum voltage* $U_{max} = 10\,\mathrm{V}$ *for a dewar being in vertical position.* **d)** *Measurement of the output voltage under the influence of inclination and axial rotations, performed with box 2 and 3 only.* **e)** *Temperature of the endcap as ATC(4) was in position* $(45\,°, 0\,°)$, $(45\,°, 120\,°)$ *and* $(45\,°, 240\,°)$. **f)** *Temperature of the endcap whith ATC(4) being in position* $(90\,°, 0\,°)$ *and* $(90\,°, 120\,°)$.

is shown in diagram b) of figure 6.17. The readjustment of box 3 has been successful since all curves are overlapping now which is also shown in diagram c). All curves have an identical slope, which is comparable to the simulations of $C(t)$, so that **all LN_2-read-out-devices are performing well and working identically.** Each position-dependent measurement is characterised by three quantities: the operation time τ, the minimum voltage output U_{min} and the maximum voltage output U_{max} of the LN_2-read-out-device. Table 6.3 shows the average of these quantities which has been taken over the four measurements with each box at one inclination. The variation of $\bar{U}_{max}$ has already been discussed in section 6.2 and is related to the inclination-dependence of the surface $S(\theta)$. The average operation time $\bar{\tau}$ is varying for each inclination. The biggest discrepancy of $\bar{\tau}$ is observed between the measurements with $\theta = 45\,^\circ$ and $\theta = 90\,^\circ$ which is nearly 8 %. Considering axial rotations, diagram d) in fig. 6.17 shows a different situation: All curves have their minimum nearly at $t = 20\,\mathrm{h}$. The average operation time of these four curves is $\bar{\tau} = (19.95 \pm 0.06)\,\mathrm{h}$. The difference between this operation time and the measured ones in table 6.3 is not reasonable. A possible explanation for this is displayed in diagram e)-f) in fig 6.3, which show the measured temperature at six positions on the endcap. The red points in diagrams e) and f) indicate

Inclination θ[°]	$\bar{\tau}$[h]	$\bar{U}_{min}$[V]	$\bar{U}_{max}$[V]
0	17.58 ± 0.11	5.05 ± 0.07	9.84 ± 0.03
45	16.69 ± 0.3	5.12 ± 0.1	10.38 ± 0.07
90	18 ± 0.25	5.33 ± 0.11	10.91 ± 0.1

Table 6.3: *Taken average of the operation time. minimum and maximum output U_{min}, U_{max} of the measurements shown in diagram a)-c) of figure 6.17.*

the temperature of the endcap as the cryostat was in position $(45\,^\circ, 0\,^\circ)$ and $(90\,^\circ, 0\,^\circ)$ respectively. In these positions, the endcaps temperature varies between 17 °C and 18 °C. But the temperature changes up to 20 °C when the cryostat is rotated around its own axis, which is a clear hint for a heat loss inside the cryostat through thermal radiation. This has an influence on the consumption and seems to be position-dependent in this case. The existence of this extra heat loss has already been observed in chapter 4. The last issue to discuss is the variation of $\bar{U}_{min}$ for each inclination. Considering table 6.3 the minimum output-voltage seems to increase with increasing inclination which is not reasonable, since an empty dewar should show a position-independent minimum. The filling-capacity C is measured between the inner and outer cylinder inside the dewar. Hence the inner cylinder does not reach until the dewars ground, the capacity-measurement will display an empty dewar, but there is still an amount of liquid nitrogen inside which cools the system. This fact might be a possible explanation for the variation of $\bar{U}_{min}$.

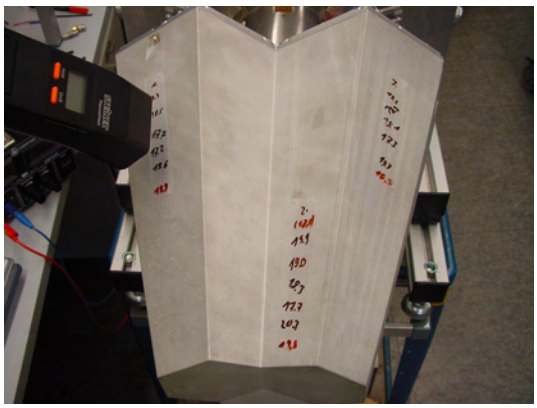

Figure 6.18: *The temperature of the endcap was measured at six different positions with an infrared-thermometer.*

6.4 First summary and discussion of the results

The measured results displayed in figure 6.17 show that the simulations of $C(t)$ which have been discussed in section 6.1.4 are working and that **the dewars filling-nozzle seems to have a negligible influence on the filling capacity measurement.** All LN_2-read-out-devices are working identically and deliver reproducible results. The average operation time $\bar{\tau}$ which is displayed in table 6.3 varies in a range of 45 min within the errors between each inclination-dependent measurement. This variation of the operation time is much smaller than observed in the measurements which have been investigated in section 6.2. Noticing that and considering the unique operation time displayed in diagram d) of fig. 6.17 and the position-dependent temperature of the endcap leads to the conclusion that **the consumption of liquid nitrogen inside a dewar is inclination-independent.**
Referring to this result, each AGATA-detector in the AGATA-array will have the same position-independent consumption of liquid nitrogen which is advantageous for monitoring the liquid nitrogen level inside a dewar.
Referring to these results, the results gained in chapter 4 and equation 6.21, the operation time τ of an AGATA-dewar is given by:

$$\tau = \frac{V_0}{|\nu|} = \frac{V_0}{|m \cdot P + \nu_0|} \tag{6.22}$$

The numerator V_0 contains all information about the dewar (length, radius, maximum filling height,etc.) and the amount of liquid nitrogen inside it. The denominator contains all information about the liquid nitrogen consumption (e.g. electronics, cabling, crystals, etc.). Diagram a) of figure 6.19 shows a simulation of the operation time as a function of the applied heating power. Furthermore the volume V_0 of liquid nitrogen inside the dewar has been varied. In order to confirm the validity of equation 6.22, an operation time-measurement has been performed with ATC(4) being in position $(90\,°, 120\,°)$. The capacity has been read out with box 2, as the heating power P of the caddock was increased stepwise. Diagram b) in fig. 6.19 displays the results of this measurement. At first the heating power has been increased from 0 W to 6 W in steps of 2 W (see green data-points in diagram b)). After increasing, the heating power was decreased in steps of 1 W (see red data-points i diagram b)). The red and green curve shown in diagram b) are a fit of equation 6.22 to the

measured data. Both curves are not identical. After being heated up, the cryostat needs a certain time to cool down and to accumulate to the new adjusted heating power. Diagram c) displays all consumption measurements which have been performed with ATC(2) and ATC(4). The green and red curve refer to the measured data shown in diagram b). Since both curves are nearly overlapping, the difference between the consumption measured with increasing power P and decreasing power is marginal. The orange curve indicates a higher liquid nitrogen consumption than the green curve for example. Although the cryostat is the same. But this difference is caused by the position dependent heat loss through thermal radiation inside cryostat. Referring to the equation: $\Delta Q_V \cdot \rho_{LN_2} \cdot \nu = \kappa \cdot (P + P_0)$, which has been discussed in chapter 4, the factor κ can be determined for the green and red curve: $\kappa_{green} = (0.81 \pm 0.08)$ and $\kappa_{red} = (0.84 \pm 0.02)$. Thus 80 % of the radiation emitted by the caddock is injected into the cooling finger which is a reasonable value.
The consumption of liquid nitrogen is higher for ATC(2) than for ATC(4) (see blue curve). But this result does not surprise since ATC(2) is fully equipped with three Ge-crystals and the complete electronics inside the cold part.

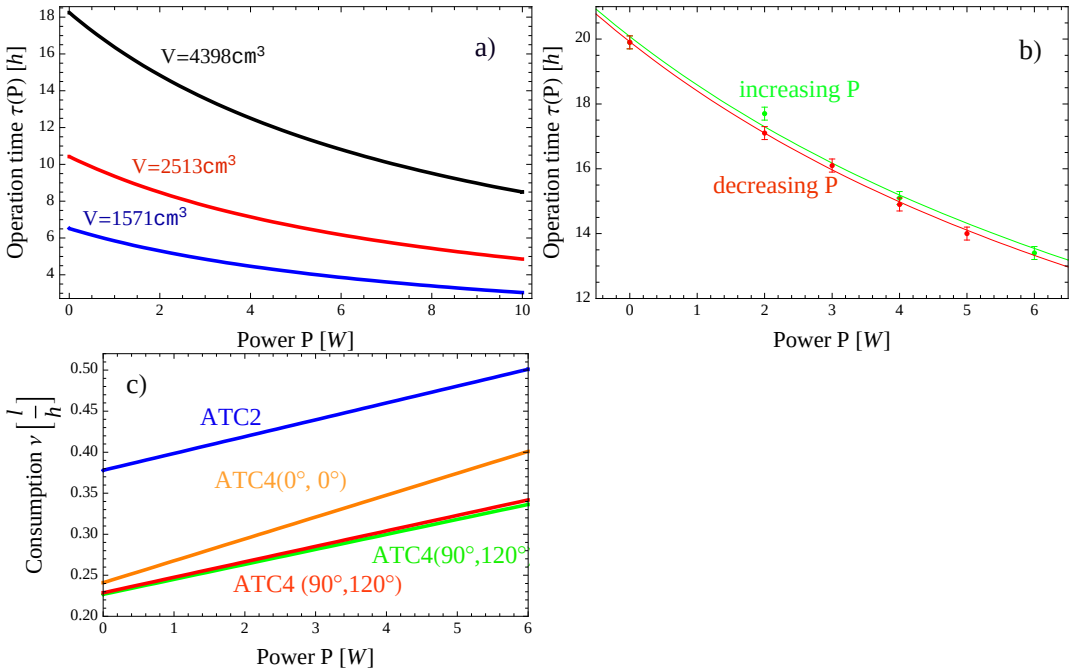

Figure 6.19: *Simulation of τ for an ideal dewar with radius $R = 10\,\text{cm}$, total height $h_0 = 29\,\text{cm}$ and a filling-nozzle with length $l_f = 15\,\text{cm}$.* **a)** *Plot of the operation time τ as a function of the applied heating power for three different volumes V_0. The volume of liquid nitrogen has been set at a fixed value of $120 \cdot \pi\,\text{cm}^3$ and the consumption was set to $\nu(P) = 27.66\frac{\text{cm}^3}{\text{Wh}} \cdot P + 241\frac{\text{cm}^3}{\text{h}}$.* **b)** *Measured operation time $\tau(P)$ for ATC(4) being in position $(90\,°, 120\,°)$. The green data points represent the measured operation with increasing power P, whereas the red data points represent the measured operation time with decreasing power. The green and red curves are regressions through the data-points referring to equation 6.22. The volume of liquid nitrogen inside the dewar has been assumed to be $V_0(90\,°) = 4555\,\text{cm}^3$ which leads to the following parameter found for the green curve: $m_{green} = (18.26 \pm 1.83)\frac{\text{cm}^3}{\text{Wh}}, \nu_{0,green} = (226.8 \pm 4.9)\frac{\text{cm}^3}{\text{h}}$. The parameters found for the red curve are: $m_{red} = (18.85 \pm 0.4)\frac{\text{cm}^3}{\text{Wh}}, \nu_{0,red} = (228.7 \pm 1.2)\frac{\text{cm}^3}{\text{h}}$.* **c)** *Plot of the consumption ν as a function of the heat loss P for the triple clusters: ATC(2) and ATC(4). The blue curve is a linear regression through the measured consumption of ATC(2) which was discussed in chapter 4. The orange curve reveals the measurement done with ATC(4), which was also discussed in chapter 4. The consumptions of ATC(4) referring to the measured operation time in diagram b) are indicated by the green (increasing heating power) and red (decreasing heating power) curve..*

Chapter 7

Summary and outlook

The main goal of this thesis was to test and to charatcerise a novel liquid nitrogen fill level meter. The experiments done within this thesis point out that the liquid nitrogen fill level meter is working and delivers reproduceable results which are comparable to a direct measurement of the liquid nitrogen filling height.
By using this capacitive liquid nitrogen read out, the warming-up and cooling-in-process of an AGATA-triple-cluster were investigated and quantified.
The consumption of liquid nitrogen was measured and discussed in chapter 4 for three different triple cluster under different conditions. These measurements point out that the consumption of liquid nitrogen is strongly influenced by the cabling inside the cold part of an AGATA-cryostat and the applied low-voltage-power. Moreover the liquid nitrogen consumption depends linearly on the applied heating power coming from the crystals, the electronics, the internal cabling etc.
In chapter 5 a novel capacitive LN_2-read-out was introduced which uses a ratiometric method for measuring the filling capacity. The advantage of this method is that small changes of the filling capacity ($\sim 15\,\%$) are detected with high accuracy.
Four of these new devices were developed by the electronic workshop at IKP Cologne and tested at the AGATA-triple-cryostat ATC(4). All devices perform well and work identically. The extra capacity of the BNC-cable, which was used for measuring the variation range of the filling capacity, needs to be compensated.
The issue how horizontal inclination or axial rotations influence the capacitive read out was discussed in chapter 6. For this purpose calculations were done to determine the volume and surface of a liquid inside an ideal cylinder. By parameterising the filling capacity with the surface and the volume with the measuring time, the filling capacity was calculated for different inclination. These results show an inclination dependence of the measuring capacity. These results of the inclination-dependent capacity measurements show:

- a good agreement with the calculation. Thus the theoretical model is working.
- that the filling capacity depends on horizontal inclination but is not affected by axial rotations.
- the consumption of liquid nitrogen does not depend on inclination and axial rotations.

- the dewar's filling-nozzle has a negligible influence on the capacity measurement and the consumption of liquid nitrogen.

Based on the results of this thesis, additional LN_2-read-out-devices will be produced to provide a LN_2-monitor for each AGATA-triple-cryostat in the array. The monitor implies that the variation ΔC of the filling capacity between a full and empty dewar is determined for each AGATA-cryostat. A performance-test of the AGATA-cryostat needs to include a specification of ΔC. The final LN_2-monitor should avoid the capacity of the BNC-cabling which affects the adjustment of the device.
Since the consumption is independent of any inclination or rotation of the detector, a common threshold-voltage for all detectors in the AGATA-array may defined. If the automatic filling system of the array is not working or damaged and if the LN_2-level inside a dewar is below the threshold a system-independent forcefill will be started and fill the cryostat before it warms up, in order to protect it.

Appendix A

Warming-up-process

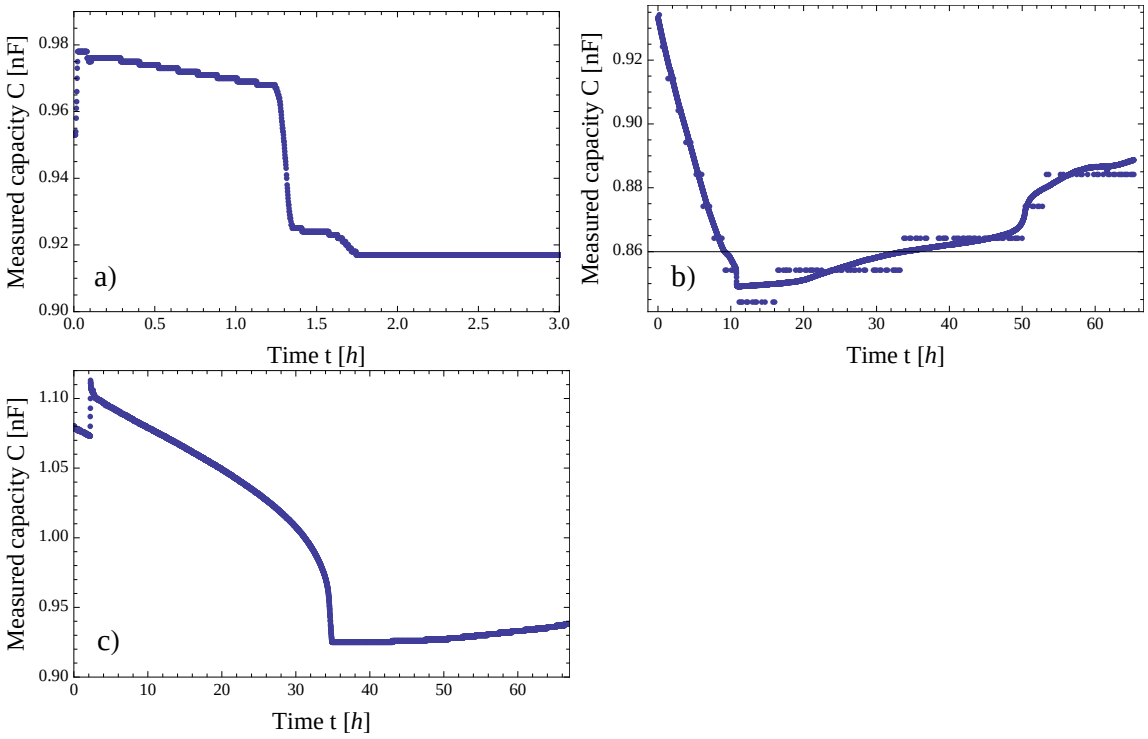

Figure A.1: *Measured capacity C as a function of time t during the warming-up-processes of:* **a)** *ATC(2).* **b)** *ATC(3). After* 60 h *this warming-up-process is still not finished. The measured capacity C shows a chaotic behaviour after $t = 30$ h.* **c)** *ATC(4). The cryostat was in horizontal position during this measurement.*

Appendix B

Consumption measurements

B.1 Measured capacities and filling heights during the consumption measurements of ATC(2)

	HV, LV ON		HV, LV OFF	
time [h]	C[pF]	h_1[cm]	C[pF]	h_2[cm]
0	$1,126 \pm 5$	-	$1,129 \pm 5$	-
1	$1,115 \pm 5$	13 ± 2	$1,120 \pm 5$	13 ± 2
2	$1,104 \pm 5$	11.5 ± 0.5	$1,113 \pm 5$	12.4 ± 0.5
3	$1,093 \pm 5$	10.3 ± 0.5	$1,101 \pm 5$	10.7 ± 5
4	$1,082 \pm 5$	8.8 ± 0.5	$1,092 \pm 5$	9 ± 0.5
5	$1,071 \pm 5$	7.5 ± 0.5	$1,082 \pm 5$	8.1 ± 0.5
6	$1,059 \pm 5$	6.2 ± 0.5	$1,072 \pm 5$	7.1 ± 0.5
7	$1,050 \pm 5$	5.1 ± 0.5	$1,063 \pm 5$	6.2 ± 0.5

Table B.1: *Measured filling height h as a function of time for ATC(2) under different conditions (high and low voltage/ high and low voltage off). The filling height was checked every hour. The filling hight for $t = 0\,\mathrm{h}$ could not be determined, because the dewar was at maximum filling-level and an opening would have caused a burst of LN_2. This is also the reason why the error of h is $2\,\mathrm{cm}$ at $t = 1\,\mathrm{h}$. The filling capacity was additionally checked every hour.*

LV ON, ramping HV and XIA

time [h]	C[pF]	h[cm]	C[pF]	h[cm]
0	$1,130 \pm 5$	-	$1,130 \pm 5$	-
1	$1,119 \pm 5$	13 ± 2	$1,119 \pm 5$	13.4 ± 2
2	$1,109 \pm 5$	11 ± 0.5	$1,107 \pm 5$	10.5 ± 0.5
3	$1,097 \pm 5$	9.8 ± 0.5	$1,097 \pm 5$	9.1 ± 5
4	$1,086 \pm 5$	8.5 ± 0.5	$1,085 \pm 5$	8.2 ± 0.5
5	$1,074 \pm 5$	7.5 ± 0.5	$1,074 \pm 5$	7.1 ± 0.5
6	$1,063 \pm 5$	6.3 ± 0.5	$1,063 \pm 5$	6 ± 0.5
7	$1,053 \pm 5$	5.3 ± 0.5	$1,052 \pm 5$	5 ± 0.5

Table B.2: *Measured filling height as a function time for ATC(2). The low voltage was applied and the high voltage has been ramped up in irregular steps. The XIA-electronics was running additionally, as the room temperature increased about* $2\,^{\circ}\mathrm{C}$. *This measurement was performed twice, thus the measured filling heights and capacities are similar.*

B.2 The capton-cable-test

B.2.1 Measured capacities and filling heights during the consumption measurements of ATC(3)

old cabling			capton-cabling		
Time [h]	C[pF]	h[cm]	Time [h]	C[pF]	h[cm]
0	$1,051 \pm 5$	-	0	$1,037 \pm 5$	-
2.17	$1,025 \pm 5$	10.4 ± 0.5	1	$1,023 \pm 5$	10.8 ± 0.5
3.75	$1,006 \pm 5$	8.5 ± 0.5	2	$1,012 \pm 5$	9.7 ± 0.5
5.17	989 ± 5	6.9 ± 0.5	4	981 ± 5	$6,5 \pm 0.5$
6.67	971 ± 5	5 ± 0.5	5	965 ± 5	5.1 ± 0.5
8.17	953 ± 5	3.2 ± 0.5	6	952 ± 5	3.6 ± 0.5
9.5	945 ± 5	1.7 ± 0.5	7	937 ± 5	2.1 ± 0.5

Table B.3: *Measured capacities and filling-hights for ATC(3). The left column represents the data for ATC(3) with the old cabling, whereas the data measured with the capton-cabling is displayed in the right column.*

B.2.2 LN_2-consumption calculated by the measured filling heights

The measured filling heights are plotted as a function of time in fig. B.1. Using the linear function: $h(t) = m \cdot t + b$ for fitting the measured data, leads to the consumption $\nu = \frac{m}{b} \cdot 4.5\,\mathrm{l}$ and operation time $\tau = \frac{b}{m}$ (see chapter 4). The calculated values are displayed in table B.4.

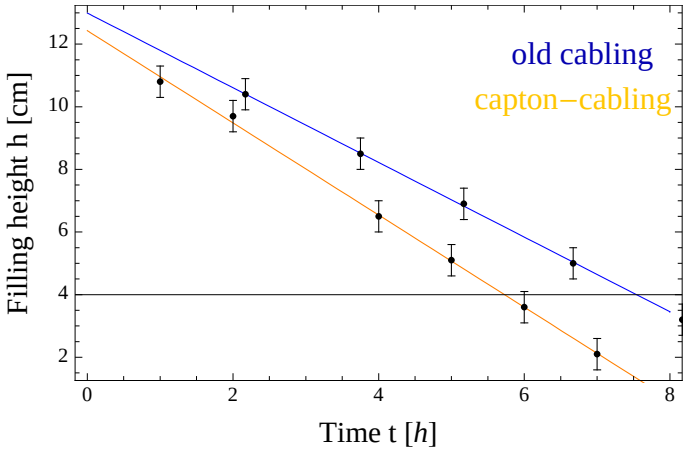

Figure B.1: *Plot of the measured filling height h as a function of time. The blue and orange curve are linear regressions through the measured data points. Their functions are given by:* $h_{old} = (-1.19 \pm 0.01)\frac{\text{cm}}{\text{h}} \cdot t + (12.99 \pm 0.06)\text{cm}$ *and* $h_{capton} = (-1.47 \pm 0.03)\frac{\text{cm}}{\text{h}} \cdot t + (12.43 \pm 0.12)\text{cm}$. *The gradient of each curve indicates the consumption of liquid nitrogen*

Cabling	$\nu[\frac{\text{ml}}{\text{h}}]$	τ[h]
old cabling	412 ± 4	10.9 ± 0.1
Capton	509 ± 11	8.8 ± 0.2

Table B.4: *Liquid nitrogen consumption and operation time of ATC(3) for two different cablings. The calculated values refer to the measured filling heights.*

B.3 LN_2-consumption and operation time of ATC(4) after a cooling-in-process

Time interval Δt[h]	ν[ml/h]	τ[h]
1.64	997 ± 44	4.51 ± 0.2
1.92	554 ± 21	8.13 ± 0.31
3	332 ± 15	13.54 ± 0.61
5	270 ± 11	16.67 ± 0.69
6.73	242 ± 9	18.57 ± 0.71

Table B.5: *Measured consumption ν and operation time τ after a cooling-in-process as a function of the time interval Δt where the consumption did not change.*

B.4 Measured filling capacity as a function of time for different loads at ATC(4)

The results of the consumption measurements are displayed in fig. B.2 and fig. B.3, as the parameters of the linear regressions are shown in table B.6. The consumption ν for one load has been calculated by $\nu(P) = \frac{\bar{m}}{\Delta C} \cdot 4.5\,\mathrm{l}$ (see chapter 4), as $\Delta C = 130\,\mathrm{pF}$ for ATC(4).

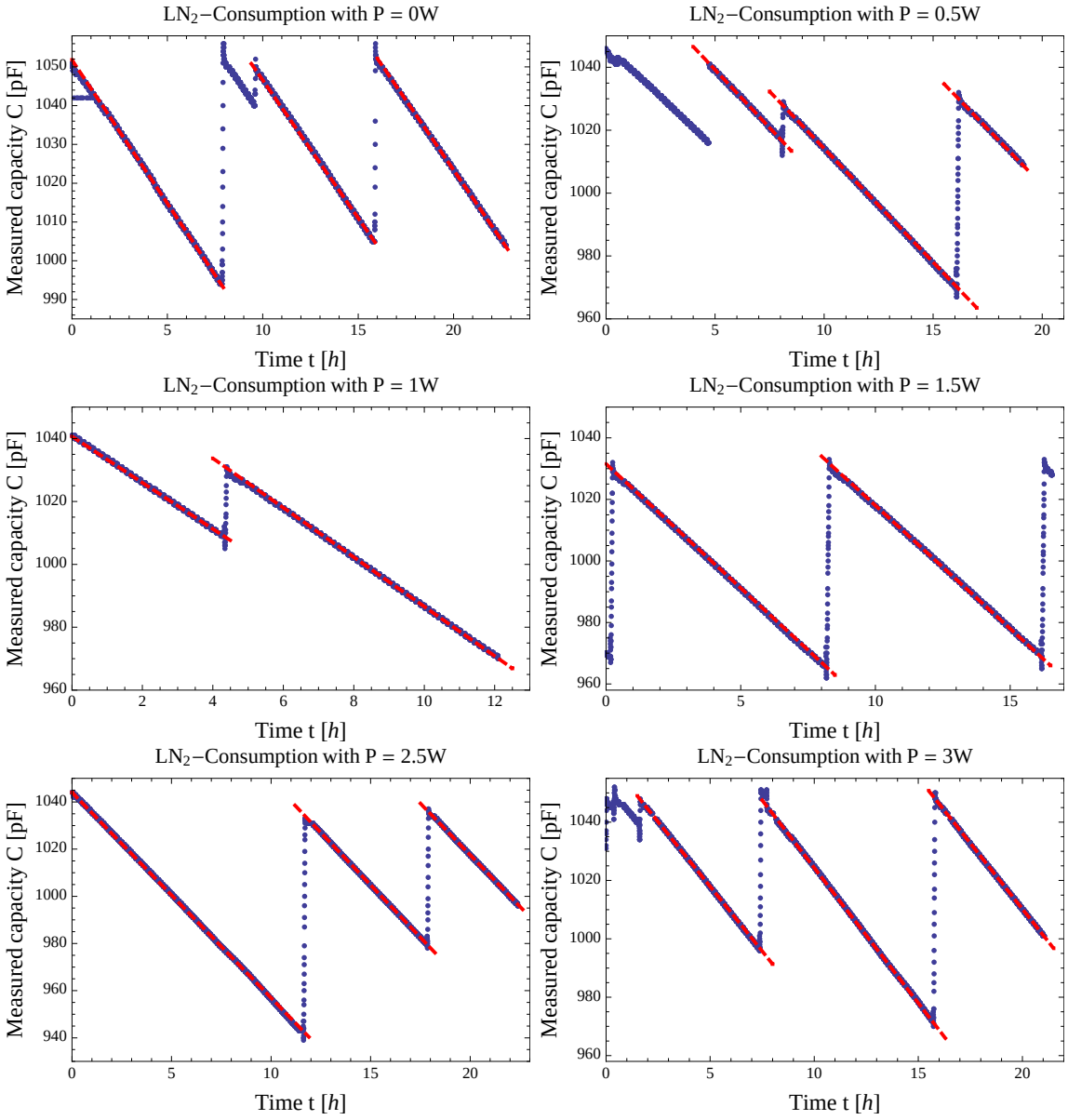

Figure B.2: *Measured filling capacity C as a function of the time t for different heat loads P. The red lines are linear regressions through the measured data.*

$P[W]$	$m[\frac{\text{pF}}{\text{h}}]$	b[pF]	$\bar{m}[\frac{\text{pF}}{\text{h}}]$	$P[W]$	$m[\frac{\text{pF}}{\text{h}}]$	b[pF]	$\bar{m}[\frac{\text{pF}}{\text{h}}]$
0	$-\frac{37}{5}$	$\frac{5259}{5}$		0.5	-7.24	1086.62	
	$-\frac{64}{9}$	$\frac{3353}{3}$	-7.24 ± 0.14		-7.37	1076.05	-7.25 ± 0.12
	$-\frac{36}{5}$	$\frac{5837}{5}$			-7.14	1145.43	
1	-7.86	1065.14		1.5	-8.07	1031.53	
	-7.35	1040.68	-7.61 ± 0.36		-8	1098	-8.04 ± 0.05
2	-8.3	1027.45		2.5	-8.75	1192.5	
	$-\frac{25}{3}$	1095	-8.23 ± 0.15		-8.89	1138.11	-8.78 ± 0.1
	-8.06	1156.1			-8.71	1044.07	
3	-8.86	1062.27		4	-9.8	1043	
	-9.27	1117.09	-9.04 ± 0.21		-10	1150	-9.93 ± 0.12
	-9	1190.25			-10	1230	
5	-11.07	1045.07		6	-11.36	1042.82	
	$-\frac{67}{6}$	$\frac{6983}{6}$	-11.08 ± 0.09		-12	1117	-11.71 ± 0.28
	-11	1246.4			-11.64	1161.18	
					-11.84	1260.26	
7	-12.5	1053.5					
	-12.67	1154.33	-12.46 ± 0.23				
	-12.22	1250.4					

Table B.6: *Parameter m and b of the linear function $C(t) = m \cdot t + b$ which has been regressed to the measured data. $\bar{m}$ is the mean value of all gradients m referring to one load P.*

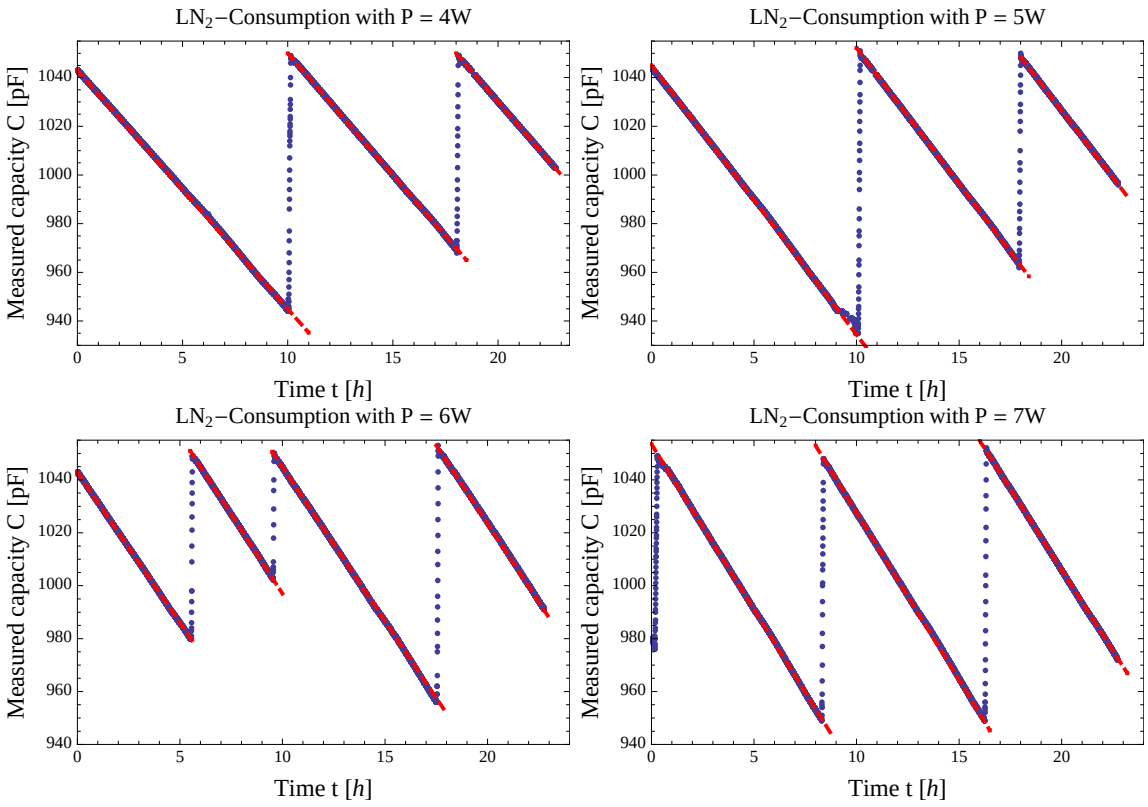

Figure B.3: *Measured filling capacity C as a function of the time t for different heat loads P. The red lines are linear regressions through the measured data.*

Appendix C

The C/V-transcenducer

C.1 Pin out and component placement specification of the CAV414

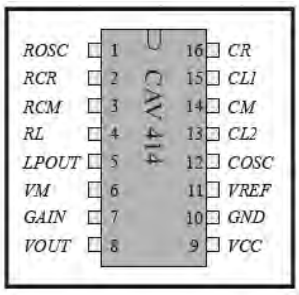

PIN	NAME	DESCRIPTION
1	*RCOSC*	Oscillator current definition
2	*RCR*	Current setting for integrator C_R
3	*RCM*	Current setting for integrator C_M
4	*RL*	Gain setting
5	*LPOUT*	Low pass filter output
6	*VM*	Reference voltage 2.V
7	*GAIN*	Output stage gain setting
8	*VOUT*	Voltage output
9	*VCC*	Supply voltage
10	*GND*	IC ground
11	*VREF*	Reference voltage 5V
12	*COSC*	Reference oscillator capacitor
13	*CL2*	Low pass 2, capacitor for 3dB corner frequency
14	*CM*	Sensor measurement capacitor
15	*CL1*	Low pass 1, capacitor for 3dB corner frequency
16	*CR*	Sensor reference capacitor

Figure C.1: *Pin out of the CAV 414 [Gmb08].*

C.2 Increasing and decreasing the gain

Considering chapter 5, the gain of a LN_2-read-out-device is given by: $G = \frac{U_G}{U_0+O}$. Decreasing the gain is described by:

$$G^{-1}(C) := \frac{U_0 + O}{U_G} = \frac{1}{\alpha} + \frac{b_0 - \frac{1}{\alpha} \cdot (b_G - O)}{U_G} \tag{C.1}$$

Considering an output-voltage $U = U_0 + O$ with gain $G = 1$ and offset $O \neq 0$ leads to the output: $U_G = GU = GU_0 + GO$ if the gain is changed to $G \neq 1$. Changing the gain back to $G = 1$ leads to the original output voltage U: $G^{-1}(U_G) = G^{-1}GU = U_0 + O$. But if the offset is changed by $\tilde{O}$ before changing back the gain leads to a different situation: the output-voltage is $\tilde{U} = U_G + \tilde{O} = GU + \tilde{O}$. Decreasing the gain now by G^{-1} changes $\tilde{U}$ to:

$$G^{-1}(\tilde{U}) = G^{-1}GU + G^{-1}\tilde{O} = U + G^{-1}\tilde{O} \tag{C.2}$$

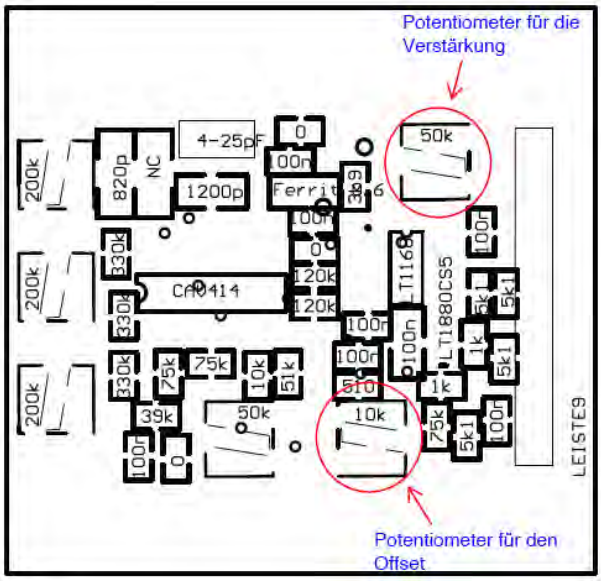

Figure C.2: *Component placement specification of the* LN_2*-read-out-device which has been developed in cologne.*

Thus the beginning value U has an extra offset $G^{-1}\tilde{O}$, because the offset has been changed between increasing and decreasing the gain. Increasing the gain again by $\tilde{G}$ leads to:

$$\tilde{G}(U + G^{-1}\tilde{O}) = \tilde{\alpha} + \frac{b_{\tilde{G}} + \tilde{\alpha} \cdot (b_0 + O + G^{-1}\tilde{O})}{U_0 + O + G^{-1}\tilde{O}} \tag{C.3}$$

The extra offset $G^{-1}\tilde{O}$ appears in every new adjustment of gain and offset. **The previous information about gain and offset effects every new adjustment of them.** This has to be considered when adjusting gain and offset of the read-out-device. Figure C.2 displays a general layout diagram of the read-out-device.

C.3 Measuring U_0, U_{max} and G_{max} for box 1,3 and 4

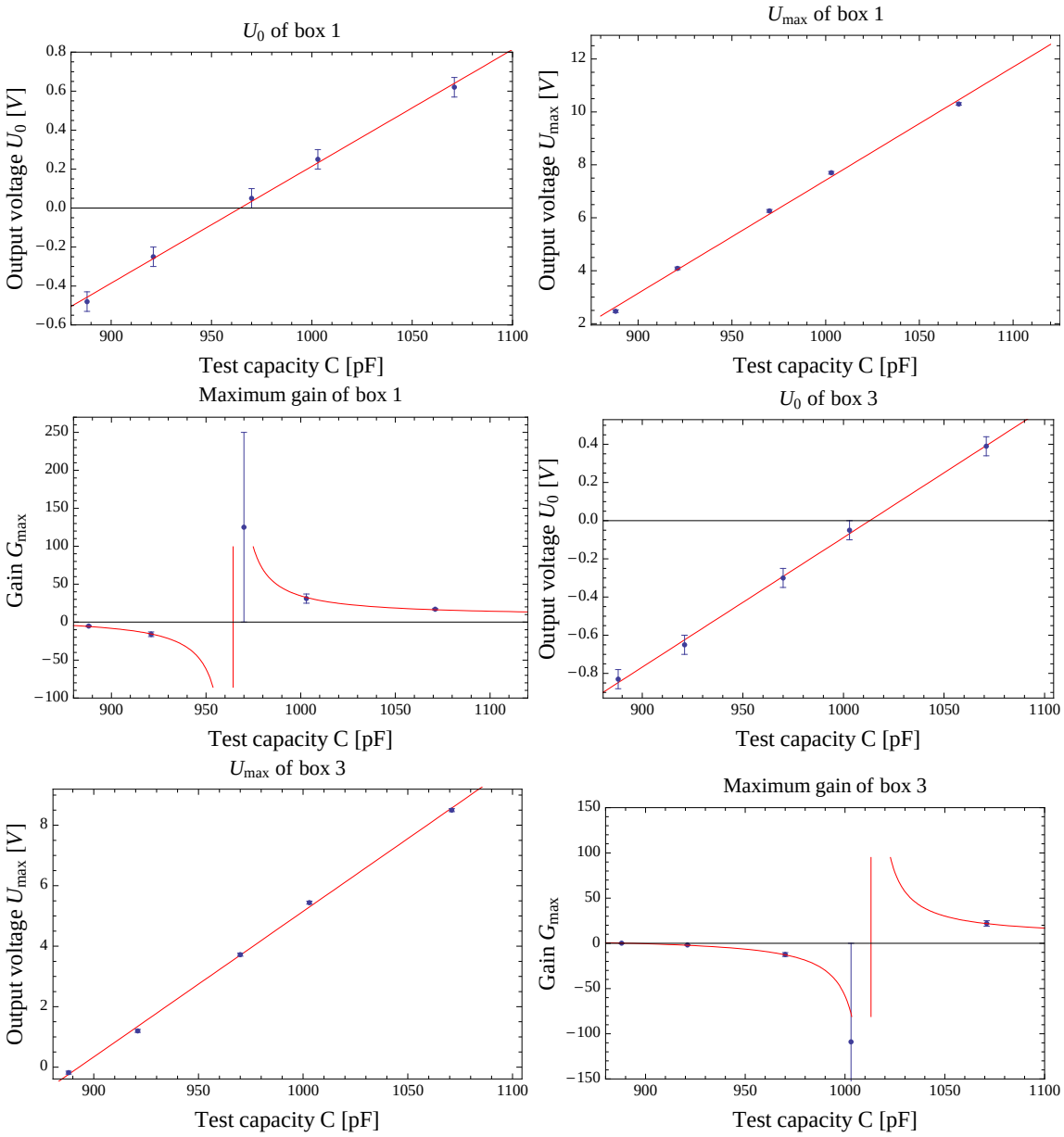

Figure C.3: *Measured output voltages U_0, U_{max} and maximum gain G_{max} for box 1 and 3 as function of the test capacity C.*

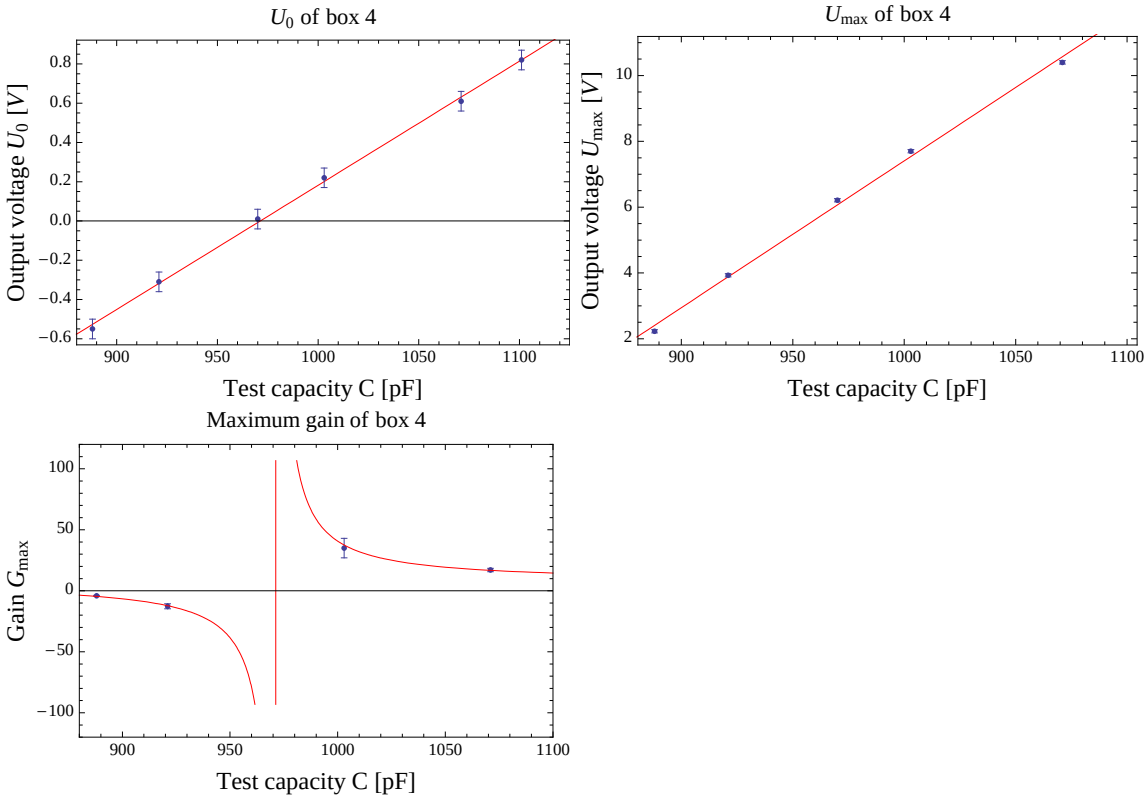

Figure C.4: *Measured output voltages U_0, U_{max} and maximum gain G_{max} for box 4 as function of the test capacity C.*

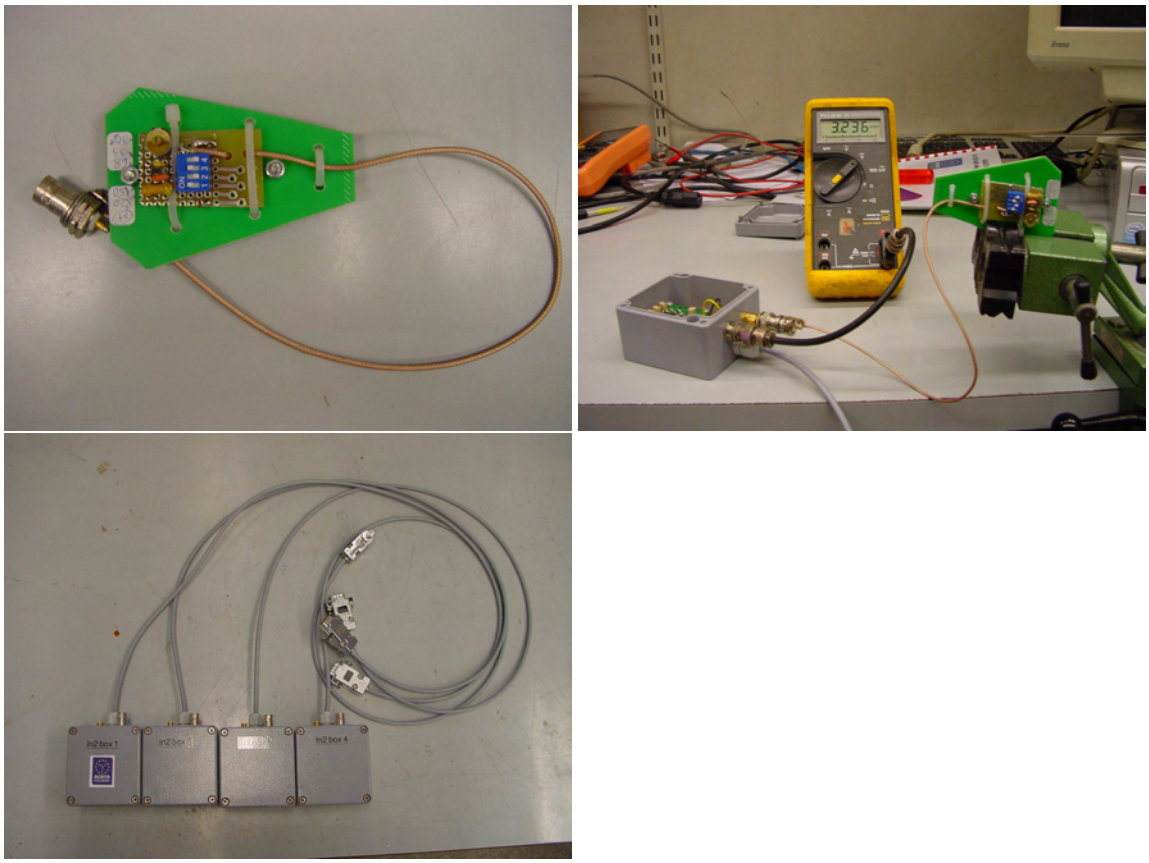

Figure C.5: **Left:** *Capacitive dummy which is able to simulate capacities between* 888 pF *and* 1030 pF. **Right:** *Measuring device for testing and adjusting the boxes: The capacitive dummy is connected to the read-out-device. The output-voltages are measured with a multimeter.* **Down left:** *Photograph of all* LN_2*-read-out-devices.*

Appendix D

Simulation of $S(\theta)$ and $V(\theta)$

The simulation of the surface S and the volume V of a liquid inside an ideal cylinder with radius R height h_0 and inclination θ is related to a theoretical model as described in chapter 6. The equations for S and V are given by:

$$S(\theta) = \begin{cases} S_{wdg}\Theta(k) + S_{seg}\Theta(-k) - \delta S_{wdg}\Theta(\theta_{crit} - \theta), & \theta < 90\,^\circ \\ S_{90}, & \theta = 90\,^\circ \end{cases} \quad \text{(D.1)}$$

$$V(\theta) = \begin{cases} V_{wdg}\Theta(k) + V_{seg}\Theta(-k) - \delta V_{wdg}\Theta(\theta_{crit} - \theta), & \theta < 90\,^\circ \\ V_{90}, & \theta = 90\,^\circ \end{cases} \quad \text{(D.2)}$$

D.1 The correction terms δS_{wdg} and δV_{wdg}

The correction terms δS_{wdg} and V_{wdg} are related to the fact that the liquid inside the cylinder for a certain inclination θ has a smaller surface/ volume than predicted by the formulas of S_{wdg} and V_{wdg}. Figure D.1 shows an ideal

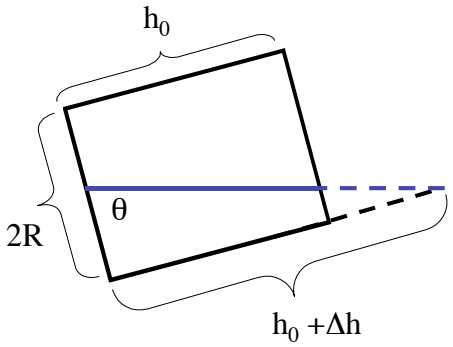

Figure D.1: *2d-cut through an ideal cylinder with radius R, height h_0 and inclination θ.*

cylinder with a liquid inside. The surface and volume of the liquid are thus given by:

$$V = V_{wdg}(h_0 + \Delta h) - \underbrace{V_{wdg}(\Delta h)}_{=\delta V_{wdg}} \quad \text{(D.3)}$$

$$S = S_{wdg}(h_0 + \Delta h) - \underbrace{S_{wdg}(\Delta h)}_{=\delta S_{wdg}} \quad \text{(D.4)}$$

The correction terms are gained from these equations: $\delta V_{wdg} = V_{wdg}(\Delta h)$ and $\delta S_{wdg} = S_{wdg}(\Delta h)$. The height Δh depends on the filling-level inside the dewar which will be discussed in the following sections.

D.2 Simulation of S and V for a constant volume V

Figure D.2 shows a two dimensional cut through an ideal cylinder with a liquid inside. The cylinder is inclined by the angle θ. The volume of the liquid inside the cylinder is inclination independent: $V(0\,^\circ) = \mathrm{V}(\theta) = \mathrm{V}(\theta_{\mathrm{crit}})$. Thus the filling level h for each inclination is determined by this condition. In order to realise an inclination independent volume V of the liquid, an imaginary filling nozzle with length l_f and diameter d is introduced. The diameter of this filling nozzle is a function of the inclination, so that the volume of the liquid is always constant. The function $d(\theta)$ can be found by solving the equation:

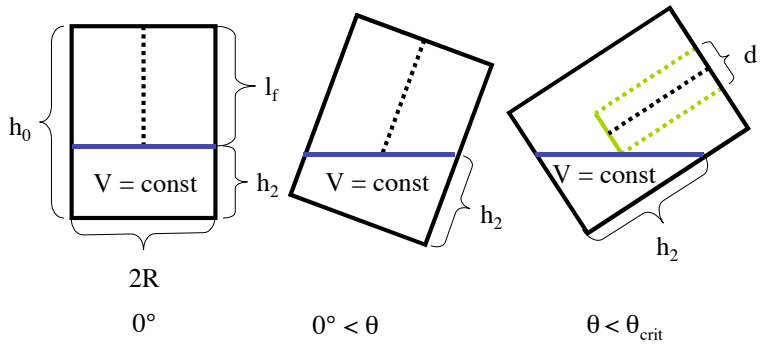

Figure D.2: *2d-cut through an ideal cylinder with a liquid inside. The filling height h of the liquid inside the dewar is determined by an imaginary filling nozzle (dashed lines) with constant length l_f and diameter d. In order to remain the volume of the liquid constant for each inclination, the diameter d has to be a function of the inclination θ as shown in this drawing: $d(\theta = 0\,^\circ) = \mathrm{d}(\theta) = 0$, but $d(\theta_{crit}) \neq 0$. Thus the height h_2 is given by: $h_2 = (h_0 - l_f) + (R - d(\theta)/2) \cdot \tan\theta$. This leads to: $\Delta h = (R - d(\theta)/2) \cdot \tan\theta - l_f$ for a given inclination.*

$$V(\theta, d(\theta), (h_0 - l_f), R) \stackrel{!}{=} (h_0 - l_f) \cdot \pi \cdot R^2 \tag{D.5}$$

for $d(\theta)$, as $V(\theta, d(\theta), (h_0 - l_f), R)$ is the volume of a liquid inside an ideal dewar with radius R, height h_0, nozzle-lentgh l_f and inclination θ. The expression $(h_0 - l_f) \cdot \pi \cdot R^2$ represents the volume of the liquid being in vertical position $\theta = 0\,^\circ$. Equation D.5 has been solved for an ideal dewar with $R = 10\,\mathrm{cm}$, $h_0 = 29\,\mathrm{cm}$ and $l_f = 18\,\mathrm{cm}$ and $l_f = 21.5\,\mathrm{cm}$. The blue data-points in figure D.3 represent the results $d(\theta)$ of solving equation D.5 for inclination angles from $40\,^\circ$ to $90\,^\circ$. The inclination angle θ_{crit} at which the imaginary filling-nozzle becomes important for the calculations of S and V is given by:

$$\tan\theta_{crit} = \frac{(h_0 - l_f)}{R} \Leftrightarrow \theta_{crit} = 48\,^\circ(\mathrm{l_f} = 18\,\mathrm{cm}),\ \theta_{\mathrm{crit}} = 37\,^\circ(\mathrm{l_f} = 21.5\,\mathrm{cm}) \tag{D.6}$$

Thus inclination angles smaller than $40\,^\circ$ are negligible for calculating $d(\theta)$. The red curves in fig. D.3 are a polynomial fit to the data-points:

$$d(\theta) = a \cdot \theta^5 + b \cdot \theta 14 + c \cdot \theta^3 + d \cdot \theta^2 + e \cdot \theta + f \tag{D.7}$$

As a, b, c, d, e, f are fit-parsmeters. The volume in diagram a) is related to a filling height $h = 11\,\mathrm{cm}$ in vertical dewar-position, whereas the volume in

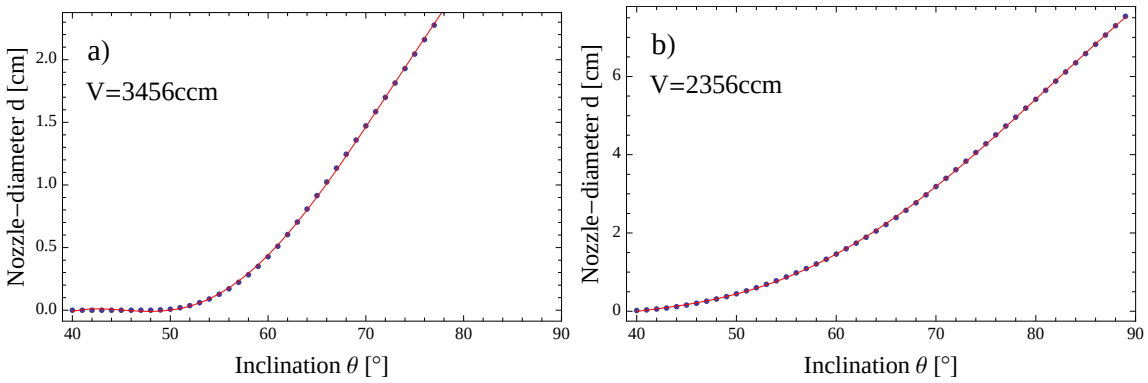

Figure D.3: **a)** *Plot of the nozzle-diamteer d as a function of the inclination θ for a constant volume $V = 3456\,\mathrm{cm}^3$.The function $d(\theta)$ is given by:* $d(\theta) = 8.01 \cdot 10^{-8}\,\mathrm{cm} \cdot \theta^5 - 2.65 \cdot 10^{-5}\,\mathrm{cm} \cdot \theta^4 + 3.42 \cdot 10^{-3}\,\mathrm{cm} \cdot \theta^3 - 0.21\,\mathrm{cm} \cdot \theta^2 + 6.37\,\mathrm{cm} \cdot \theta - 73.87\,\mathrm{cm}$. **b)** *Plot of $d(\theta)$ for a volume $V = 2356\,\mathrm{cm}^3$, as the function of the diameter is:* $d(\theta) = 9.17 \cdot 10^{-9}\,\mathrm{cm} \cdot \theta^5 - 4.14 \cdot 10^{-6}\,\mathrm{cm} \cdot \theta^4 + 6.53 \cdot 10^{-4}\,\mathrm{cm} \cdot \theta^3 - 4.43 \cdot 10^{-2}\,\mathrm{cm} \cdot \theta^2 + 1.38\,\mathrm{cm} \cdot \theta - 16.52\,\mathrm{cm}$.

diagram b) is related to a filling height $h = 7.5\,\mathrm{cm}$ in vertical dewar-position. All calculations considering $S(\theta)$ and $V(\theta)$ have been done with *mathematica*. Figure D.4 displays an extract from the program which was used for the simulation of $S(\theta)$ and $V(\theta)$, as the parameters of equations B.3 and B.4 are defined in this part (see mathematica-guide):

- **f[x_, y_, z_] = ⋯**: Defines a function $f(x, y, z)$ depending on three or even more variables.
- **HeavisideTheta[...]**: Refers to the step-function and is used for defining the surface and volume of the liquid over the full inclination-range from $0\,^\circ$ to $90\,^\circ$.
- **Tan[x Degree]**: Defines the trigonometrical function $\tan(x)$, as the angle x is given in $^\circ$.

The part of the program where the surface $S(\theta)$ and volume $V(\theta)$ are visualised is displayed in fig. D.5, as the following commands were used [x]:

- **Plot[**$f(x)$**, {**x**,** x_{min}**,** x_{max}**}]**: Generates a plot of the function $f(x)$ beginning at $x = x_{min}$ and ending at x_{max}.
- **PlotStyle**: Defines characteristics (like colour or thickness) of the plotted curve.
- **Frame**, **FrameLabel**: Defines a frame with a labelling.
- **PlotRange**: Defines the range of the plot which shall be shown.
- **PlotLabel**: Defines a labelling of the plot.

```
R = 10; L = 29; aw[x_, di_, H_] = Sqrt[2 * R * (L - H + (R - di / 2) * Tan[x Degree]) / Tan[x Degree] -
    ((L - H + (R - di / 2) * Tan[x Degree]) / Tan[x Degree])^2]; ϕw[x_, di_, H_] =
 π / 2 + ArcTan[((L - H + (R - di / 2) * Tan[x Degree]) / Tan[x Degree] - R) / aw[x, di, H]];
awm[x_, di_, H_] = Sqrt[2 * R * (-H + (R - di / 2) * Tan[x Degree]) / Tan[x Degree] -
    ((-H + (R - di / 2) * Tan[x Degree]) / Tan[x Degree])^2]; ϕwm[x_, di_, H_] =
 π / 2 + ArcTan[((-H + (R - di / 2) * Tan[x Degree]) / Tan[x Degree] - R) / awm[x, di, H]];
vw[x_, di_, H_] = Tan[x Degree] / 3 * (aw[x, di, H] * (3 * R^2 - (aw[x, di, H])^2) +
     3 * R^2 * ((L - H + (R - di / 2) * Tan[x Degree]) / Tan[x Degree] - R) * ϕw[x, di, H]) *
   HeavisideTheta[(R + di / 2) * Tan[x Degree] - (L - H)] +
  π * R^2 * (L - H - di / 2 * Tan[x Degree]) * HeavisideTheta[(L - H) - (R + di / 2) * Tan[x Degree]];
vwm[x_, di_, H_] = Tan[x Degree] / 3 * (awm[x, di, H] * (3 * R^2 - (awm[x, di, H])^2) +
    3 * R^2 * ((-H + (R - di / 2) * Tan[x Degree]) / Tan[x Degree] - R) * ϕwm[x, di, H]);
sw[x_, di_, H_] = (2 * R * Tan[x Degree] *
    (aw[x, di, H] + ((L - H + (R - di / 2) * Tan[x Degree]) / Tan[x Degree] - R) * ϕw[x, di, H]) *
    HeavisideTheta[(R + di / 2) * Tan[x Degree] - (L - H)] +
   2 * π * R * (L - H - di / 2 * Tan[x Degree]) * HeavisideTheta[L - H - (R + di / 2) * Tan[x Degree]]);
swm[x_, di_, H_] = 2 * R * Tan[x Degree] *
  (awm[x, di, H] + ((-H + (R - di / 2) * Tan[x Degree]) / Tan[x Degree] - R) * ϕwm[x, di, H]);
vg[x_, di_, H_] = vw[x, di, H] - HeavisideTheta[(R - di / 2) * Tan[x Degree] - H] * vwm[x, di, H];
sg[x_, di_, H_] =
 sw[x, di, H] - HeavisideTheta[(R - di / 2) * Tan[x Degree] - H] * swm[x, di, H];
nu = π * R^2 * (L - H) / 20; d1[x_, H_] =
 (8.007236605879354`*^-8 * x^5 - 0.00002653176171680337` * x^4 + 0.003421330672866954` * x^3 -
    0.21252849253009456` * x^2 + 6.366501773577047` * x - 73.86869199399531`) *
  HeavisideTheta[Tan[x Degree] - (L - H) / R]; d2[x_, H_] =
 (9.167396979646134`*^-9 * x^5 - 4.1384187688018035`*^-6 * x^4 + 0.0006530677570700743` * x^3 -
    0.04428623326084718` * x^2 + 1.3809034538376617` * x - 16.521762597525587`) *
  HeavisideTheta[Tan[x Degree] - (L - H) / R];
```

Figure D.4: *Extract from the program which was used for simulating the surface S and volume V for a liquid inside an ideal cylinder, as the volume of the liquid has to remain constant. This part of the program defines all parameters of the cylinder and the parameters of $S(\theta)$ and $V(\theta)$ as they were discussed in chapter 6.*

```
Plot[{vg[x, d1[x, 18], 18], vg[x, d2[x, 21.5], 21.5]},
 {x, 0.01, 89}, PlotStyle → {{Thick, Green}, {Thick, Red}},
 Frame → True, PlotRange → {{0, 90}, {2000, 4000}}, FrameLabel →
  {Style["Inclination θ [°]", FontSize → 13], Style["Volume V(θ) " [cm^3], FontSize → 13]},
 PlotLabel → "green: h=11cm, red: h=7.5cm"]
Plot[{sg[x, d1[x, 18], 18], sg[x, d2[x, 21.5], 21.5]}, {x, 0.01, 89},
 PlotStyle → {{Thick, Green}, {Thick, Red}}, Frame → True, FrameLabel →
  {Style["Inclination θ " [°], FontSize → 13], Style["Surface S(θ) "[cm^2], FontSize → 13]},
 PlotRange → {{0, 90}, {400, 840}}, PlotLabel → "green: h=11cm, red: h=7.5cm"]
```

Figure D.5: *Visualisation of $S(\theta)$ and $V(\theta)$ using the parameters defined in fig. D.4.*

D.3 Simulation of S and V for a refilled dewar

If the dewar is refilled with a liquid for each inclination, the calculation of $S(\theta)$ and $V(\theta)$ is very simple, since no imaginary nozzle with an inclination dependent diameter is needed. If the filling nozzle is longer than $\frac{h_0}{2}$ the volume changes as function of the inclination θ, whereas the filling height h remains constant and isdetermined by the length l_f of the filling nozzle:

$$h = h_0 - l_f = \text{const.} \tag{D.8}$$

Figure D.6 shows the simulation of $S(\theta)$ with respect to $V(\theta)$ for a liquid inside an ideal cylinder. The structure of this program is mainly the same as used in the programs before, whereas the surface $S(\theta)$ is plotted with respect to the volume $V(\theta)$ for a given angle θ. The definitions of all parameters which

```
G = Green; B = Blue; Rd = Red; Yl = Yellow; Oe = Orange; Bk = Black;
Clear[i]; w = 1; y = 1; n = 0; R = 10; L = 29; H = 15; d = 0; Label[begin];
i = w++; γj = Input["Bitte Winkel in ° angeben"] Degree;
a[x_] = Sqrt[2 * R * x / Tan[γj] - (x / Tan[γj])^2];
ϕ[x_] = π / 2 + ArcTan[(x / Tan[γj] - R) / a[x]]; vi[x_] =
 (Tan[γj] / 3 * (a[x] * (3 * R^2 - (a[x])^2) + 3 * R^2 * (x / Tan[γj] - R) * ϕ[x]) * HeavisideTheta[
     2 R * Tan[γj] - x] + π * R^2 * (x - R * Tan[γj]) * HeavisideTheta[x - 2 * R * Tan[γj]]);
si[x_] = (2 * R * Tan[γj] * (a[x] + (x / Tan[γj] - R) * ϕ[x]) * HeavisideTheta[2 * R * Tan[γj] - x] +
   2 * π * R * (x - R * Tan[γj]) * HeavisideTheta[x - 2 * R * Tan[γj]]);
V[x_] = vi[x] - HeavisideTheta[x - L] * HeavisideTheta[Tan[γj] - H / (R - d / 2)] * (Tan[γj] / 3 *
     (a[(x - L)] * (3 * R^2 - (a[(x - L)])^2) + 3 * R^2 * ((x - L) / Tan[γj] - R) * ϕ[(x - L)]));
S[x_] = si[x] - HeavisideTheta[x - L] * HeavisideTheta[Tan[γj] - H / (R - d / 2)] *
   (2 * R * Tan[γj] * (a[(x - L)] + ((x - L) / Tan[γj] - R) * ϕ[(x - L)]));
s90[x_] = (2 * ArcCos[(R - x) / R] * R * L); v90[x_] = R / 2 * s90[x] - L * (R - x) * Sqrt[2 * R * x - x^2];
p90 = ListLinePlot[Table[{v90[x], s90[x]}, {x, 0, R - d / 2, 0.01}], PlotStyle → {Thick, Red}];
p[i] = ListLinePlot[Table[{V[x], S[x]}, {x, 0.001, L - H + (R - d / 2) * Tan[γj], 0.01}],
  PlotStyle → {Thick, Input["Welche Farbe? (G,Rd,B,Oe,Bk)"]}];
r = Input["Erneute Eingabe?"]; If[r > 0, Goto[begin]];
tab = Table[p[k], {k, 1, i}]; Show[tab, p90, Frame → True,
 FrameLabel → {Style[V / cm^3, FontSize → 13], Style[S / cm^2, FontSize → 13]},
 PlotRange → {{0, v90[R]}, {0, s90[R]}}]
```

Figure D.6: *Program for simulating the surface $S(\theta)$ and volume $V(\theta)$ for a liquid inside an ideal cylinder with radius $R = 10\,\text{cm}$, height $h_0 = 29\,\text{cm}$, filling-nozzle-length $l_f = 15\,\text{cm}$ and nozzle-diameter $d = 0$.*

are needed for calculating $S(\theta)$ and $V(\theta)$ are integrated in one loop, so that several plots of S vs. V for different angles are possible. The important steps of this program shall be described in the following:

1. Definition of the parameters R, d, $H = l_f$ and $L = h_0$ for the ideal cylinder.

2. **Label[begin]**: Beginning of the loop. The command **Input["Bitte Winkel in ° eingeben"** demands the operator to define an inclination angle θ.

3. Definition of all parameters Φ, a for the calculation of S and V.

4. **ListLinePlot[Table[{V[x], S[x]}...]]**: Generates a table of pairs $(V(\theta), S(\theta))$ for a specified angle θ which are plotted afterwards.

5. **Input["Welche Farbe? (G, Rd, B, Oe, Bk)"]**: The colour of each plot can be chosen here.

6. **r=Input["Erneute Eingabe?"]**: Asks the operator for another iteration with a different inclination angle. The command **If[r>0,Goto[begin]]** terminates the iteration if the answer is no.

7. **Table[p[k],...]**: Each $V-S$-plot referring to one inclination is collected in a table and finally plotted in one common diagram by the command **Show[...]** if the iteration is terminated.

For practical reasons the calculations and plots of $S(\theta)$ and $V(\theta)$ for angles between $0\,^\circ$ and $89\,^\circ$ are separated within this program from the calculations/plots of $S(90\,^\circ)$ and $V(90\,^\circ)$. Figure D.7 shows the generated output of the program for two different angles.

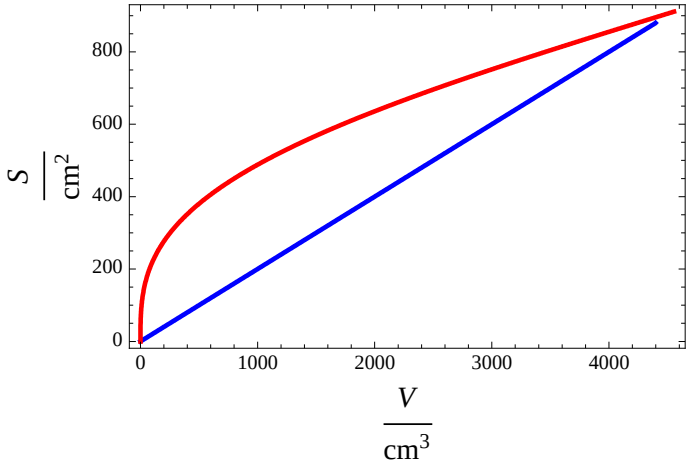

Figure D.7: *Output of the program: Plot of the surface $S(\theta)$ with regard to the volume $V(\theta)$ for the angles $\theta = 0\,^\circ$ (blue curve) and $\theta = 90\,^\circ$ (red curve).*

D.4 Simulating the filling capacity $C(t)$

The simulation of the filling capacity as a function of the time is similar to the simulations discussed before, as the formulas 6.20 and 6.21 are used. Figure D.8 and D.9 show the simulation of the filling capacity $C(t)$ as a function of time t. The case of a constant amount of liquid nitrogen inside an inclined dewar is displayed in fig. D.8, whereas the case of a dewar which is refilled with LN_2 for each inclination is shown in fig. D.9.

```
G = Green; B = Blue; Rd = Red; Yl = Yellow; Oe = Orange; Bk = Black; Clear[i]; w = 1; y = 1; n = 0;
R = 10; L = 29; H = 21.5; Label[begin]; i = w++; γj = Input["Bitte Winkel in ° angeben"] Degree;
d = d2[γj, H]; a[x_] = Sqrt[2 * R * x / Tan[γj] - (x / Tan[γj])^2];
ϕ[x_] = π / 2 + ArcTan[(x / Tan[γj] - R) / a[x]]; vi[x_] =
 (Tan[γj] / 3 * (a[x] * (3 * R^2 - (a[x])^2) + 3 * R^2 * (x / Tan[γj] - R) * ϕ[x]) * HeavisideTheta[
     2 R * Tan[γj] - x] + π * R^2 * (x - R * Tan[γj]) * HeavisideTheta[x - 2 * R * Tan[γj]]);
si[x_] = (2 * R * Tan[γj] * (a[x] + (x / Tan[γj] - R) * ϕ[x]) * HeavisideTheta[2 * R * Tan[γj] - x] +
   2 * π * R * (x - R * Tan[γj]) * HeavisideTheta[x - 2 * R * Tan[γj]]); V[x_] =
 vi[x] - HeavisideTheta[x - L] * HeavisideTheta[Tan[γj] - H / (R - d2[γj, H] / 2)] * (Tan[γj] / 3 *
     (a[(x - L)] * (3 * R^2 - (a[(x - L)])^2) + 3 * R^2 * ((x - L) / Tan[γj] - R) * ϕ[(x - L)]));
S[x_] = si[x] - HeavisideTheta[x - L] * HeavisideTheta[Tan[γj] - H / (R - d2[γj, H] / 2)] *
   (2 * R * Tan[γj] * (a[(x - L)] + ((x - L) / Tan[γj] - R) * ϕ[(x - L)]));
s90[x_] = (2 * ArcCos[(R - x) / R] * R * L); v90[x_] = R / 2 * s90[x] - L * (R - x) * Sqrt[2 * R * x - x^2];
p90 = ListLinePlot[Table[{(v90[R - d2[89, H] / 2] - v90[x]) * 20 / (π * R^2 * (14)),
    8.854 * 10^(-2) / (R * Log[10 / 9.82]) * (2 * π * R * L + 0.4 * s90[x])},
   {x, 0, R - d2[89, H] / 2, 0.01}], PlotStyle → {Thick, Red}];
p[i] = ListLinePlot[Table[{(V[L - H + (R - d2[γj, H] / 2) * Tan[γj]] - V[x]) * 20 / (π * R^2 * (14)),
    8.854 * 10^(-2) / (R * Log[10 / 9.82]) * (2 * π * R * L + 0.4 * S[x])},
   {x, 0.001, L - H + (R - d1[γj, H] / 2) * Tan[γj], 0.01}],
  PlotStyle → {Thick, Input["Welche Farbe? (G,Rd,B,Oe,Bk)"]}];
r = Input["Erneute Eingabe?"]; If[r > 0, Goto[begin]];
tab = Table[p[k], {k, 1, i}];
angle = Show[tab, p90, Frame → True, FrameLabel → {Style["Time t "[h], FontSize → 13], Style[
     "Simulated capacity C(t) "[pF], FontSize → 13]}, PlotRange → {{0, 14}, {891, 1040}}]
```

Figure D.8: *Simulation of $C(t)$ for a constant amount of liquid nitrogen inside the dewar. The model of an imaginary filling-nozzle with varying diameter $d(\theta)$ was used here.*

```
G = Green; B = Blue; Rd = Red; Yl = Yellow; Oe = Orange; Bk = Black; Clear[i]; w = 1; y = 1; n = 0;
R = 10; L = 29; H = 15; Label[begin]; i = w++; γj = Input["Bitte Winkel in ° angeben"] Degree;
d = 2; a[x_] = Sqrt[2 * R * x / Tan[γj] - (x / Tan[γj])^2];
ϕ[x_] = π / 2 + ArcTan[(x / Tan[γj] - R) / a[x]]; vi[x_] =
 (Tan[γj] / 3 * (a[x] * (3 * R^2 - (a[x])^2) + 3 * R^2 * (x / Tan[γj] - R) * ϕ[x]) * HeavisideTheta[
     2 R * Tan[γj] - x] + π * R^2 * (x - R * Tan[γj]) * HeavisideTheta[x - 2 * R * Tan[γj]]);
si[x_] = (2 * R * Tan[γj] * (a[x] + (x / Tan[γj] - R) * ϕ[x]) * HeavisideTheta[2 * R * Tan[γj] - x] +
   2 * π * R * (x - R * Tan[γj]) * HeavisideTheta[x - 2 * R * Tan[γj]]);
V[x_] = vi[x] - HeavisideTheta[x - L] * HeavisideTheta[Tan[γj] - H / (R - d / 2)] * (Tan[γj] / 3 *
     (a[(x - L)] * (3 * R^2 - (a[(x - L)])^2) + 3 * R^2 * ((x - L) / Tan[γj] - R) * ϕ[(x - L)]));
S[x_] = si[x] - HeavisideTheta[x - L] * HeavisideTheta[Tan[γj] - H / (R - d / 2)] *
   (2 * R * Tan[γj] * (a[(x - L)] + ((x - L) / Tan[γj] - R) * ϕ[(x - L)]));
s90[x_] = (2 * ArcCos[(R - x) / R] * R * L); v90[x_] = R / 2 * s90[x] - L * (R - x) * Sqrt[2 * R * x - x^2];
p90 = ListLinePlot[Table[{(v90[R - d / 2] - v90[x]) * 20 / (π * R^2 * (L - H)),
    8.854 * 10^(-2) / (R * Log[10 / 9.82]) * (2 * π * R * L + 0.4 * s90[x])},
   {x, 0, R - d / 2, 0.01}], PlotStyle → {Thick, Red}];
p[i] = ListLinePlot[Table[{(V[L - H + (R - d / 2) * Tan[γj]] - V[x]) * 20 / (π * R^2 * (L - H)),
    8.854 * 10^(-2) / (R * Log[10 / 9.82]) * (2 * π * R * L + 0.4 * S[x])},
   {x, 0.001, L - H + (R - d / 2) * Tan[γj], 0.01}],
  PlotStyle → {Thick, Input["Welche Farbe? (G,Rd,B,Oe,Bk)"]}];
r = Input["Erneute Eingabe?"]; If[r > 0, Goto[begin]];
tab = Table[p[k], {k, 1, i}];
angle = Show[tab, p90, Frame → True, FrameLabel → {Style["Time t "[h], FontSize → 13], Style[
     "Simulated capacity C(t) "[pF], FontSize → 13]}, PlotRange → {{0, 22}, {890, 1070}}]
```

Figure D.9: *Simulation of $C(t)$ for a dewar which is refilled with liquid nitrogen for each inclination.*

D.5 Measured filling capacity as a function of the inclination for a given filling height

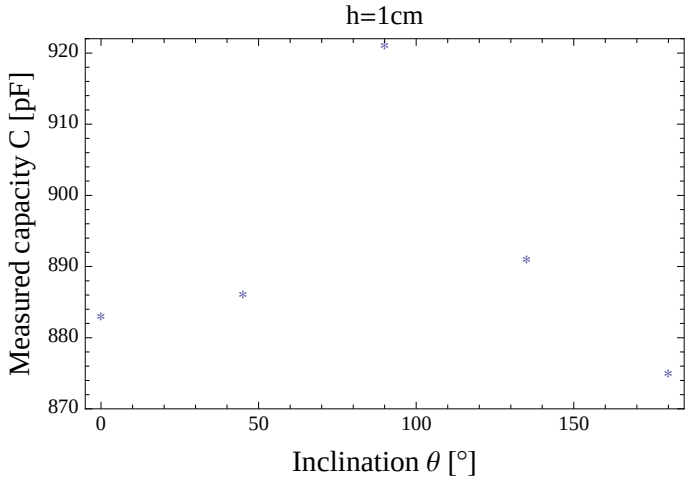

Figure D.10: *Measured filling capacity C as a function of the inclination θ. The dewar was filled with liquid nitrogen, when being in vertical position. The filling height was* 1 cm. *After filling the dewar has been inclined. This measurement was done by Heinz Georg Thomas (CTT Montabaur).*

Bibliography

[APG] Inc. Automation Product Group. Dielectric constants. Weppage. Available from World Wide Web: `www.apgsensors.com`.

[Cob41] James Dillon Cobine. *Gaseous Conductors*. Dover Publications, Inc., 1941.

[DB01] J. Cresswell G. Duchêne J. Eberth W. Gast J. Gerl W. Korten I. Lazarus R.M. Lieder J. Simpson D. Weisshaar D. Bazzacco, B. Cederwall. Agata - technical proposal for an advanced gamma tracking array for the european gamma spectroscopy community. Pruposal, September 2001. Available from World Wide Web: `http://www-win.gsi.de/agata/Publications/Agata_pub-proposal.pdf`.

[Dem04] Wolfgang Demtröder. *Experimentalphysik 2 Mechanik und Wärme*. Springer-Verlag, 3 edition, 2004.

[Dem05] Wolfgang Demtröder. *Experimentalphysik 3, Atome, Moleküle und Festkörper*. Springer-Verlag, 3 edition, 2005.

[EH05] Jürgen Gutekunst Ekbert Hering, Klaus Bressler. *Elektronik für Ingenieure und Naturwissenschaftler*. Springer-Verlag, 5 edition, 2005.

[Gmb08] Analog Microelectronics GmbH. Cav414-capacity/voltage (c/v-) transducer ic with adjustable output voltage. Datasheed, May 2008. Available from World Wide Web: `http://www.analogmicro.de/english/index.html`.

[JE08] John Simpson Jürgen Eberth. From ge(li) detectors to gamma-ray tracking arrays - 50 years of gamma spectroscopy with germanium detectors. *Science Direct*, 60, 2008.

[Kit06] Charles Kittel. *Einführung in die Festkörperphysik*. Oldenbourg, 14 edition, 2006.

[Koj07] Ivan Kojouharov. Cryogenic electronics and signal in/out specification for ad autofill. Technical report, GSI Darmstadt, June 2007.

[pas09] [online]November 2009 [cited December 2009]. Available from World Wide Web: `http://en.wikipedia.org/wiki/Paschen's_law`.

[pt1] [online, cited December 2009]Available from World Wide Web: `http://www.picotech.com/applications/pt100.html`.

[Rai99] Wilhelm Raith. *Bergmann, Schaefer Lehrbuch der Experimentalphysik, Band 2*, volume 2. de Gruyter, 1999.

[Rot79] Alexander Roth. *vacuum technology*. north-holland, 3 edition, 1979.

[Tec00] Linear Technology. Lt1168 low power, single resistor gain programmable precision instrumentation amplifier. Datasheed, 2000. Available from World Wide Web: `http://cds.linear.com/docs/Datasheet/1168fa.pdf`.

[Thr08] Stefan Thränert. *Charakterisierung mikro- und mesoporöser Gläser mit Hilfe der ortho-Positronium Lebensdauer-Spektroskopie*. PhD thesis, Martin-Luther-Universität Halle-Wittenberg, July 2008. Available from World Wide Web: `http://sundoc.bibliothek.uni-halle.de/diss-online/08/08H200/t8.pdf`.

[Wei09a] Eric W. Weisstein. Cylindrical segment. Webpage, 2009. Available from World Wide Web: `http://mathworld.wolfram.com/CylindricalSegment.html` [cited December 2009].

[Wei09b] Eric W. Weisstein. Cylindrical wedge. Webpage, 2009. Available from World Wide Web: `http://mathworld.wolfram.com/CylindricalWedge.html`.

Acknowledgement

It would not have been possible to write this thesis without the tremendous help and support of many people which I would like to thank. Many thanks to:

- Prof. Dr. Peter Reiter for assigning this thesis, having considerable ideas and his unlimited support during my examination period and during the period of writing this thesis.
- Dr. Bart Bruyneel for reading and correcting this thesis and many useful discussions which were a big help.
- Dr. Jürgen Eberth for introducing me into the complex field of detector-physics and always having time for a short discussion.
- Dr. Gheorghe Pascovici for developing the LN_2-read-out-device and teaching me in detail its working principle.
- Gristoph Goergen and the IKP electronics workshop for producing the read-out-modules, repairing many many broken potentiometers and having always time for answering my questions.
- Dr. Heinz Georg Thomas for supporting me with many information and useful ideas about AGATA-crystats.
- The AGATA-group members: Benedikt Birkenbach, Herbert Hess and Andreas Wiens. They introduced me into the AGATA-project and showed me elaborately how to handle and work with these delicate systems.
- The rest of the Reiter-Group: Kerstin Geibel, Tanja Kotthaus, Michael Seidlitz, Burkhard Siebeck and Andreas Wendt who provided a favourable working atmosphere.
- The whole IKP team for always being friendly and helpful.
- My fellow students: Alkiviadis Baviolis, Lukas Fink, Patrick Iserhardt, Sebastian Standop, Alexander Stolz and Christoph Trabant who are really friends and were always present and helped me to cope with my studies.
- My Kendo-sensei: Roland Niewerth, Hak-Seung Shin, Mitsuhiro Takamura and all members of the Kendo-Dojo-Cologne for the unique and inspiring training and many many Ji-Geikos (also those in the tavern).
- My parents Dagmar and Wolfgang, my brother Oliver for their love and support during my whole studies and helping me to cope with all problems during that long time.

- My deceased science teacher Dr. Wilfried Zeiske who teached me a lot in physics and was a great mentor.
- All my friends (especially Bernd Körperich) who also supported me and helped me to have a great time.
- My girlfriend Susanne for her love, her tremendous help and patience

Erklärung

Hiermit bestätige ich, dass ich meine Diplomarbeit selbstständig angefertigt und keine anderen als die angegebenen Quellen und Hilfsmittel benutzt, sowie Zitate kenntlich gemacht habe.

Köln, den 18.Dezember 2009

Daniel Lersch